# DEVELOPMENTAL SIMULATION OF THE ADULT CRANIAL MORPHOLOGY OF *AUSTRALOPITHECUS SEDIBA*

A Dissertation

by

KEELY BRITT CARLSON

Submitted to the Office of Graduate and Professional Studies of
Texas A&M University
in partial fulfillment of the requirements for the degree of

DOCTOR OF PHILOSOPHY

| | |
|---|---|
| Chair of Committee, | Darryl J. de Ruiter |
| Committee Members, | Lori Wright |
| | David Carlson |
| | Thomas J DeWitt |
| Head of Department, | Cynthia Werner |

August 2014

Major Subject: Anthropology

ABSTRACT

The present study involves the developmental simulation of the adult cranial morphology of the newly discovered species, *Australopithecus sediba. Au. sediba* has been the focus of considerable discussion and debate in paleoanthropology, following its announcement as a new species in 2010. The unique mosaic morphology of the Malapa hominins - with features aligning them to both earlier species of australopith as well as later *Homo* - has led some to hypothesize that *Au. sediba* represents the best candidate ancestor to the genus *Homo*. To date, only a single, relatively complete cranium has been recovered from the Malapa fossil site, belonging to the type specimen designated MH1. While its second molars are erupted and in occlusion, the third molars remain in the crypt, indicating the juvenile status of MH1. Some commentators have suggested that, because MH1 was a juvenile, its morphology may have changed substantially as it progressed towards adulthood. Further, these changes may have been significant enough to alter current interpretations of its morphological affinities, including traits thought to align *Au. sediba* with the genus *Homo*. As such, understanding the degree and nature of change to be expected to occur between second and third molar eruption is of crucial importance.

The present study has addressed this problem using 3D geometric morphometric techniques for the developmental simulation of the MH1 fossil cranium. Landmark-based developmental vectors were acquired from three extant hominoid species, including chimpanzees (*Pan troglodytes*), gorillas (*Gorilla gorilla*), and modern humans

(*H. sapiens*). Vectors were separated by sex to control for the influence of secondary sexual characteristics and applied to the reconstructed MH1 cranium. Six virtual adult crania were generated in total, a male and female from each of the three extant hominoid species used in simulation. In order to understand the morphological affinities of these generated adults in a broader comparative context, multivariate tests were carried out using a sample of non-robust hominin crania.

The results indicate that the majority of morphological changes expected to occur between second and third molar eruption are related to puberty. Results acquired from principal components analysis (PCA) and Procrustes distance matrix analysis indicate that all simulated adult crania of *Au. sediba* show greater similarities to one another than to other hominin species. All simulated *Au. sediba* adults consistently clustered together with the original juvenile cranium in PCA, separate from other hominin taxa. Results acquired from distance matrices also indicate that variation within the sample of simulated adult *Au. sediba* crania does not exceed that of other extant hominoid species, regardless of the developmental vector applied. Therefore, the results of this study provide empirical support for a separate, species-level diagnosis for *Au. sediba*, and further indicate the need to account for sexual dimorphism in morphometric studies of developmental simulation.

# DEDICATION

This dissertation is dedicated to my beloved grandfather, Milo E. Carlson. Thank you for sparking my curiosity and broadening my imagination. Without your life and legacy, I would never have become Dr. Keely Carlson.

# ACKNOWLEDGEMENTS

First of all, I would like to express my immense gratitude to my committee chair, Dr. Darryl de Ruiter for his encouragement and guidance throughout my years of graduate study. I would also like to thank my committee members, Dr. Lori Wright, Dr. David Carlson, and Dr. Thomas DeWitt for their support throughout the course of this research. My thanks also go to the entire Malapa Research Team, and Dr. Lee Berger in particular, for providing me with the life-changing opportunity to participate in this exciting and ground-breaking project. I would also like to thank Dr. Kieran McNulty and Dr. John Soderberg for generously providing their specialized knowledge and advice.

I also would like to offer my gratitude to various funding sources for this research: Texas Academy of Science Student Research Award, Sigma Xi Grant-in-Aid of Research, Vision 2020 Dissertation Enhancement Award (College of Liberal Arts, Texas A&M University), Program for the Enhancement of Creative and Scholarly Activities (Texas A&M University), and Texas A&M University Department of Anthropology. I would also like to acknowledge Lyman Jellema of the Cleveland Museum of Natural History, Stephany Potze of the DITSONG: National Museum of Natural History, Brendon Billings of the Raymond A. Dart Collection of Human Skeletons, Dr. Charles Musiba of the University of Colorado Denver, as well as Agness Gidna and Dr. Paul Msemwa of the National Museum of Tanzania for their access and assistance with museum collections.

I would also like to offer a very special thank you to my boyfriend Jonathan Walker, along with my wonderful friends (a.k.a. the 'wolfpack') for their moral support. Finally, I would like to thank my parents, Gene and Cynthia Carlson, for their endless love and encouragement.

# NOMENCLATURE

| | |
|---|---|
| 3D | Three-dimensional |
| GPA | Generalized Procrustes analysis |
| M1-stage | First molars erupted and in occlusion |
| M2-stage | Second molars erupted and in occlusion |
| M3-stage | Third molars erupted and in occlusion |
| MASL | Meters above sea level |
| MH1 | Malapa hominin 1 |
| MH2 | Malapa hominin 2 |
| UNESCO | United Nations Educational, Scientific and Cultural Organization |
| PCA | Principal components analysis |

TABLE OF CONTENTS

Page

LIST OF FIGURES

LIST OF TABLES

# 1. INTRODUCTION

## 1.1 Introducing the genus *Homo*- a synopsis of the debate

The focus of the present study involves the developmental simulation of the adult cranial morphology of the newly discovered species, *Australopithecus sediba*, for which only a single, juvenile cranium belonging to the type specimen (MH1) is currently available for morphological comparison. This species of australopith was hypothesized by Berger and colleagues (2010) to represent the best candidate ancestor to the genus *Homo*, or a close sister group to that taxon. However, the sub-adult status of the MH1 cranium has been the focus of considerable criticism by outside commentators, signaling the need for greater understanding of the morphological changes expected to occur between MH1's current stage of development and full adulthood.

Understanding and refining our knowledge of the origin and evolution of the genus *Homo* is of central importance to the field of paleoanthropology, and to anthropology as a whole. Yet, despite countless excavations and numerous fossil discoveries, the ancestry of our genus remains the subject of heated debate, the criteria for membership continuously shifting and adjusting in line with new discoveries. While some would support a definition of our genus based on the possession of a few discrete traits, such as language abilities and tool use (Leakey et al., 1964), others now push for a more ecological and adaptively oriented approach (Wood and Collard 1999a,b). The discovery of *H. habilis* was announced in the early 1960s (Leakey et al., 1964), followed by KNM-ER 1470 in the 1970s (Leakey et al., 1973). This latter fossil was ultimately

designated as the type specimen of *H. rudolfensis* in 1986 (Alexeev, 1986), a diagnosis that was later supported by Wood (1991), and which became widely accepted following upon the discoveries of OH 65 (Blumenschine et al., 2003) and KNM-ER 62000 (Leakey et al., 2012). Blumenschine et al. (2003) and Leakey et al. (2012) noted morphological similarities between KNM-ER 1470 and fossils assigned to *Homo*. However, the distinctiveness of these taxa, as well as the limited and fragmentary nature of fossils assigned to early *Homo*, has generated uncertainty surrounding phylogenetic relationships.

No consensus opinion currently exists regarding the fossil specimens to be assigned to each species, nor the number of taxa represented in the present sample. Further complicating the issue, well-preserved post-cranial remains that can be reliably assigned to *H. habilis* and *H. rudolfensis* are virtually non-existent (Berger et al., 2010), limiting our understanding of the ecological niche occupied by either species. Some researchers have suggested that the genus *Homo* is not adaptively coherent with the inclusion of *H. habilis* and *H. rudolfensis*, as these species do not appear to have made the adaptive-grade level transition into the genus *Homo* (Wood and Collard 1999a,b). The limited cranial capacity of these species, combined with what little we know regarding their post-cranial morphology, offers little evidence to support a closer relationship to *H. sapiens* than to australopiths. Further, the adaptive strategy of *H. habilis* and *H. rudolfensis* likely was not suited for an open environment characterized by complete terrestrial bipedalism. In other words, their life history and body plan

differed substantially from what we observe in later *H. erectus* and eventually modern *H. sapiens*.

Rather, the earliest species that can be unanimously assigned to the genus *Homo* when applying an adaptive-grade level diagnosis is *H. erectus*. The overall body size and shape, combined with a reduction in gut size and increased cranial capacity all indicate an adaptive pattern more similar to that of modern humans than to australopiths. Some of the earliest fossil specimens to be confidently assigned to *H. erectus* include the KNM-ER 3733 cranium from Koobi Fora in East Africa, dated to ca.1.78 Ma, and KNM-WT 15000 dated to ca. 1.65 Ma. Moving beyond the African continent, the Dmanisi fossil locality located in the Republic of Georgia contains numerous, well-preserved cranial and post-cranial hominin remains, which have provisionally been assigned to *H. erectus.*

The Dmanisi fossil site is one of the earliest known for the genus *Homo*, and dates to ca. 1.78-1.85 Ma (Ferring et al., 2011). Until recently, the most complete crania recovered from this locality included the D2700/D2735 juvenile cranium along with an elderly, edentulous specimen designated D3444 (Lordkipanidze et al., 2006). Several other specimens have been recovered as well, including the D2280 braincase and the D2282 partial cranium. However, the recently announced, complete fossil cranium, D4500/D2600 (a.k.a. skull 5), has significantly expanded the range of morphological variation previously recognized in the Dmanisi fossil sample (Lordkipanidze et al., 2013), with cranial capacities now ranging from approximately 546cm$^3$ to 775cm$^3$.

Based on this discovery, Lordkipanidze and colleagues (2013) now argue that all of early *Homo*, in both Africa and Asia, can be subsumed within a single, highly variable and evolving lineage. However, this synonymy of early *Homo* has received considerable criticism in the months following the announcement of D4500 (Spoor, 2013; Hublin, 2014; Schwartz et al., 2014). It remains to be seen how this discovery will impact our understanding of the evolution of early *Homo*.

The debate concerning the evolution of the genus *Homo* will be described in detail in the literature and background review section of the present manuscript (section 2); here I will describe issues regarding the definition of the genus *Homo*, as well as the history and timing of fossil finds that contribute to our understanding of its origins. The literature and background section also provides a detailed description of the morphology of the *Au. sediba* cranium and our understanding of hominin sexual dimorphism set within the context of the present study. Section 3 of this manuscript includes a detailed review of the geometric morphometric techniques applied to studies of hominin ontogeny and developmental simulation. This section also covers the materials and methods used in my dissertation research, including the 3D reconstruction of the MH1 cranium. This is followed by a detailed discussion of results and conclusions (sections 4-6) with a specific focus on how these results influence our understanding of *Au. sediba* in human evolutionary history.

## 1.2 *Australopithecus sediba* and the MH1 cranium

The magnitude and complexity of the debate concerning the origins of the genus *Homo* has become yet more intense in recent years, following upon the announcement of a new species of *Homo*-like australopith, known as *Australopithecus sediba*. In 2010, Berger and colleagues announced the discovery of two well-preserved and relatively complete fossil skeletons from the Malapa fossil site, located approximately 15 km Northeast of the Sterkfontein and Swartkrans fossil localities in the Gauteng Province, South Africa. These fossil sites, along with several others including Kromdraai, Cooper's, Gladysvale, Gondolin, and Drimolen are located within an UNESCO world heritage site known as the Cradle of Humankind. Collectively, this region has produced fossil specimens putatively assigned to the taxa *H. erectus*, *H. habilis*, *Au. africanus*, *Au. "prometheus"*, and *Au. robustus*.

Dating to 1.977 ± 0.002 Ma (Pickering et al., 2011), the Malapa hominin skeletons, belonging to a juvenile presumed male (MH1) and an adult presumed female (MH2), exhibit a unique, mosaic morphology, possessing features that align them with both the genus *Homo* as well as other species of australopith. Together these specimens represent respectively the type and paratype of *Au. sediba*; however, additional skeletons representing up to six more individuals of various age groups are currently being excavated. Only one cranium has been discovered to date, belonging to the juvenile individual, MH1. The cranium itself shows remarkable preservation, possessing a complete facial skeleton and detailed surface anatomy with clearly visible suture lines.

When examining the morphology of MH1, the cranial capacity falls well within the australopithecine range at 420cm$^3$ (Berger et al., 2010). While its second molars are erupted and in occlusion, its third molars remain in the crypt, providing an age estimate of approximately 12-13 years by human standards (Berger et al., 2010). Based upon this developmental information, it is believed that MH1 had achieved approximately 95% of its expected brain growth at age of death (Berger et al., 2010; Tobias, 1971).

A recent study by Le Cabec et al. (2014) used propagation phase contrast X-ray synchrotron micro-tomography to examine the dental microanatomy and calcification of the MH1 teeth to ascertain the exact age at death for MH1. Histological analysis of incremental markings on the outer and inner tooth surfaces indicates a nine day enamel periodicity for cross-striations between neighboring striae of Retzius. By counting the striae of Retzius, and matching developmental landmarks with an enamel hypoplasia that had occurred, Le Cabec et al. (2014) were able to obtain a high-resolution estimate of 7.5 ± 0.2 years for age at death of MH1. *Au. sediba* also reveals early initiation for canine tooth development. These results indicate that *Au. sediba* showed accelerated dental development relative to moderns humans, similar to that observed in other early hominins of the Pliocene and Pleistocene (Bromage and Dean, 1985; Dean and Lucas, 2009).

When examining the craniofacial morphology of *Au. sediba*, the overall shape and cranial architecture of MH1 is distinct from *Au. afarensis* with regard to its craniofacial, mandibular, and dental characteristics (Berger et al., 2010). For example, *Au. afarensis* exhibits marked alveolar prognathism with a convex nasoalveolar clivus,

combined with curved/notched zygomaticoalveolar crests (Rak, 1983). However, alveolar prognathism is significantly reduced in *Au. sediba* and MH1 possesses straight, steep zygomaticoalveolar crests. MH1 is also distinct from *Au. garhi* and the robust australopithecine species including *Au. aethiopicus*, *Au. boisei*, and *Au. robustus* which together exhibit marked cranial cresting patterns at muscle attachment sites, combined with megadont post-canine dentition, all of which are absent from the Malapa hominins. Together, this evidence supports the distinctiveness of *Au. sediba* from other gracile australopith species from eastern Africa, as well as the robust australopith species. The closest comparison for *Au. sediba* is therefore *Au. africanus*, whose similarities are documented below.

While a detailed description of the MH1 cranium is provided below in section 2.4 of the manuscript, a brief synopsis of the morphology will now be discussed. *Au. sediba* has a mesognathic face combined with a transversely expanded cranial vault of ovoid shape. The lateral walls of the parietals show a vertical orientation, with widely spaced temporal lines. The overall outline of the facial skeleton as viewed anteriorly in *Au. sediba* is squared superiorly and then tapered inferiorly. The postorbital constriction is limited, reduced relative to earlier gracile australopiths and robust australopiths. *Au. sediba* has a moderately developed supraorbital torus combined with a shallow but distinct supratoral sulcus.

The frontal process of the zygomatic bone is primarily anterolaterally oriented and shows medial but not lateral expansion at its root, reducing the anterolateral flare of the zygomatic and zygomatic prominence as compared to *Au. africanus*. The nasal

bones of *Au. sediba* join to form a ridge along the suture, and they project slightly anteriorly as they progress towards their inferior extent. The maxilla steadily retreats away from the lateral edges of the nasal aperture producing the slight eversion of the superolateral portion of the aperture. A small anterior nasal tubercle is also present. In all these features, *Au. sediba* approaches the *Homo* condition.

*Au. sediba* differs from *Homo* and resembles *Au. africanus* with regard to several anatomical features of the craniofacial skeleton. The MH1 cranium has a robust, block-like glabellar region. The zygomaticoalveolar crest rises in a straight, steep line resulting in a high masseteric origin, with the malar root at the anterior margin of the $M^1$. A small premaxillary suture is present. A prominent canine juga is also noticeable, combined with moderately developed canine fossae; however, *Au. sediba* lacks the anterior pillars for which *Au. africanus* is typically, though not consistently, known (Rak, 1983).

Based on this intermediate morphology, as well as other features observed in the mandible and post-cranium, Berger and colleagues (2010) suggested a possible ancestor-descendant relationship between *Au. sediba* and the genus *Homo*, with the possibility of *Au. sediba* representing the direct ancestor to *H. erectus*, or else a close sister group to that ancestor. In other words, either the resemblance to the genus *Homo* observed in the Malapa hominins reflects an ancestor-descendant relationship between *Au. sediba* and the genus *Homo*, or instead these *Homo*-like traits are examples of homoplasy, the result of random genetic drift or convergent evolution. Therefore, these traits would have had to evolve a second time, independently in the genus *Homo*. This seems less parsimonious, as the majority of characters that we currently consider to be exclusive to

*Homo* would no longer provide a reliable diagnosis or contribute to a meaningful understanding of our genus.

While the cranium and other parts of the post-cranial anatomy clearly exhibit mosaic morphology similar to that observed within the genus *Homo*, the limited cranial capacity, combined with the retention of arboreal capabilities in the post-cranium, were interpreted by Berger et al. (2010) as support for an australopith-level adaptive grade. In addition to the small cranial capacity, the Malapa hominins also had a small body size of about 1.3 meters, combined with relatively long arms and curved fingers well-suited for arboreal activity. Therefore, the authors decided that the most appropriate classification for the Malapa hominins would be to the genus *Australopithecus* rather than *Homo*.

### 1.3 Response and criticisms to the announcement of *Au. sediba*

In response to the announcement, some outside commentators immediately questioned the distinctiveness of *Au. sediba* as a unique species, separate from *Au. africanus*, while others - in a diametrically opposed argument - whether this species actually should have been placed within the genus *Homo* (Balter, 2010; Cherry, 2010; Spoor, 2011; Wood and Harrison, 2011; Kimbel, 2013). Cherry (2010) described how some critics speculated as to whether *Au. sediba* was unique relative to *Au. africanus*. In this same response, the question was raised whether a thorough analysis of the variation present within the *Au. africanus* taxon had been conducted, which was argued may have encompassed that observed within the Malapa hominins. This critique was later echoed by Wood and Harrison (2011).

Balter (2010) quoted other critics as suggesting that *Au. sediba* should have been placed within the genus *Homo*, based upon the small tooth size and cusp shape of the Malapa hominins and the relative thinness of the recovered mandibles. Still others stated that *Au. sediba* had evolved too recently to have given rise to the genus *Homo*, as purported *Homo*-like fossils are found elsewhere in Africa as early as 2.35 Ma, with the A.L. 666-1 maxilla from the Hadar Formation in Ethiopia thought to represent the most persuasive example of early *Homo* pre-dating 2.0 Ma (Kimbel et al., 1996, 1997). However, the A.L. 666-1 fossil was found eroding out of a sloping surface, and its morphology is not unequivocally *Homo*-like, making the interpretation of this particular specimen uncertain (Pickering et al., 2011).

In the initial announcement of *Au. sediba*, the authors indicated that it is unlikely that Malapa represents either the first or the last appearance date for this species (Berger et al., 2010), though this cautionary statement has often been overlooked by commentators. Therefore, *Au. sediba* existed prior to its occurrence at the Malapa fossil site, and continued to exist for some amount of time after . Subsequent research has questioned the reliability of the dates associated with early *Homo* fossils dated prior to 2.0 Ma, as well as the confidence with which the preserved morphological features can be used to assign taxonomic classification to the genus *Homo* (Pickering et al., 2011).

To date the most substantive criticism of the interpretation of *Au. sediba* is linked to the juvenile status of the MH1 cranium (Balter, 2010; Cherry, 2010; Spoor, 2011; Wood and Harrison, 2011; Kimbel, 2013). This is despite the fact that juveniles of the same developmental age or younger than *Au. sediba* have served as type specimens for

hominin species in the past, including the Taung child for *Au. africanus* and OH 7 for *H. habilis*. Therefore, the fact that the MH1 type specimen is a sub-adult individual should not necessarily rule out its utility in this role. Nonetheless, critics argue that the degree of growth and development expected to occur between second (current status of MH1) and third molar eruption (adult status) would have been significant enough to alter our current interpretations of the morphological affinities of *Au. sediba*, especially those features thought to resemble later *Homo*. Spoor (2011) made note of this in particular with respect to the possibility for increased constriction of the brain case of *Au. sediba* as it progresses into adulthood- this in response to the analysis of the endocast of *Au. sediba* (Carlson et al., 2011). More recently, Kimbel (2013) criticized the use of the juvenile mandible in multivariate statistical comparisons with other species, based on the potential for continued growth and development impacting linear measurements (de Ruiter et al., 2013a).

Others argue more broadly that the morphological characteristics that seem to align *Au. sediba* with later *Homo* are simply a result of the juvenile status of MH1 (Balter, 2010). For example, Tim White of the University of California, Berkeley, is quoted in Balter (2010: 155) as stating, "These characters change as a hominin grows, and features of a young australopithecine could mimic those of ancient adult humans". Similar sentiments are listed and described in Cherry (2010) with the author stating, "... the jury will be out until more complete adult remains are described," (doi:10.1038/news.2010.171).

After carefully reviewing and examining the criticisms outlined above, it is clear that the juvenile status of MH1 is a crucial point of concern for the hypotheses presented in Berger et al. (2010). The uncertainty surrounding morphological change between the ages of second and third molar eruption is a source of major criticism for outside reviewers. An empirical, quantitative test of this criticism is required if the interpretations originally put forth in Berger et al. (2010) are to stand the test of time and hold weight in the paleoanthropological community. Equally, if the concerns relating to the juvenile status of MH1 are indeed valid, a morphometric demonstration of this developmental change is necessary to further our understanding of the taxon *Au. sediba* and to extend our knowledge of its phylogenetic relationships. As such, addressing this question has become the focus of my dissertation research.

### 1.4 Developmental simulation of the *Au. sediba* cranium

The goal of the present study is to assess the degree and nature of morphological change expected to occur between MH1's current stage of development (M2-stage, or second molars erupted and in occlusion) and full adulthood (M3-stage, or third molars erupted and in occlusion). This is to be carried out through the use of established geometric morphometric techniques designed for the analysis of ontogenetic change.

To summarize, the following hypothesis was tested: $H_0$: Species distinct morphology is not yet established by the eruption of the second molar in apes, humans, or fossil hominins, thus development in the juvenile type (MH1) is not sufficiently complete to allow for reliable phylogenetic analysis of *Au. sediba*. $H_1$: Species distinct

morphology is established by the eruption of the second molar in apes, humans, and fossil hominins, thus development in the juvenile type specimen (MH1) is sufficiently complete to allow for reliable phylogenetic analysis of *Au. sediba*.

I tested the hypothesis through three-dimensional (3D) developmental simulation of the MH1 cranium using developmental vectors obtained from M2-stage and M3-stage extant hominoid crania (*Pan troglodytes*, *Gorilla gorilla*, and *H. sapiens*). Adult individuals of extant hominoids are separated into male and female developmental vectors to control for the influence of puberty and the concomitant development of secondary sexual characteristics on the ultimate resulting form. Following upon the developmental simulation process, the simulated male and female adult *Au. sediba* crania resulting from each extant developmental vector (chimpanzee, gorilla, human) are placed into a broader comparative context with other *Au. africanus* and early *Homo* crania. Using multivariate statistical tests, such as Principal Components Analysis (PCA) and Procrustes distance matrix analysis, I am able to assess both the total variation within the sample, as well as the overall impact that the ontogenetic process would exert on our current interpretations of the morphological affinities of *Au. sediba* with other hominin species.

For example, through these tests, one can now observe whether the intra-species distance for the simulated adult *Au. sediba* crania exceeds that for extant species. If the average distance is greater than that observed for chimpanzees or humans, it may be reasonable to conclude that the remaining developmental change would have a significant impact on species diagnosis. Further, if the simulated adults fail to cluster

together in scatter plots generated through PCA, and instead are found to plot separate from one another or with representatives of other hominin species, a similar conclusion would follow.

The use of geometric morphometric methods for the purpose of developmental simulation has been previously applied to questions regarding juvenile extant and fossil specimens with considerable success (McNulty et al., 2006; Neubauer et al., 2010; Singleton et al., 2010; Gunz and Bulygina, 2012; Gunz et al., 2012). However, while previous analyses have focused on earlier stages of dental development, this study is the first to provide a highly focused examination of the changes to occur between second and third molar eruption. Additionally, this study is also the first to separate the sexes of extant species into separate developmental vectors. Previous studies involving developmental simulation have pooled sexes, thereby obscuring any changes that may have arisen as a result of puberty and the development of secondary sexual characteristics. However, the degree and patterning of puberty may have a significant on the final adult form.

As the estimated age of MH1 coincides the expected onset of puberty, it is maintained that a detailed analysis of the manner in which these secondary sexual characteristics impact the outcome of developmental simulation is of critical importance. For example, does the resulting adult *Au. sediba* cranium generated from the male gorilla developmental vector differ substantially from that generated from the female gorilla developmental vector, and if so, how does it differ? Therefore, while the methods used in the following study have been previously applied to questions of the hominin fossil

record, these results not only extend our knowledge of *Au. sediba*, but also contribute to our understanding of developmental change in hominoids as a whole.

# 2. LITERATURE AND BACKGROUND REVIEW

## 2.1 Malapa hominin site discovery and description

The Malapa hominin site was discovered in 2008 by Prof. Lee R. Berger during a geological survey of the UNESCO Cradle of Humankind World Heritage Site in the Gauteng Province, South Africa. The site is located approximately 15 km north-northeast of several well-known hominin sites including Sterkfontein, Swartkrans, and Kromdraai. Malapa, itself, is comprised of a cave system found in the stromatolite-rich dolomite with the hominin fossils located roughly 3.5 meters deep (Dirks et al., 2010) in a large peloidal sandstone classified as Facies D (Pickering et al., 2011). It sits at an altitude of 1442 masl, as an erosion-remnant of a now de-roofed cave situated within the Carletonville Dolomite Grassland (Bamford et al., 2010; Dirks et al., 2010;).

Conditions at the site allowed for excellent preservation of fossil remains, through "rapid deposition, limited transport distance, and laminar flow conditions consistent with debris flows" (Dirks et al., 2010: 207). The geology suggests rapid cementation of remains, with no evidence for carnivore/scavenging activity. At the time in which the hominins were buried, it is believed that the cave system housing the Malapa site had formed a deep, vertical shaft approximately 50 feet deep, which served as a death trap for animals wandering about the surface (Dirks et al., 2010). Most likely the hominin remains were washed into this deep vertical shaft through a single depositional event, such as a large storm inflow (de Ruiter et al., 2013b)

Originally assigned a date of 1.95-1.78 Ma (Berger et al., 2010), Pickering et al. (2011) later refined this date using paleomagnetic data and uranium-lead (U-Pb) dating of the hominin bearing deposits. The flowstone units indicate that the hominins were deposited at the site during a short geomagnetic field event, known as the Pre-Olduvai event, at approximately 1.977 Ma, allowing for a highly refined date of 1.977 ± 0.0015 million years ago. Facies D in which the hominin fossils were buried is directly underlain by flowstone 1. Flowstone 1 indicates normal magnetic polarity near its base 1 and has been dated to 2.026 ± 0.021 Ma and (Pickering et al., 2011). Flowstone 2 records evidence for reversed polarity, and was assigned an age of 2.05 to 1.91 Ma (Pickering et al., 2011). The fossil-bearing faces of D and E have been shown to be deposited between the formation of flowstones 1 and 2, indicating that the U-Pb date provided by Pickering et al. (2011) serves as an upper age limit for the hominin fossils. Therefore, Malapa is one of the most precisely dated and tightly constrained deposits from the Plio-Pleistocene in sub-Saharan Africa.

In addition to the well-preserved remains of *Au. sediba* individuals, numerous faunal specimens have been recovered from the Malapa site in a near-articulated state. These remains provide invaluable information concerning the environment and habitat of *Au. sediba*. The rich carnivore record has been the focus of particular research interest, including representatives of Canidae, Viverridae, Herpestidae, Hyaenidae and Felidae (Kuhn et al., 2011). Leopard and brown hyaena have both been identified; however, despite the prevalence of carnivore remains, there is virtually no evidence of

carnivore-damaged bones, lending credence to the death-trap interpretation for site formation (Kuhn et al., 2011).

While today a grassland biome surrounds Malapa, analysis of a carnivore coprolite located near the MH1 cranium indicates that conifer trees were present when *Au. sediba* was present (Bamford et al., 2010). Analysis of phytoliths within the coprolite also specified woody species in the area surrounding Malapa. The conifer trees identified would have preferred higher rainfall than occurs in this region today, generally forming a forest with medium light levels. This type of forest is typically restricted to mountain kloofs (Bamford et al., 2010). The combined evidence suggests that the environment at the Malapa site has not been static during the past two million years, and instead the Cradle of Humankind has undergone considerable changes in flora and fauna.

Data concerning the dietary habits of *Au. sediba* indicate that it had a diet consisting of almost exclusively $C_3$ vegetation. Plant phytoliths were extracted from the dental calculus of MH1 and MH2 and described in Henry et al. (2012). Dental microwear was also examined to provide information concerning the mechanical properties and texture of food consumed by the Malapa hominins shortly prior to their death. After examining the dental calculus, 15 dicotyledons and 9 monocotyledon morphotypes were identified, along with several indeterminate forms. However, abundant $C_4$ grass phytoliths were recovered from Facies D, although no $C_4$ morphotypes were identified in the phytoliths of the dental calculus. The results of Henry et al. (2012) indicate that *Au. sediba* most likely consumed hard food items, as well as dicotyledons such as wood, bark, leaves, and fruits, along with some grasses and

sedges. As these monocotyledons were not of the $C_4$ morphotype, results indicates that *Au. sediba* was most likely consuming tropical shade and high-water grasses and sedges. Therefore, the diet of *Au. sediba* was likely similar to that of modern savanna chimpanzees that also consume an almost exclusively $C_3$ vegetation diet, but differed significantly from the dietary habits of other known hominins that otherwise indicate higher consumption of $C_4$ plant material. This preference for $C_3$ vegetation is in spite of the fact that $C_4$ material was widely available within the local environment.

## 2.2 Defining the genus *Homo*

When discussing the genus *Homo*, and possible scenarios for its origins, it is important to have a clear view of what it means to belong to this genus. However, unlike species-level classifications, which have a relatively clear biological significance associated with the production of viable offspring, classifications above this taxonomic level are more subjective and open to debate. For many years, membership within the genus *Homo* was defined by a discrete set of criteria. This included: an erect posture with bipedal locomotion, a precision grip with a fully opposable thumb, a cranial capacity larger than that of other species within *Australopithecus*, and language capabilities (Leakey et al., 1964; Wood and Collard, 1999a,b). In their announcement of *H. habilis*, Leakey et al. (1964) lowered the 'cerebral rubicon' to 600 $cm^3$ from that of previous researchers who had set the limit between 700$cm^3$ and 800 $cm^3$. These criteria were later challenged by Wood and Collard (1999a,b) who questioned both the

biological significance of the 'cerebral rubicon', as well as the ability of researchers to determine language capabilities from fossil endocasts.

Wood and Collard (1999a,b) instead recommended a more meaningful diagnosis of the genus *Homo* based on two primary criteria. Firstly, all species within the genus *Homo* should be more closely related to *H. sapiens* than they are to australopiths, and secondly, all species within the genus *Homo* should share a common adaptive strategy for maintaining homeostasis, acquiring food, and reproduction. These traits can be inferred from overall body size and shape, the relative size of the brain, the relative size of the masticatory apparatus, locomotor repertoire, and pattern of development.

When applying these criteria to species assigned to the genus *Homo* one would expect to see complete terrestrial bipedalism and a body plan well suited for an open environment, similar to that observed in modern humans. In other words, one would recognize a larger, leaner body-frame with arm length that is significantly reduced relative to leg length. Additionally, one would observe a reduction in the overall size of the masticatory apparatus consistent with a higher-quality diet.

After applying these criteria to taxa currently assigned to the genus *Homo*, Wood and Collard (1999a,b) recommended removing *H. habilis* and *H. rudolfensis* from *Homo* on the premise that neither of these species exhibits features associated with the *Homo*-level adaptive grade. Although the problem exists that many of their criteria were based on the post-crania, which are relatively absent for both *H. habilis* and *H. rudolfensis*. The oldest species that is virtually unanimously recognized as belonging to the genus *Homo* is *H. erectus sensu lato*. Within this species, the oldest relatively complete *H.*

*erectus* cranium to be recovered in Africa is KNM-ER 3733 from the Koobi Fora Formation, located in Kenya, and dated to approximately 1.78 Ma. An *os coxa* and additional fragmented cranial remains recovered from Koobi Fora have been attributed to *H. erectus* and date to ca. 1.88-1.90 Ma; however, they are less diagnostic than KNM-ER 3733 (Wood, 1991).

Outside of Africa, the Dmanisi fossils recovered in the Republic of Georgia have been provisionally assigned to *H. erectus ergaster georgicus* (a questionable quadrinomial allocation) and date to ca. 1.77-1.85 Ma (Ferring et al., 2011). Probable *H. erectus* remains have also been recovered from the Swartkrans fossil locality in South Africa and date to ca. 1.80-1.90 Ma (Pickering et al., 2011). Collectively, these finds suggest that ca. 1.9 Ma represents a likely date for the first appearance of *H. erectus*, although it is unclear when the full suite of *H. erectus* morphologies actually appeared, given the relatively later date of KNM-ER 3733.

### 2.3 Ancestry of the genus *Homo*- a history of thought

Multiple species of australopith have been proposed as candidate ancestors to the genus *Homo*, since the discovery of the first australopith cranium/endocast belonging to the Taung child (Dart, 1925). The Taung child is the type specimen of *Au. africanus*, and was described by Raymond Dart in 1925. In the announcement of the specimen, Dart described the M1-stage (first molars erupted and in occlusion) juvenile as a "man-like ape" and highlighted its seemingly intermediate morphology between apes and modern humans, thereby suggesting an evolutionary link between *Au. africanus* and the

genus *Homo*. Dart (1925: 198) states, "It is obvious, meanwhile, that it represents a fossil group distinctly advanced beyond living anthropoids in those two dominantly human characters of facial and dental recession on the one hand, and improved quality of the brain on the other." The suggestion of a human ancestor arising on the African continent was revolutionary at the time and inspired considerable debate in light of the Piltdown man, which at the time was accepted as the probable ancestor to modern humans.

After Piltdown man was revealed to be a forgery, *Au. africanus* became the generally accepted ancestor to the genus *Homo* for a considerable period of time (Clark, 1947; Howell, 1978; Tobias, 1967a, 1980, 1991). Subsequent discoveries at Sterkfontein and Makapansgat reinforced the significance of this species as a center for discussions on human evolution. The discovery of OH 5 in 1959 indicated the occurrence of a robust species of hominin in eastern Africa, expanding the known geographic range of early hominins on the African continent. Shortly thereafter, *H. habilis* was announced (Leakey et al., 1964) and debate ensued concerning the distinctiveness of this species from *Au. africanus* (Robinson, 1965, 1966; Tobias, 1966).

However, the announcement of *Au. afarensis* in East Africa, and the famous Lucy (A.L. 288-1) skeleton, resulted in uncertainty regarding the evolutionary relationship between *Au. africanus* and the genus *Homo* (Johanson and White, 1979). In their discussion of the phylogenetic relationships of gracile australopiths, Johanson and White (1979) suggested that *Au. afarensis* may, in fact, represent the ancestor to the genus *Homo*. In light of their new discoveries, Johanson and White (1979) proposed an

alternative interpretation of hominin phylogenetic relationships indicating that *Au. africanus* may have exclusively given rise to the robust australopith lineage in southern Africa. They based this argument on the presence of derived characteristics shared between *Au. africanus* and the robust specimens, including, "... stronger molarization of the premolars, increased relative size of the postcanine dentition, increased buttressing of the mandibular corpus in the symphyseal region, and increased robustness of the corpus itself," (Johanson and White, 179: 328).

In his descriptive analysis of australopithecine facial morphology, Rak (1983) highlights additional morphological features aligning *Au. africanus* with *Au. robustus*, including the shared presence of a straight, steeply ascending zygomaticoalveolar crest, anterior pillars, a pronounced, anterolaterally flaring zygomatic prominence, and an upwardly tapering contour of the facial mask. Likewise, Rak (1983) notes morphological features in *Au. afarensis* that align it with later *Homo* including sharp lateral edges of the pyriform aperture and a curved zygomaticoalveolar crest.

However, cladistic analyses complicated taxonomic discussions by regularly placing *Au. africanus* or an *Au. africanus*-like species as the likely sister-taxon to the genus *Homo* (Eldredge and Tattersall, 1975; Delson et al., 1977; Skelton et al., 1986; Chamberlain and Wood, 1987; Skelton and McHenry, 1992; Strait et al., 1997; Strait and Grine, 2004). For example, Skelton et al. (1986) and Skelton and McHenry (1992) propose that *Au. afarensis* is the ancestor to all later hominids. Further, their phylogenetic analyses imply that *Au. africanus*, or a species similar to *Au. africanus* gave rise to both the robust australopith lineages and the genus *Homo*. These results

therefore indicated that perhaps *Au. africanus* should not be discounted as a potential ancestor to later *Homo*.

The story became yet more multi-faceted in later years. In 1999, Asfaw and colleagues announced the discovery of a new hominid species from Ethiopia, *Au. garhi*. The authors suggested that this species, dating to 2.5 Ma, might also represent a candidate ancestor to the genus *Homo*. The primary evidence used to support this claim was the geographic location and time period (between 2 and 3 million years ago) in which this species was recovered, which they argue coincides with their expectations for the ancestor to the genus *Homo*. Further, they did not recognize any morphological characteristics that would preclude this species from giving rise to later *Homo*. However, the presence of megadont postcanine dentition and a sagittal crest bring uncertainty regarding the alignment of this species with later *Homo*.

In 2001, Leakey and colleagues described a new specimen, KNM-WT 40000, dating to 3.5 million years of age, to which they assigned a new genus and species, *Kenyanthropus platyops*. The authors recognized morphological similarities between KNM-WT 40000 and *H. rudolfensis* specimen KNM-ER 1470. Based upon this evidence, they suggested that *K. platyops* may have shared a close phylogenetic relationship with *H. rudolfensis* and may therefore represent the ancestor to the genus *Homo* via this lineage. They go on to suggest that if *H. rudolfensis* is to be removed from the genus *Homo* it should be placed in *Kenyanthropus* rather than *Australopithecus*.

These suggestions have considerable ramifications. If it were proven that *K. platyops* gave rise to the genus *Homo* it would mean that *Australopithecus* is a dead-end

lineage that was not involved in human origins. However, these interpretations have been criticized as KNM-WT 40000 suffers from severe expanding matrix distortion (White, 2003). Therefore, morphological interpretations based on this material may be unreliable.

Most recently, however, a complete skull, D4500, was described from the Dmanisi fossil locality (Lordkipanidze et al., 2013). In their announcement of this fossil, which they refer to as "skull 5", the authors argue that the range of morphology present within the Dmanisi sample serves as evidence for a single evolving lineage of early *Homo*. They attribute dissimilarities among fossils as simply a reflection of population-level intraspecific variation combined with change over time. The authors further state that the similarities observed between skull 5 and other early *Homo* fossils including A.L. 666-1, OH 65, and KNM-ER 1470 falsify a scenario in which *Au. sediba* is the ancestor to the genus *Homo*. They compare this variation to that observed in various extant hominoid species, such as chimpanzees, bonobos, and humans, and designate the Dmanisi sample as *H. erectus ergaster georgicus*.

Spoor (2013) provided comments on Lordkipanidze et al. (2013) criticizing the quadrinomial classification of the Dmanisi hominins, which he states is not recognized by the International Code of Zoological Nomenclature. Spoor (2013) further states that the evidence used by Lordkipanidze et al. (2013) to subsume *H. habilis*, *H. rudolfensis*, and *H. erectus* within a single lineage is weak. He goes on to state, "It is doubtful whether analyses of overall cranial shape have the diagnostic power to distinguish between closely related taxa," (Spoor, 2013: 453). He also criticizes the lack of

systematic examination of the morphological features that was provided, as well as their failure to distinguish between primitive and derived traits. Such a distinction is usually required to ascertain phylogenetic relationships between taxa. Spoor (2013) instead suggests that the projecting face, limited brain size, and large cheek teeth of skull 5 support an interpretation in which the Dmanisi hominins represent a population of *H. erectus* individuals that recently diverged from "... a more generalized form of early *Homo*" (Spoor, 2013: 453). He also suggests that the evidence is in line with an instance of centrifugal speciation, in which the peripheral populations, such as that at Dmanisi retain primitive features. Hublin (2014) also responded to Lordkipanidze et al. (2013), noting that the variation within the Dmanisi sample may be largely inflated by the inclusion of both sub-adult individuals, such as D2700, as well as elderly, edentulous specimens (D3444). D3444 in particular suffers from a high-degree of alveolar resorption. This leads Hublin (2014: 84) to state, "When all this is taken into account the claim that there is complete overlap between the morphology of *H. erectus* and other African early *Homo* becomes questionable." He further notes that while hybridization may have occurred between hominin lineages, this likely did not account for the majority of variation observed in the fossil record and questions the considerable 'lumping' that would be necessary to accommodate the taxonomic scheme proposed in Lordkipanidze et al. (2013).

## 2.4 Earliest evidence of the genus *Homo*

Several fossils have been proposed as early representatives of the genus *Homo* dating prior to 2.0 million years ago. In East Africa, this sample includes the UR 501 mandible from the western shore of Lake Malawi with a claimed date of 2.5-2.3 Ma, the Chemeron temporal fragment, KNM-BC1, with a claimed date of ca. 2.4 Ma, and the A.L. 666-1 maxilla from the Maka'amitalu Basin of the Busidima Formation at Hadar, possibly dating to 2.35 Ma. Additional remains attributed to *Homo* that may date prior to 2.0 Ma include cranial fragments from South Africa, such as Sts 19 (Kimbel and Rak, 1993), Stw 53 (Hughes and Tobias, 1977; Cronin et al., 1981; Wood, 1987; Wood, 1992; Curnoe and Tobias, 2006) Stw 151 (Moggi-Cecchi et al., 1998), certain isolated teeth from Sterkfontein Member 5 (Pickering et al., 2011), and a series of isolated teeth from the Omo Shungura Formation (Howell et al., 1987).

There is considerable discussion regarding what materials comprise Member 5 and the associated deposits at Sterkfontein. A later phase of Member 4 is among the associated deposits (Pickering et al., 2011). However, the provenience of fossils recovered from the deposits is uncertain as the actual deposits have been largely removed from their original setting (Pickering et al., 2011). Moreover, all of these specimens have variably been assigned to *Au. africanus* as well as early *Homo*. The cranial base, Sts 19 (which possibly dates to 2.7-2.5 Ma) is described by Kimbel (2009) as being found in a rubble dump associated with Member 4 (see Broom et al., 1950). Features found in its sphenoid and temporal bone were described as potentially aligning it with the genus *Homo* (Clark, 1977). Dean and Wood (1982), however, rejected this

supposition and maintained that it was a morphological variant of *Au. africanus*, while Kimbel and Rak (1993) assigned it to *Homo*. Ahern (1998) later strongly challenged this assignment. Pickering et al. (2011) describe the controversy over this fossil in their supplementary material, stating that the current evidence is not adequate to assign these remains to the genus *Homo* and that it is also unclear as to whether or not it predates 2.0 Ma.

Stw 53 has been widely regarded as belonging to early *Homo*. In its original description, by Hughes and Tobias (1977), the authors present this specimen as a likely representative of the genus *Homo*, stating that it derives from Member 5 at Sterkfontein. The association with stone tools in this member was thought to strengthen the likelihood that this specimen might represent *Homo*. They described morphological features aligning it with the genus *Homo*, including a "well-filled vault in the temporal fossa" (Hughes and Tobias, p. 311) and temporal lines that were well separated from the midline. They interpret this latter trait as aligning it with *H. habilis*, and also recognize a similarity in brow morphology with that of OH 24. While Hughes and Tobias (1977) acknowledge that the calvaria of Stw 53 is quite small, they maintain that these features indicate a large brain relative to body size. Clarke (1985) described Stw 53 as morphologically similar to *H. habilis* specimen OH 24, which he viewed as evidence for an evolutionary link between *Au. africanus* and the genus *Homo*. In a recent reconstruction of the cranial fragments, Curnoe and Tobias (2006) describe Stw 53 as remarkably similar to *H. habilis* in its morphological characteristics. While Stw 53 was originally thought to derive from Member 5 at Sterkfontein, it has since been associated

with a separate deposit that may represent a later phase of Member 4 dating to 2.6-2.0 Ma (Kuman and Clark, 2000; Clark, 2008; Pickering et al., 2011). If this age were to be proven correct, Stw 53 would be the earliest representative of early *Homo* in the southern African region (Pickering et al., 2011).

Some have challenged the taxonomic assignment of Stw 53 to the genus *Homo* (Clarke, 2008; Berger et al., 2010), noting numerous morphological features of the Stw 53 cranial fragments that clearly align it with *Au. africanus*. This list includes, but is not limited to: anterior pillars, a straight, steep zygomaticoalveolar crest, closely spaced temporal lines, marked post-orbital constriction, considerable subnasal prognathism, both medial and lateral expansion of the frontal process of the zygomatic bone, a flat nasoalveolar clivus, and a saddle-shaped nasal region. More recently, it has been suggested that Stw 53 represents an entirely new species, *H. gautengensis* (Curnoe, 2010). However, in light of the above morphological features that support the taxonomic assignment of this fossil *Au. africanus*, the hypothesis argued by Curnoe (2010) lacks empirical support. Pickering et al. (2011: 3) also challenge the assignment to *H. gautengensis* in their supplementary material, stating "... there is little reason to consider '*H. gautengensis*' to be a valid taxon. The preponderance of anatomical evidence indicates that Stw 53 is best considered a (possibly later) form of *Au. africanus* that is not especially closely affiliated with early *Homo*...".

Pickering et al. (2011) also discuss Stw 151, which is made up of associated teeth and bone fragments belonging to an individual of approximately 5 years of age (Moggi-Cecchi et al., 1998). These remains supposedly derive from the same time period as Stw

53 between 2.0-2.6 Ma, although some suggest that this deposit could date much more recently, to less than 1.8 Ma (Pickering and Kramers, 2010; Herries and Shaw, 2011). Stw 151 has also been said to be more derived towards *Homo* than that of other *Au. africanus* specimens from Sterkfontein Member 4 (Moggi-Cecchi et al., 1998) primarily with regard to maxillary and mandibular dimensions of the first molar, as well as other features related to the temporal bone. However, Pickering et al. (2011) maintain that the general morphology observed with regard to cranial and dental characters of Stw 151 align this individual with *Au. africanus*.

The KNM-BC1 specimen is comprised of a partial right hominid temporal that is missing part of its squamous portion. This specimen was discovered in 1965 by John Kimbengich and was announced in 1967 (Martyn, 1967; Tobias, 1967b), and was later relocated by Hill and colleagues in 1992. As described by Martyn (1967: 478), "The fossil was found weathered out on the surface of an exposure of the Upper Fish Beds at J.M. 85 in a small tributary of the Kapthurin River ... There is little doubt that the fossil came from the Upper Fish Beds and not from a higher horizon in the Chemeron Beds...". Hill et al. (1992) attempted to relocate and date this site, thereby obtaining $^{40}Ar/^{39}Ar$ ages of approximately 2.4 Ma. However, their provenience for the fossil is questionable, given that it was recovered weathered out of a sloping plane. Hill et al. (1992) claimed that the Chemeron temporal fragment resembled later *Homo* with regard to its medially positioned mandibular fossa that is primarily located under the middle cranial fossa, and a sharp petrous crest. The medial position of the mandibular fossa relative to the lateral wall of the braincase was believed to indicate brain expansion. The exposure of the

tegmen tympani within the upper limits of the mandibular fossa, the possession of an anteromedial recess, as well as a couple other traits, such as a sagittally convex tympanic laterally, were interpreted as sufficient evidence to attribute KNM-BC1 to *Homo* sp. indet. However, the doubtful provenience of this specimen, combined with the uncertainty with which these morphological features can be used for aligning fossil specimens with later *Homo* have been discussed by Kimbel (2009). Kimbel (2009) describes the presence and degree of expression for these features as varying widely across hominin taxa. Further, Lockwood et al.'s (2002) analysis indicated that KNM-BC1 does not possess features that uniquely align it with *Homo*. It has even been suggested by Asfaw et al. (1999) that it may be an *Au. garhi*. Pickering et al. (2011 som: 4) state, "... the utility of these characters for phylogenetic interpretations is uncertain, as they all tend to vary across hominin taxa, and the specimen does not exhibit any unique affinity to specimens considered to belong to early *Homo*".

The UR 501 specimen described by Schrenk et al. (1993) consists of a mandibular corpus represented by two joining parts recovered from Unit 3A in the Uraha Hill in the Chilumba area of Malawi. Like KNM-BC1, this fossil was also discovered on a sloping surface. It was believed to be recovered from Unit 3A (a ferruginous calcimorphic paleosol) based upon the presence of a ferric cementing agent found in the calcerous matrix on the right side of the mandible (Beltzer and Ring, 1995). However, Unit 3B is also a ferruginous calcimorphic paleosol, and the fossil may therefore date to 2.0-1.5 Ma in accordance with dates assigned to this stratigraphic layer (Pickering et al., 2011). UR 501 was biochronologically dated to 2.4 Ma based on associated fauna. The

authors describe aspects of the corpus dimensions, morphological features, and dental characteristics that they believe align it with *H. rudolfensis* specimens, such as the KNM-ER 1802 mandible from Koobi Fora (see also Bromage et al., 1995). These features include the overall large size of the anterior and postcanine dentition, the relatively thick molar enamel, as well as the double, plate-like lower roots of the fourth premolar. Bromage et al. (1995) assigns a tentative date of 2.5-2.3 for UR 501, stating, "The faunal assemblage associated with UR 501 represent various time spans, but the one time span that can be narrowly embraced by all taxa is 2.5-2.3 Ma," ( Bromage et al, 1995: 102). Kimbel (2009), however, questions the reliability of this date, due to the broad span of time encompassed by the fauna (from roughly 3 Ma to less than 2 Ma). Pickering et al. (2011) also criticize the faunal lists and interpretations used to date this specimen, and note that considerable admixture between time spans adds substantial uncertainty to a date of 2.5 Ma for UR 501.

Isolated teeth from Omo, along with a fragmentary mandible have been described as resembling early *Homo* in Members E (2.4-2.36 Ma), F (2.36-2.33 Ma), and G (2.33-1.9 Ma) within the Omo Shungura Sequence (Howell et al., 1987; Suwa et al., 1996). While they were designated "aff. *Homo* sp. indet", these specimens were described as showing the greatest overall similarity to *H. rudolfensis* (Suwa et al., 1996). Pickering et al. (2011) criticized the analyses that were used to align these specimens with *Homo*, as well as the resolving power of the supposedly diagnostic characters. An isolated right mandibular molar, designated KNM-WT 42718 from the Lokalalei fossil locality was dated to 2.34 Ma (Prat et al., 2005). Metric and other morphological

features were thought to align this specimen with early *Homo*. In the comparative metric analyses of Prat et al. (2005), in which KNM-WT 42718 was said to plot outside the range of *Au. africanus*, it was noted that KNM-WT 42718 only exceeded this range when Stw 80, Sts 24, and Stw 151 were excluded from the *Au. africanus* sample. While Pickering et al. (2011) acknowledge that Stw 80 might belong to the genus *Homo*, they criticize the exclusion of Sts 24 and Stw 151. Pickering et al. (2011) further state that, had the authors included all mandibular first molars of *Au. africanus*, KNM-WT 42718 would have fallen within the range of this taxon. This enlarged hypodigm would also have reduced their posterior probability from $p$=0.8033 to $p$=0.5409.

The last, and possibly most important fossil to be discussed, is A.L. 666-1. A.L. 666-1 is a fragmented hominid maxilla with partial dentition recovered from a layer 80cm below the Bouroukie Tuff 3 (BKT-3 tephra) of the Maka'amitalu Basin of the Busidima Formation in Ethiopia. It was said to be in close proximity to Oldowan stone tool artifacts. Kimbel et al. (1996: 550) describe the recovery of the A.L. 666-1 maxilla from a "...low, steep hill of undifferentiated silts capped by a small patch of a heavily weathered sandstone". The Oldowan tools associated with the maxilla were located at the base of the hill. They suggested that A.L. 666-1 had only been exposed for a short period of time based upon the position of the freshly broken pieces of the maxilla. A "trial excavation" was carried out to try to determine its source horizon; however, no other parts of the maxilla were recovered. Therefore, its provenience cannot truly be certain. However, Kimbel et al. (1996) believed that it came from the lithic-bearing, silt horizon based upon the silt matrix found in the maxillary sinus cavities/anterior tooth

alveoli, as well as a root cast found in one maxillary sinus. The authors used $^{40}Ar/^{39}Ar$ dating taken from three samples of the BKT-3 layer. They decided on using an integrated age which "sums the total gas from all grains in the subset..."(Kimbel et al, 1996: 553). This provided them with an age of 2.33±0.06 Ma. They additionally note that this date is in agreement with biochronological evidence from the site. The presence of *Theropithecus oswaldi* remains provides a maximum age of ca 2.4 Ma. However, the presence of *Metridiochoerus modesti*, a species with a reliable first appearance datum of 1.89 Ma (White, 1995), in the same deposit, renders the date of this deposit uncertain.

In their description of the fossil, Kimbel et al. (1996) note that the A.L. 666-1 maxilla is characterized by a wide and deep palate with a parabolic dental arcade, mild subnasal prognathism, a flat nasoalveolar clivus that angles sharply to the floor of the nasal cavity with a distinct spinal crest, and a square anterior maxillary profile. They mention that this last feature, in particular, aligns it with later *Homo* specimens. Additional *Homo*-like dental features include a narrow $M^1$ crown, and a rhomboidal shaped $M^2$. Using these features for support, A.L. 666-1 was assigned to *Homo* sp. aff. *H. habilis*. Later, Kimbel et al. (1997) outlined additional features expressing similarity with the genus *Homo*. Kimbel (2009) states that the overall morphology of A.L. 666-1 aligns this fossil closely with KNM-ER 1813, L. 894-1, and material from Bed I and lower Bed II at Olduvai Gorge. Generally speaking, this fossil is believed to provide some of the best evidence for the earliest appearance of *Homo*, but the associated dates are unreliable for the reasons previously outlined. Additionally, the majority of these morphological features are not exclusive to the genus *Homo*, but are also shared with

*Australopithecus*, weakening their utility for conclusive taxonomic designation of this specimen (Pickering et al., 2011).

## 2.5 Description of the MH1 cranium

As a means to compliment the geometric morphometric analysis which forms the bulk of the present study, I provide here a detailed, qualitative description of the MH1 cranium. The excellent preservation of the surface anatomy of MH1 allows for in-depth examination of the craniofacial skeleton for the species *Au. sediba*. The intermediate, or mosaic, anatomy is reflected in multiple aspects of the facial skeleton, with morphological features aligning it with both *Au. africanus* and later representatives of the genus *Homo*. As the palate remains encased in matrix, the description of the fossil from inferior perspective is based on a 3D print-out of a synchrotron scan of the cranium.

**Description**

The cranium itself shows remarkable preservation, possessing a complete facial skeleton and detailed surface anatomy with clearly visible suture lines. The right half of the cranium is missing posterior to the coronal suture following loosely along the coronal and sagittal suture lines. The left half of the cranium is largely complete until approximately the lambdoid suture, with most of the cranial base missing as well as the occipital bone. Most of the cranial sutures have not yet fused, and some displacement is observed along the suture lines. The missing parietal bone on the right-hand side, along

with several cracks and the disarticulated zygomatic bone, were successfully dealt with and repaired through virtual reconstruction and mirror imaging of a synchrotron scan. This reconstruction process is described in detail later in the manuscript (section 3.1).

The face of MH1 is rather small, generally aligning with other non-robust australopiths or early *Homo* (de Ruiter et al., in preparation). The lateral margins of the MH1 face run vertically and parallel forming a rectangular outline, rather than upwardly tapering, diamond-like outline observed in *Au. africanus*. The overall superior facial breadth makes up 84% of mid-facial breadth in this specimen (de Ruiter et al., in preparation). The forehead of MH1 slopes gently away posterosuperiorly from the shallow, but clearly recognizable, supratoral sulcus. The supratoral sulcus serves to define a supraorbital torus with sharply angled lateral corners, similar to the pattern seen in early *Homo*. This arrangement further contributes to the squared off upper facial profile.

The frontal bone has a somewhat rounded appearance from frontal aspect, and the preserved left parietal shows slight bossing. The moderately pronounced supraorbital tori join to merge with a block-like glabellar prominence at midline. The glabella has a small depression at midline, and shows an overall similarity to *Au. africanus* and the Sts 71 specimen, in particular (de Ruiter et al., in preparation). The supraorbital tori show a slight inferolateral slope; however, they are oriented primarily upon a horizontal plane.

The lateral margin of the orbit is oriented anterolaterally in a slightly concave arc, as observed in *Homo* (de Ruiter et al., in preparation). The orbital midline

represents the highest point of the orbit, with a sweeping inferomedial corner. MH1 has a small, but recognizable zygomatic prominence that does not flare anterolaterally to the extent of *Au. africanus*. The anterior and lateral faces of the zygomatic join at a roughly 90˚ angle that is marked by a slight zygomatic prominence (de Ruiter et al, in preparation). The frontal process of the zygomatic faces primarily anterolaterally, and shows only medial expansion at its root, rather than the combined medial and lateral expansion observed in representatives of *Au. africanus*. This is largely responsible for the reduced anterolateral expansion of the zygomatic in MH1 relative to that observed in *Au. africanus*.

The infraorbital plane joins the alveolar plane at roughly a 90˚ angle (de Ruiter et al., in preparation). The infraorbital foramina are located high upon the infraorbital region (two are present on the right side of the face and one on the left), approximately 13mm inferior to zygooorbitale. MH1 has moderately pronounced canine juga, but does not exhibit the column-like anterior pillars seen in *Au. africanus* or *Au. robustus*. As such, MH1 also does not possess a maxillary furrow. The canine juga and lateral crests are the only features to slightly disrupt the otherwise smooth surface of the gently rounded nasoalveolar clivus. Canine fossae are also recognizable posterior to the lateral margins of the canine juga.

The inferior nasal bridge resembles early *Homo* in that it is elevated relative to the infraorbital region (de Ruiter et al., in preparation). The nasals widen superiorly and narrow approximately one-third of the way down, only to widen to their greatest extent at their inferior margin. The nasals have a "pinched" morphology, forming a ridge at

midline, similar to that of *Au. africanus* specimen Sts 52. Overall, MH1 has a mildly projecting nose. The frontal processes of the maxilla rise on either side to meet the nasals, enhancing this projecting appearance. The inferolateral margins of the nasal aperture are rounded.

Traces of a premaxillary suture can be observed near the superolateral margins of the nasal aperture (de Ruiter et al., in preparation). The nasal aperture has a maximum width of 26mm across and a height of 22mm (from rhinion to the anterior nasal tubercle) as noted in Berger et al. (2010), and is responsible for less than half of the complete nasal height (de Ruiter et al, in preparation). The overall shape of the aperture is similar to that seen in *Au. africanus* specimens, such as Sts 5, although MH1 has a small anterior nasal tubercle - a trait not associated with *Au. africanus*. A spinal crest demarcates the nasal aperture, as well as low and rounded lateral crests (de Ruiter et al., in preparation). The superior portions of the lateral borders of then nasal aperture are somewhat thin, but thicken as they approach the inferior border of the nasal aperture. The inferior border of the nasal aperture grades smoothly and continuously into the nasoalveolar clivus and lacks a distinct nasal sill, such as that seen in *Au. africanus*. A ridge is present in the position of the intermaxillary suture that runs from the anterior nasal spine to prosthion. The nasoalveolar clivus is visible from lateral perspective, indicating that this portion of the face is placed anteriorly to the lateral borders of the nasal aperture as well as the canine juga.

The anterior dentition is set in a gentle arch, while the post-canine dentition follows a parasagittal orientation, posterior to the canine jugum. The

zygomaticoalveolar crest rises steeply in a long, straight line from the alveolar plane to the point of masseteric origin, similar to the arrangement seen in Sts 71 and Sts 52 (Sts 5 has a more horizontal orientation). MH1 does not possess a malar notch, nor is there any horizontal orientation to this feature.

From lateral view, the cranium is long and rounded in its profile. The root of the zygomaticoalveolar crest is located at $P^4/M^1$. An acute angle is formed by the frontal and temporal processes of the zygomatic at jugale. The posterior edge of the frontal process of the zygomatic has a posteriorly angled projection, known as the marginal process. However, the meeting of the frontal process of the zygomatic and the zygomatic process of the frontal transitions smoothly with relatively little angulation. Any concavity is limited primarily to the lateral margin of the orbit, similar to that of *Homo*. The superior edge of the temporal process of the zygomatic is positioned slightly superior to the inferior margin of the orbit. The temporal crest is seen to originate at the angled projection at the posterior edge of the frontal process of the zygomatic and runs along the superior edge of the supraorbital torus until turning posteriorly at the medial wall of the temporal fossa at an approximately 90˚ angle.

The temporal bone is interesting in that it intercedes between the parietal and sphenoid. It is additionally characterized by a long, horizontal squamosal suture that indicates little overlap of the temporals over the parietals (de Ruiter et al., in preparation). Parietal striae are present and visible, becoming more pronounced towards the posterior extent, spreading away from the squamosal suture and covering nearly half the distance to the temporal lines. The lateral surface of the temporal turns gently

inwards near the sphenosquamosal suture. However, a weak ridge of bone interrupts this trend, beginning at the temporal line on the parietal and following the coronal suture inferiorly. The ridge continues beyond the squamosal suture and across a flange of bone that intercedes between the parietal and sphenoid

The entire infraorbital region of the MH1 cranium, including the moderately projecting nose, is visible from lateral perspective, as a result of the reduced zygomatic prominence. However, the most prominent feature from lateral perspective is the large, inferoanteriorly sloping glabellar prominence. This, combined with the slight concavity of the lateral margin of the orbit, allow the superomedial corner of the orbit to be viewed from lateral perspective.

The vault of MH1 is long and ovoid when viewed from superior aspect, showing limited postorbital constriction, similar to the degree observed in later representatives of the genus *Homo* (de Ruiter et al., in preparation). The prominent temporal lines are widely spaced, and advance very little upon the posterior aspect of the supraorbital torus (de Ruiter et al., in preparation). The temporal lines run along the medial wall of the temporal fossa and do not approach midline, aligning MH1 with early *Homo*. The temporal lines continue on in the posterior direction along the parietals in a subtle convex arch until they eventually curve inferiorly and finally anteriorly to join the supramastoid crest. However, there is no evidence for a compound temporal/nuchal crest (de Ruiter et al., in preparation).

The zygomatic arch of the MH1 cranium is lightly built containing a relatively limited temporal foramen, which is smaller than that of *Au. africanus* and *H. habilis*,

placing it within the range of *H. erectus* (de Ruiter et al., in preparation). This is partially a result of the reduced lateral expansion of the zygomatic arch/zygomatic prominence from that observed in *Au. africanus* and *Au. robustus*, as well as a reduction in post-orbital constriction. The arch maintains a parasagittal orientation throughout its length. From inferior perspective one can see that the zygomatic arch turns posteriorly at roughly a 90 degree angle from the zygomatic prominence.

The palate is relatively deep along its entire extent, with the lateral sides of the palate rising steeply towards the alveolar margin. The shape of the dental arcade is generally that of a parabola, expressed as a gentle arch formation, intermediate to that described in *Au. africanus* and later *H. erectus*. This pattern differs, however, from that of earlier representatives of *Australopithecus* in East Africa. The overall shape of the palate is most similar to KNM-ER 3733, although it is narrower across is width.

From inferior perspective, it is also clear that the zygomatic has a reduced degree of lateral flare as compared to *Au. africanus*. Whereas the transition from the zygomatic prominence to the zygomatic arch forms at approximately a right angle in *Au. africanus* specimens when viewed from inferior perspective, this transition is reduced to a more acute angle in MH1. Further, and coinciding with this observation, the temporal foramen enclosing the temporalis muscle is far narrower in MH1. In this respect, MH1 approaches the condition of later *Homo*.

## 2.6 Additional remains of *Au. sediba*

**Endocast of *Au. sediba***

The intermediate, mosaic morphology observed in the cranium of *Au. sediba* is reflected in both the endocast and post-cranium of this species as well. In an analysis of the endocast as described in Carlson et al. (2011), a virtual model of the brain of *Au. sediba* was constructed by Carlson et al. (2011) by careful segmentation of a phase contrast x-ray synchrotron microtomography scan of the cranium, allowing for a high-resolution 3D model to be produced. Due to the excellent preservation of the MH1 cranium, combined with the young age at death of the individual, the convolutions and relative dimensions of the endocast could be examined in great detail. This model could then be compared with endocasts of both extant hominoids, including *P. troglodytes* and modern *H. sapiens*, as well as endocasts of other hominin species.

The overall convolution patterns appear similar to that of other australopiths, such as Sterkfontein Type 2 and Sts 60. However, a frontal petalia is present on the right-hand side of the brain, with a larger right frontal lobe relative to the left. The presence of a frontal petalia has been linked to handedness in modern humans (LeMay, 1992), perhaps indicating the ability for tool use and precision motor skills in *Au. sediba*.

The temporal poles of MH1 are more centrally projecting, similar to that observed in modern humans and chimpanzees and differing from that of other australopiths (such as Sts 5 and Sts 60 of *Au. africanus*). The shape of the inferior frontal gyrus also differs anteriorly from other australopith endocasts currently available for comparison in South Africa, as well as that observed in apes. It is suggested that the

bulge recognized on the MH1 endocast may be related to increased local neural interconnectivity in area 45, or Brodmann's area of the brain, which is related to language abilities. Increased neural interconnectivity was also suggested in accordance with the tension-based folding theory of neural morphogenesis for BA 10, or the anterior-most region of the prefrontal cortex, of *Au. sediba*. The olfactory bulbs are also positioned posteriorly in MH1. Therefore, despite the small brain size of MH1, we do observe some morphological changes similar to that observed in later *Homo*. The overall results of the analysis by Carlson et al. (2011) indicate that neural reorganization in the orbitofrontal region likely preceded brain enlargement in hominins.

**The hand and upper arm of *Au. sediba***

Perhaps one of the most exciting finds to come out of the Malapa hominin discovery is the excellent preservation of hand and wrist bones; these elements are commonly missing even from well-preserved and relatively complete skeletons, such as A.L. 288-1 and KNM-WT 15000. All metacarpals and phalanges belonging to MH2 have been extracted, with the exception of the distal phalanges, which are preserved, but have not yet been extracted from the encompassing matrix. Only the pisiform is missing from the wrist.

When looking at the hand in articulation with the upper arm, the most striking feature is the elongated thumb and relatively short fingers (Kivell et al., 2011). The hand of *Au. sediba* appears to have been capable of fine motor manipulation and an opposable grip (Kivell et al., 2011). Other derived features include a well-developed

flexor pollicis longus muscle, expanded apical tufts, well-developed intrinsic muscles of the thumb, and a *Homo*-like scaphoid (Kivell et al., 2011). Should *Au. sediba* prove not to be the ancestor to the genus *Homo*, these seemingly derived traits would have had to evolve twice in separate lineages.

Certain australopith-like features are retained, however, including a strong flexor apparatus and intermediate phalangeal curvature, traits generally associated with arboreal capabilities (Kivell et al., 2011). Overall, when studying the hand, one observes a clear example of the mosaic morphology of this species. While we do not yet have evidence that *Au. sediba* was a stone tool producer, we do know that it had the fine motor capabilities to do so.

**The pelvis of *Au. sediba***

The pelvis is one of the most informative parts of the hominoid skeleton with regard to life-history characteristics. Of particular interest to paleoanthropology, is the relationship between encephalization/bipedal locomotion, and the anatomical changes that were made to accommodate these adaptations. Until recently, the majority opinion in paleoanthropology was that the structural changes observed in the pelvis of later *Homo* collectively represent an adaptive response to increased brain size and the concomitant obstetric demands (Simpson et al., 2008). However, the discovery of *Au. sediba*, for which two partial pelves are preserved, has forced the paleoanthropological community to rethink this long-standing interpretation. The MH1 individual preserves

the left ischium, along with the right and left ilia. MH2 preserves the partial left and complete right pubic bones, as well as the right sacrum and ilium.

Many of the derived *Homo* features, long presumed to be associated with giving birth to large-brained neonates, are identified in the pelvic remains of MH1 and MH2 (Kibii et al., 2011). Traits associated with other members of *Australopithecus* include relatively small sacral and coxal joints, along with a long pubic ramus. Further, the biacetabular diameter is large, similar to that of other australopiths. However, traits aligning it with *Homo* include "...more vertically oriented and sigmoid-shaped iliac blades, greater robusticity of the iliac body, sinusoidal anterior iliac borders, shortened ischia, and more superiorly oriented pubic rami" (Kibii et al., 2011: p. 1407).

The birth canal of *Au. sediba* is relatively large and rounded, while the brain of this species remains quite small. Therefore, if *Au. sediba* does in fact represent the ancestor to the genus *Homo*, we interpret that obstetric accommodations to increased brain-size in neonates was not the driving force influencing the evolution of pelvic architecture (Kibii et al., 2011). This instead forces us to examine other possible explanations for the changes observed over time, including locomotor behavior favoring an enlarged pelvic outlet.

**The foot and ankle of *Au. sediba***

Preserved foot and ankle bones, like the hand and wrist, are rare finds in the hominin fossil record. However, these skeletal remains are crucial towards explaining both the transition to bipedal locomotion, as well as later changes in bipedalism

throughout time. This includes the transition from habitual to obligate terrestrial bipedalism, for which the time period in which *Au. sediba* was recovered is especially critical to our interpretations. The architecture of the *Au. sediba* foot tells a surprising story of a unique form of bipedal behavior, unlike that of other hominins, yet retaining some arboreal capabilities (Zipfel et al. 2011).

The ankle bones of MH2 actually remain in articulation, held together by surrounding matrix, and thus were reconstructed virtually using CT scans to allow for individual examination (Zipfel et al. 2011). The MH2 individual preserves a distal tibia, talus, and calcaneus (the only adult remains from the early hominin fossil record), while a calcaneus apophysis and two partial metatarsals are associated with MH1. A distal tibia is also preserved, but its association with a specific individual is presently uncertain. Some ape-like features include the relatively gracile body of the calcaneus combined with a robust medial malleolus. However, the overall morphology of the talocrural joint is similar to that of humans (Zipfel et al. 2011).

**Thorax and spinal column of *Au. sediba***

The overall number and preservation state of both the ribs and spinal column have allowed for reliable reconstruction of the body shape of *Au. sediba* by Schmid et al. (2013) and Williams et al. (2013). The thorax is important in informing us with regard to locomotor patterns, especially concerning the relative degree of arboreality in this species (Schmid et al., 2013). Great apes tend to possess a more conically shaped rib cage, allowing for a wider range of motion in arboreal climbing and suspension

activities. However, we observe a more barrel-shaped thorax in modern humans, with a mediolaterally broadened upper rib cage related to a greater emphasis on bipedal walking and running (Schmid et al., 2013). Schmid and colleagues (2013) describe the upper thorax as relatively ape-like in shape, with a mediolaterally expanded rib cage between the first and sixth ribs that form "... a typical ape-like apex," (Schmid et al., 2013: 1234598-2). In addition to this, the authors suggest that - based upon the vertical reorientation and increased curvature in the iliac blades derived towards *Homo*- the lower thorax could not have been that of the ape-like condition. Examination of the slender ninth rib is thought to support this hypothesis.

Partial vertebral columns are preserved for both the MH1 and MH2 individuals. The morphology of the vertebral column, and its association with bipedal locomotion in humans, is well-established. The s-shaped curvature of the vertebral column and the relative diameter of each respective vertebrae as they progress in size from C1-L5 aid in the transmission of weight and shock and serve to balance the upper-body on top of two legs. Williams et al. (2013) provide a detailed analysis of the vertebrae preserved for *Au. sediba*, a rare find considering that the only two hominin species for which vertebrae are well preserved prior to 50 thousand years ago include the *Au. africanus* partial skeletons Sts 14 and Stw 431, and the *H. erectus* partial skeleton KNM-WT 15000.

Of particular interest is the transition from thoracic to lumbar vertebrae. This transition can be defined as both the last rib-bearing vertebra, as recognized by the presence or absence of costal facets, or by the relative orientation of the superior and inferior articular facets. For modern hominoids, these transitional characteristics

generally coincide at the same position along the vertebral column. However, the vertebrae associated with KNM-WT 15000 may follow a different form with "... five nonribbed lumbar vertebrae and six vertebrae with sagitally oriented upper articular facet," (Williams et al, 2013: 1232996-1). This is the same pattern which is said to be exhibited in Sts 14. In addition, the last rib-bearing vertebra associated with Sts 14 is also said to resemble the lumbar vertebrae in certain aspects of its structure. Therefore, understanding the timing and nature of the thoraco-lumbar transition of the vertebral column is important for paleoanthropologists.

Currently, six rib-bearing and non-rib-bearing vertebrae are associated with MH1, while seven rib-bearing vertebrae along with a penultimate and ultimate lumbar were assigned to MH2. The latter vertebrae associated with MH2 were actually discovered in articulation both with each other as well as the articular facets of the sacrum (Williams et al, 2013). The most caudal thoracic vertebra associated with MH2 has a complete costal facet, while it also exhibits curved and dorsomedially directed superior and inferior articular facets. Overall, Williams et al. (2013) concluded that five non-rib-bearing lumbar vertebrae were present in *Au. sediba* along with five sacral elements, similar to that seen in most modern humans. Williams et al. (2013) further interpreted the lumbar dorsal wedging observed in MH1 and MH2 as evidence for lumbar lordosis or an adaptation to bipedal locomotion along with upright posture in *Au. sediba*. The ability for flexion and extension of the torso is also inferred based on the presence of six vertebrae that possess curved and sagitally oriented articular facets on the zygopophyses, which also serves to limit the rotation of the torso. The increased degree

of lordosis is thought to assist in positioning the center of gravity of the trunk more posteriorly, when combined with an anterior position for the shoulder joint. Overall, *Au. sediba* would have had a flexible lower back (Williams et al., 2013).

### 2.7 Sexual dimorphism and puberty in extant hominoids

As the period of maturation between second and third molar eruption generally coincides with puberty in hominoids, this topic warrants greater discussion and consideration within the present manuscript. Three extant species were used for developmental simulation in the present study (*P. troglodytes*, *G. gorilla*, and *H. sapiens*, see Section 3.3, which collectively exhibit widely varying life-histories and mating strategies. These variations, in turn, are reflected in their respective craniofacial and post-cranial anatomies.

Sexual dimorphism in form refers to any morphological or physiological feature that differs between males and females (Plavcan, 1999) and represents the most basic product of sexual selection. The shortage of mates, or the unequal distribution of resources in the environment, represents the foundation for sexual selection and is driven by the two primary forces of mate choice and mate competition. A wide range of sexual dimorphism exists within the world of primates, ranging for minimal to extreme.

While most haplorhine males are larger than females, far less dimorphism is generally observed in strepsirhine species (Plavcan, 1999). Most sexual dimorphism in primates is believed to be the product of male competition, with male reproductive success limited by the number of females that are available to mate with (Plavcan,

1999). This is perhaps best summarized in the following quote from Boesch and Boesch-Ackermann (2000: 43), "Females are the determining element in population dynamics; they are the limiting resource for the males, and their life history strategies determine how a given population will evolve".

Extant species characterized by a monogamous mating pattern with minimal male competition tend to exhibit a lesser degree of sexual dimorphism when compared to species for which heavy male competition is essential for successful reproduction. For example, the gibbons and siamangs (Hylobatidae) of Southeast Asia and Malaya have males and females of similar body size. Hylobatids form monogamous pair-bonds with family groups composed of two parents and their offspring.

Conversely, in groups formed around a harem-type social structure wherein males monopolize and defend access to females, sexual dimorphism can become highly marked. The gorilla (*G. gorilla* and *G. beringei*) is the most sexually dimorphic of the African great apes, with males weighing up to 450 pounds. Male gorillas are on average twice the size of females (Smith and Jungers, 1997). Upon reaching sexual maturity, males further develop numerous cranial features associated with the onset of puberty, such as large brow ridges and prominent cresting patterns that together produce a large, crest upon the back of the skull. The face becomes more prognathic with large, dimorphic canine teeth, and overall the architecture of the skull assumes a more rugged appearance.

Chimpanzees (*P. troglodytes*) exhibit a promiscuous, multi-male and multi-female hierarchical group pattern and are intermediate with regard to sexual

dimorphism. While males do develop masculine cranial features upon reaching puberty, such as enhanced brow-ridges and facial prognathism, the changes observed are considerably more limited than that observed in gorillas. The most prominent difference observed in the facial architecture between adult males and females is in relation to canine tooth size.

When comparing the life-history patterns of gorillas and chimpanzees, there are several significant differences. Research indicates that the onset of menarche occurs earlier in female gorillas as compared to chimpanzees (Shea, 1985). Further, while male means for size dimensions for both species generally exceed female means throughout life, females commonly exceed males while undergoing a female growth spurt in adolescence. This growth spurt occurs between second and third molar eruption in chimpanzees and between first and second molar eruption in gorillas (Shea, 1985). Nonetheless, dental eruption occurs at roughly the same chronological age and sequence in both chimpanzees and gorillas (Shea, 1985). Harcourt et al. (1980) report that female gorillas reach sexual maturity at approximately 8 years of age, while female chimpanzees achieve this developmental landmark slightly later between 9-10 years of age. Male gorillas and chimpanzees will begin to breed at approximately 15 and 13 years of age respectively. The inter-birth interval for chimpanzees is reported between 61 and 86 months for wild chimpanzees (Boesch and Boesch-Ackermann, 2000), with a median birth interval of 45.5 ± 1.2 months is reported for gorillas (Galdikas and Wood, 1990).

Chimpanzees and gorillas also have widely different forms of social organization. As previously mentioned, gorillas exhibit a male-dominated form of social organization, in which the group is dominated by a single silverback male, while also containing sexually mature, non-reproducing young adult males. While most studies focus on mountain gorillas, Parnell (2002) found that, excluding solitary males, mean group size for the western lowland gorillas at Mbeli Bai was 8.4±SD 4.3. Further, all groups contained a single fully mature male; however, emigrating males did not form bachelor groups, but remained solitary. Competition for access to reproductively viable females is high, wherein young, sexually mature males are forced to either fight dominant silverbacks for access to their females, or otherwise lure females away from outside groups. For example, Gibbons (2001) describes an instance where a DNA study confirmed that a single male gorilla, named Titus, fathered nine out of the ten offspring in his group.

Female gorillas generally leave their natal group and join a separate group with a dominant silverback upon reaching reproductive maturity. Similarly, female chimpanzees will also emigrate from their natal groups upon reaching sexual maturity, usually at about 11 years of age (Boesch and Boesch-Ackermann, 2000). Interestingly, female chimpanzees frequently exhibit a period of "adolescent sterility" (Boesch and Boesch-Ackermann, 2000) after emigrating to a new group that lasts an average of 32 months.

Chimpanzees exhibit what is known as a "fission-fusion" form of social organization (Boesch and Boesch-Ackermann, 2000), in which individuals join together

to form unstable, temporary groupings that break up and reform variably throughout the day. Unlike gorillas, in which typically only a single, dominant male has access to reproductively viable females, chimpanzees exhibit a promiscuous form of sexual behavior. Both males and females within a group form strict social hierarchies that are connected to increased breeding rights for males (i.e. greater access to fertile females). Males often perform displays to establish their dominance and intimidate their opponents, or may engage in violent behavior to secure their rank.

Social hierarchies for females are generally associated with greater access to food resources, and offspring of high-ranking females also tend to enjoy a higher-ranking and greater likelihood of success throughout their lives. Females exhibit sexual swellings during estrous, signaling their receptivity to mating. This is also argued to represent a sort of "social passport" when females leave their natal group to join an outside group, thought to enhance their chances for being successfully assimilated into the new group through increased male tolerance and support (Boesch and Boesch-Ackermann, 2000). A female in estrous may copulate with multiple males during this time of fertility. To increase their chances for paternity, dominant males may attempt to restrict access of other males to specific females for the duration of her estrous.

Humans have a reduced degree of sexual dimorphism relative to most anthropoid primates, with significant overlap between sexes in both body and canine size. Humans are slightly more dimorphic than gibbons, but are less dimorphic than either chimpanzees or bonobos (Plavcan, 2012). Generally, however, males are about 7-15% taller than females (Smith and Jungers, 1997; Gustafsson and Lindenfors, 2004).

Males and females can also be distinguished through the development of secondary sexual characteristics following puberty.

Human males usually have a more robust craniofacial skeleton with larger and more pronounced sites of muscle attachment. Males generally have a larger glabella and brow ridge, as well as a more pronounced external occipital protuberance. When examining the post-cranium, males tend to have larger, more rugged-looking and heavier bones, with the architecture and shape of pelvis allowing for correct male/female classification at 95% accuracy (White and Folkens, 2000). In addition to these features, Plavcan (2012) lists numerous other distinguishing traits, including, but not limited to: enlarged breasts, narrower rib cages, relatively wider pelves, thicker subcutaneous fat distribution, and a relatively narrower waist in females. With regard to males Plavcan (2012) notes that males tend to possess broadened shoulders, relatively greater upper body strength, thick body hair, and limited subcutaneous fat relative to females, amongst other traits.

Aggressive behaviors and violence observed in human males have been linked to sexual dimorphism using models based on observations in nonhuman primates (Dixson, 2009; Sefcek et al., 2009; Puts, 2010). However, Plavcan (2012) states that canine dimorphism in humans falls at the low range when compared to other nonhuman primates, with male canines approximately 10% larger than that of females. Humans are further distinct from other African great apes (with the exception of the bonobo, *P. paniscus*) with regard to concealed ovulation, or hidden estrus, meaning that there are no visible changes in their external anatomy at or near the peak of female fertility.

## Sexual dimorphism in the hominin fossil record

When examining sexual dimorphism in the hominin fossil record, we are of course limited to the analysis of skeletal remains. Plavcan (2012) warns that skeletal dimorphism and body size dimorphism do not always represent a one-to-one connection, which can hamper our understanding of the biological significance surrounding these features. Nonetheless, he goes on to state that, "Even so, skeletal and cranial dimorphism are strongly correlated with body mass dimorphism across primates," (Plavcan, 2012: 49). Analysis of sexual dimorphism is also critical to our understanding of human evolutionary history as it provides a valuable insight into the social behavior of our ancestors.

Minimal dimorphism in canine tooth size has long been one of the defining features of the hominin clade (Brace, 1972; Wolpoff, 1976; Greenfield, 1992; White et al., 2009). This derived characteristic extends back to our earliest purported ancestors, including *Ardipithecus ramidus* (White et al., 2009), *Sahelanthropus tchadensis* (Brunet et al., 2002), and *Au. anamensis* (Plavcan et al., 2009; Ward et al., 2010). Yet, despite the relatively small canine cusp size observed in australopiths, many researchers have argued for substantial sexual dimorphism in the *Au. afarensis* taxon (Richmond and Jungers, 1995; Lockwood et al., 1996; Harmon, 2006; Scott and Stroik, 2006; Gordon et al., 2008; Kimbel and Delezene, 2009), one of the only species for which we have considerable post-cranial remains. However, others have questioned the veracity of this conclusion (Reno et al., 2003, 2010), instead suggesting that *Au. afarensis* may have had a human-like pattern of sexual dimorphism. In their analysis of digit ratios of both

extant and extinct hominoids, Nelson and colleagues (2011) also suggest a lesser degree of dimorphism for *Au. afarensis* than had been previously believed. However, the methods and samples employed in these latter analyses have been brought into question (Plavcan, 2012).

Lockwood (1999) carried out a bootstrapping analysis using craniodental remains of *Au. africanus* individuals. His results led him to suggest a high degree of sexual dimorphism for *Au. africanus*, greater than that of humans or chimpanzees. He further states that this places *Au. africanus* at a level similar to that of *H. habilis*, but less than that of the robust species from east Africa, *Au. boisei*. Despite the apparent variation in craniofacial morphology, the relative canine tooth size of *Au. africanus* remains quite small. This, in turn, is reflected in the facial skeleton, with the supraorbital and glabellar regions, for example, showing a greater degree of sexual dimorphism between specimens than the curvature of the infraorbital surface.

McHenry and Coffing (2000) provide body weight estimates for males and females for each species of australopith and early *Homo*. They provide a weight estimate of 41 kg for *Au. africanus* males and 30 kg for females, with a difference of $23cm^3$ for stature. This height and weight disparity was reduced to an estimate of 37 kg for *H. habilis* males and 32 kg for *H. habilis* females, with a difference of $31cm^3$ for stature. The statures listed here come from McHenry (1991). McHenry (1991) states that body weight was estimated through calculating stature using Olivier's (1976) correlation analysis for humeral, femoral, and tibial lengths, while deriving weight from stature through the power curve provided in Jungers and Stern (1983). It is unclear,

however, exactly what criteria were used to provide these estimates for *H. habilis*. However, McHenry (2000) notes that available information concerning the body of *H. habilis* indicates that it more greatly resembled to *Australopithecus* as opposed to *H. rudolfensis* or later *Homo*.

When assessing the level of dimorphism in the *Au. sediba* taxon, we are limited to a single cranium. However, dental, mandibular, and post-cranial remains are available for comparison between individuals. While still a sub-adult, MH1 is presumed to be a male based upon the overall development of the supraorbital region, the pronounced canine juga, and the eversion of the gonial angle of the mandible. Also, the muscle scars found across the skeleton were large and rugose. The pelvic remains also indicate that this individual was a male (Berger et al., 2010; Kibii et al., 2011). These characteristics would not be dimorphic at this age in modern *H. sapiens*. Further, while still a juvenile, MH1 had already achieved a greater body size than MH2, and the molar occlusal surface was 8.1-10.7% larger than that of MH2 (Berger et al., 2010).

The recovery of an additional piece of the MH2 mandible has also allowed for additional comparison of both mandibular and tooth morphology, including canine size (de Ruiter et al., 2013a). The MH1 canine is roughly 9.6% larger than that of MH2 in mesio-distal breadth and about 20% larger in bucco-lingual breadth, making for an overall size difference of 15% between the MH1 and MH2 canines. Using the "mean" estimation method for canine dimorphism, this value is less than that of the presumed highly dimorphic *Au. afarensis* and *Au. boisei* with values of 21% (de Ruiter et al., 2013a). However, it remains slightly greater than that of *Au. africanus* and *Au. robustus*

(11%), *H. erectus* (13%), and the least dimorphic hominoid species, *H. sapiens* with a value of 7% (de Ruiter et al., 2013a),. Therefore, canine dimorphism is present and observable in the *Au. sediba* taxon, greater than that of modern *H. sapiens*, but reduced compared to earlier *Au. afarensis* and east African robust species. Clearly, future fossil discoveries and an increased sample size for *Au. sediba* will help elucidate the extent and exact degree to which sexual dimorphism was inherent in this species.

With regard to the behavior and social organization of australopiths, strontium isotopes have provided a unique insight into ranging and residence patterns for australopith species of southern Africa, including the taxa *Au. africanus* and *Au. robustus*. Copeland et al. (2011) conducted a strontium ($^{87}Sr/^{86}Sr$) isotopic analysis of australopith tooth-crowns from the Sterkfontein Valley using laser ablation techniques. Strontium isotope ratios tend to reflect local geology, making them a useful tool for assessing movement across landscapes. Strontium is ingested by animals through food and water and then incorporated into body tissues and dental enamel where they can be sampled. The heterogenous geological landscape of Sterkfontein Valley allows for a high-resolution analysis of movement and dispersal across the region.

Using only the largest and smallest individuals as designated male and female hominoids, the authors used only teeth that were more than one standard deviation above or below the mean. Results of this analysis indicate that smaller individuals (n=4), more likely to represent female individuals, showed a higher-proportion of non-local strontium isotopic signatures. Conversely, larger individuals (n=6), more likely to represent male individuals, were more likely to exhibit local strontium isotopic compositions.

Interestingly, no statistically significant differences were detected between the proportion of non-locals found for the *Au. robustus* versus the *Au. africanus* sample. When specifically examining specimens that were more than one standard deviation above and below the mean (i.e. most likely to represent males and females), Copeland et al. (2011) found that 75% of the smaller teeth showed non-local strontium signatures, while only 17% of the larger teeth were non-local. This data was interpreted as evidence for a female pattern of dispersal from natal groups. As discussed previously, this behavior is commonly observed in female chimpanzees, bonobos, and gorillas.

When placing this discussion of both past and present sexual dimorphism in the focus of the current study, the available data would suggest that *Au. sediba* likely did exhibit some level of sexual dimorphism, more so than that observed in modern *H. sapiens*. However, the morphological variation expressed between sexes in the *Au. sediba* taxon was also unlikely to be as extreme as that of highly dimorphic extant species, such as modern gorillas. Therefore, the developmental trajectories acquired from extant chimpanzees and possibly modern humans (see Section 4) are more likely to provide a representative model of development in *Au. sediba*, with the gorilla developmental trajectory providing the most extreme possible outcome.

# 3. MATERIALS AND METHODS

## 3.1 Geometric morphometrics

### Introduction to geometric morphometrics

Morphometrics is the study of biological shape (Slice, 2007). The comparison and examination of anatomical form has been a defining element of biological science for centuries (Adams et al., 2004). However, the past twenty years has witnessed remarkable advances in the quantification of form through biometry, leading to the advent of three-dimensional landmark-based methods. Three-dimensional landmark coordinates can be acquired directly from specimens using a MicroScribe 3D digitizer, or they can be collected from 3D renderings of specimens produced from computed-tomography (CT) scans, synchrotron scans, or through the collection of surface scans using a 3D laser scanner, such as the NextEngine 3D laser scanner used in the present study. Three-dimensional coordinates are then collected from these scans using specialized software programs.

After acquiring the raw data for use in shape comparisons, statistical analyses of 3D landmark data first require the superimposition and alignment of coordinates through generalized Procrustes analysis (GPA). GPA involves the superimposition of landmark coordinates through the translation of landmark configurations to the same centroid, scaling these configurations to a common centroid size, and rotation, thereby removing extraneous variation in a sample related to location, orientation, and size. Forms are fitted as closely together as possible through minimizing the sum of squared distances

between homologous landmarks (Richtsmeier et al., 1992). The resulting centered, scaled, and rotated coordinates belong to a consensus configuration known as Procrustes shape coordinates. Morphometric techniques and multivariate statistics can then be applied to this data set to explain variation within and among groups and samples.

## Geometric morphometrics, hominin ontogeny, and developmental simulation

The focus of the present study is the analysis of developmental patterning and the potential influence that these shape changes exert on our interpretations of the morphological affinities of sub-adult individuals. Previous studies have used morphometric techniques to assess the age at which species-distinct morphology is established in primates and the degree of post-natal divergence present in ontogenetic trajectories across species (Richtsmeier and Walker, 1993; Ponce de León and Zollikofer, 2001; Ackermann and Krovitz, 2002; Bastir and Rosas, 2004; Cobb and O'Higgins, 2004; Mitteroecker et al., 2004; McNulty et al., 2006; Bastir et al., 2007; Cobb and O'Higgins, 2007; Neubauer et al., 2010; Singleton et al., 2010; Singleton, 2012; Gunz and Bulygina, 2012; Gunz et al., 2012). Studies of primate/hominin craniofacial growth and development have indicated that species-specific morphologies are established quite early in ontogeny, and are clearly developed by the age of first molar eruption (Ponce de León and Zollikofer, 2001; Ackermann and Krovitz, 2002; McNulty et al., 2006; Singleton et al., 2010). After reaching this developmental landmark, species appear to follow more-or-less parallel ontogenetic trajectories through

to adulthood (Ponce de León and Zollikofer, 2001; Ackermann and Krovitz, 2002; McNulty et al., 2006; Singleton et al., 2010).

However, other geometric morphometric studies indicate that, while many species-level differences are established pre-natally, postnatal divergence in ontogenetic trajectories is a significant factor in shaping adult morphology (O'Higgins, 2000a,b; O'Higgins et al., 2001; Cobb and O'Higgins, 2004). Mitteroecker et al. (2004) employed geometric morphometrics to compare the ontogenetic sequence of apes and modern humans in shape space. The results show a pattern of general divergence, with the youngest specimens showing greater morphological resemblance than adult specimens. Mitteroecker et al. (2004) argue that previous studies, such as that of Ackerman and Krovitz (2002), whose findings indicate parallel ontogenetic trajectories in shape space, are connected to the focus on higher stages of dental development. Mitteroecker et al. (2004) conclude that shape changes that distinguish humans from the great apes appear to emerge earlier in ontogeny than those separating the great ape species from one another.

Multiple researchers have used geometric morphometric techniques to virtually "grow up" juvenile fossil crania and examine subsequent developmental changes in shape. Richtsmeier and Walker (1993) applied 3D geometric morphometric methods to a paleoanthropological investigation by conducting a developmental simulation of the juvenile *H. erectus* cranium, designated KNM-WT 15000. The authors used Finite-Element Scaling Analysis and Euclidean distance matrix analysis for the creation and comparison of the simulated forms using Eskimo-based (*H. sapiens*) and chimpanzee-

based (*P. troglodytes*) models. They noted remarkable similarity with regard to adolescent growth patterning both between sexes as well as within and between species. This led them to remark that, "Many of the morphological criteria that contribute to primate species designation are present at birth and certainly well established by adolescence," (Richtsmeier and Walker, 1993: 408-409).

Ponce de León and Zollikofer (2001) later examined Neanderthal and modern human ontogeny and reached the conclusion that taxon-specific differences in morphology arose early in ontogeny for both phylogenetic lineages, and further, that this divergence was followed by parallel developmental patterns. Ackermann and Krovitz (2002) further explored this development, calculating growth matrices as the proportional change implicated in the conversion of a juvenile to adult form. The authors used EDMA to examine differences in both facial shape and growth patterns among five hominoid species. Growth patterns between species were quantified by comparing like growth matrices as ratios, thus producing a growth difference matrix. The results of this analysis indicated that the general facial shape for adult individuals is largely set by the time of eruption of the first permanent molar. While taxon-specific patterns may be identified during subsequent development, these do not significantly alter the essential species-specific facial shape, and thus between-species differences are the consequence of early ontogenetic processes. They go on to elaborate that, "... these later growth patterns are so similar that applying differing species growth patterns does not alter the unique aspects of the starting species' overall form" (Ackermann and Krovitz, 2002: 146) with gorillas representing a possible exception. This latter point is

an interesting observation, considering that gorillas are the most sexually dimorphic of the great ape species.

Mitteroecker et al. (2004) conducted a geometric morphometric analysis examining the ontogenetic trajectories of *H. sapiens* and the great apes. This research was conducted in light of the then recent discoveries indicating that chimpanzees are more closely related to humans than they are to gorillas. With regard to craniofacial morphology, however, the great apes appear more similar to one-another than to humans. Their results also indicated that species-specific morphologies are established during the early stages of human ontogeny as a result of small genetic differences and that these morphologies further diverge post-natally. Additionally, differences that separate *H. sapiens* from great apes seem to arise earlier than those that separate the different species of great apes.

Like Richtsmeier and Walker (1993), McNulty et al. (2006) also performed a developmental simulation for an extinct hominin, *Au. africanus*. McNulty et al. (2006) used the Taung child (the type specimen for *Au. africanus*) to estimate the adult form of this individual. Here the authors applied the developmental trajectories from extant hominids including *G. gorilla*, *H. sapiens*, *P. paniscus*, and *P. troglodytes*, having collected three-dimensional landmark data from both adult and juvenile individuals. The specimens were divided based upon dental eruption sequence in an effort to assure that all stages of growth and development, as well as sex, were well represented.

Developmental trajectories were estimated for each extant hominine species to assess differences in the pattern and amount of shape change (i.e. angle and magnitude

respectively). The developmental trajectories of different species were applied to extant juveniles to assess the impact of using incorrect hominine trajectories on the resulting form. Four simulations of the adult Taung individual were produced based upon the pattern of development observed in extant species. These models were then compared to one another statistically. The simulated Taung adults produced through this analysis were remarkably similar, with only small distances observed between the four adult models. When compared to only Sts 5 (*Au. africanus*) and SK 48 (*Au. robustus*), the Taung child was consistently shown to be most similar to Sts 5. When compared to a broader set of fossils, the simulated Taung adults were most similar to Sterkfontein, specimen Sts 71. Overall, these results support the conspecificity of the Sterkfontein specimens included in this study (Sts 5 and Sts 71) and the Taung child.

More recently, a developmental simulation was conducted for the extant mangabey species, *Rungwecebus kipunji* (Singleton et al., 2010). This is a critically endangered species found in the Southern Highlands of Tanzania for which only a single M1-stage juvenile was available for study. Therefore, the adult cranial morphology was unknown at the time of the publication (Singleton et al., 2010). The authors used similar methodology to that described in McNulty et al. (2006) for the developmental simulation (dental stage regression), and then followed this reconstruction with a phenetic analysis of the adult model. Developmental trajectories were calculated using cercopithecine crania derived from all papionin genera in addition to two cercopithecine outgroups. The simulated *R. kipunji* cranium was visualized by applying the morphing function in Landmark Editor® software (Wiley et al., 2005) to a 3D laser scan created using a

NextEngine desktop 3D laser scanner®. Principal components analysis was then applied to the simulated *R. kipunji* adults in comparison to other papionin adults. Procrustes distances were calculated between individual simulated *R. kipunji* adults and the average simulated adult and then compared with the species distributions. Procrustes distances were also applied to assess the affinities of the simulated *R. kipunji* adults to other species. It was found that the estimated adult cranial morphology for the *R. kipunji* individual tended to be similar to that observed in other mangabeys, and showed the greatest morphological similarity to *Lophocebus aterrimus*. However, it remained significantly different from this taxon with distances that are equivalent to those recognized in other papionin genera. These results therefore suggest that *R. kipunji* is a distinct phenon of generic status.

Singleton (2012) further investigated studies of papionin development, examining questions relating to the age at which differentiation of cranial shape is established in combination with other questions regarding environmental influences on cranial shape and ontogenetic development. Singleton (2012) notes that, by necessity, we must rely upon extant models when examining the developmental foundation concerning the morphological evolution of hominin species, especially considering the limited number of juvenile hominin crania available for analysis. The results of her analysis indicate that macaques have a common postnatal growth pattern, despite considerable genetic and morphological diversification. Therefore, research continues to indicate that species-specific cranial morphology is the result of prenatal morphogenesis and is established by early juvenile stages. By using papionins, the author has further

demonstrated that this is a general phenomenon, and that early pattern formation/diagnostic traits are present in early infancy and remain stable through postnatal ontogeny. Singleton (2012: 514) goes on to state, "It seems increasingly clear that early morphogenesis is the primary determinant of cranial shape, making juvenile morphology reliably predictive of adult form."

Gunz and Bulygina (2012) also used dental stage via regression (McNulty et al., 2006) to predict adult morphology of the Teshik-Tash child, which has been interpreted to represent both a Neandertal and an early modern human by different researchers (Weidenreich, 1945; Gremiatsky, 1949; Jelinek et al., 1969; Vlcek, 1991; Stefan and Trinkaus, 1998; Rosas, 2001; Trinkaus, 2003; Wolpoff et al., 2004; Trinkaus, 2006; Glantz et al., 2009; Hublin, 2009; Kharitonov, 2009). They projected the simulated adult individuals into Procrustes shape space of the original sample to assess whether these individuals fell within the range of variation for adult Neandertals or modern humans. This was followed by a phenetic analysis to assess the morphological affinities of Teshik-Tash, which indicated a greater alignment with the Neandertal species.

The present research employs the dental stage via regression model for developmental simulation outlined in McNulty et al. (2006), Singleton et al. (2010) and Gunz and Bulygina (2012). While these methods are both well-established and highly effective, no study has yet been conducted that applies a highly focused approach to the development of secondary sexual changes between second and third molar eruption, and further, these studies usually pool sexes, therefore blurring any morphological changes that may be related to puberty. By testing the hypothesis that MH1 is sufficiently

developed to all for reliable morphological comparison, this study extends the results to include *Au. sediba*, thereby expanding our knowledge of this species.

**Multivariate tests**

When conducting a shape-based analysis of morphological features, one must choose the most appropriate morphometric applications that will provide a thorough and accurate description of any trends and patterns within the data set. Producing high-quality visualizations of these results and processes is usually a corollary goal of morphometric research. Fortunately, the advent of 3D geometric morphometric techniques and 3D scanning technology has provided a number of means towards achieving both objectives.

The focus of the present study, as previously discussed, is to test whether or not MH1 is sufficiently developed at age-of-death to allow for reliable morphological comparison with other hominin species. This is to be accomplished by both producing accurate 3D renderings of the adult morphology of *Au. sediba*, as well as placing the resulting simulated adults in a broader comparative context within the hominin fossil record. The multivariate tools and comparative analyses chosen for use in the present study involve the application of thin-plate splines, principal components analysis (PCA) and the calculation of Euclidean (Procrustes) distances. Thin-plate splines were chosen for their ability to provide accurate renderings of adult morphology through interpolation, while PCA and Euclidean distances were used to simplify trends and

describe shape-based comparisons within- and between- groups of specimens. These three morphometric tools will now be reviewed in detail.

*Thin-plate spline transformation*

As discussed above, the focus of morphometric research is the description and comparison of biological shape. This often requires the ability to identify and describe shape-based change through illustrations, for which thin-plate splines can provide an invaluable tool. Thin-plate splines are designed for morphing objects between a reference and target form through interpolation between corresponding landmarks. While the mathematics supporting interpolation is relatively new, the actual concept that forms the foundation of thin-plate spline analysis is quite simple, dating back to D'arcy Thompson's (1917) use of transformation grids. These grids were used to warp one object into another, the differences of which could then be depicted through the size and orientation of grid squares.

Today, with rigorous mathematical techniques for support, the thin-plate spline method functions on the basis of minimizing the bending energy of deformation between homologous coordinates for reference and target specimens (O'Higgins, 2000a; Bookstein, 1991). By assigning correspondences between landmarks, one can interpolate shape transformations between a reference and target form. Essentially, the reference specimen is 'warped' into the target specimen using these homologous landmark points.

One of the primary advantages of thin-plate spline is the ease with which high-quality visualizations are generated allowing one to create detailed descriptions of shape-based change between forms. Thin-plate spline interpolation was used in the present study to create 3D visualizations of the simulated adult *Au. sediba* crania. A synchrotron scan of the juvenile MH1 individual was morphed into the simulated adult coordinates by assigning correspondences between the juvenile and adult landmarks, thereby creating a reference and target form. The 3D renderings of adults that were produced using the original scan could then be used to describe and interpret developmental changes in morphology between second and third molar eruption.

*Principal components analysis*

Principal components analysis (PCA) is perhaps the most widely used technique for describing broad-scale trends in multivariate data sets. PCA is an ordination method, for which the aim is to condense the information represented by a large number of variables into a smaller number of new variables, while at the same time minimizing the total information lost (Abdi and Williams, 2010; Shennan, 1997). In biological anthropology, these data are normally comprised of either a set of measurements or 2D/3D landmark coordinates with which one hopes to identify shape-based similarities and differences among specimens.

Each specimen can be understood as a point in space, and there are as many dimensions to this space as there are variables. The position of the specimen within this space is designated by the variables used to define it. However, some of these variables

will be correlated with one another, and the distribution of items within this space may not be equal in all directions. One must identify the orientation and length of these different axes across which the specimens are distributed (Shennan, 1997).

By applying PCA to this type of data set, one hopes to create an accurate depiction of the interactions between objects (such as crania) and variables in a space illustrated through a small number of dimensions. The ultimate goal of this reduction of variables through ordination is to allow for an easier interpretation of trends within a data set by minimizing redundant information. Ordination involves the rotation of the axes formed by an original variable coordinate system and transforming these to create new orthogonal or perpendicular axes. The new axes are then referred to as principal axes and correspond to the directions of maximum variation contained by the original observations (Campbell and Atchley, 1981).

If there is covariation between variables, these variables can then be summarized using a smaller number of variables, in essence, providing a summary variable for the data (Shennan, 1997). For example, when considering scattergrams produced through basic bivariate regression, the existence of strong trends indicates that variation in one variable can be explained through another (Shennan, 1997). The new variables produced through ordination allow for simplified scattergrams to be produced that can allow one to take note of and understand any groupings or trends within the data set under study. For the present study, these scattergrams can allow us to identify groupings of hominin crania based on morphological similarities.

When examining a principal component plot, the first axis or component, is the longest and represents the greatest amount of variation within the sample. The orientation and length of this axis will cut through the longest part of the point scatter. This, in turn, is followed by the second axis, which is slightly shorter, cutting through the second longest dimension of the point scatter. However, this axis must be orthogonal (perpendicular) to the first. A useful visual exercise for explaining this process is to picture a scatter of points in the shape of an American football. The longest axis of variation will cut through the length of the ball. The second axis is formed at a right angle to this and will cut through the width of the football. The total number of principal components is equal to one less than the sample size included in the analysis (n-1), with the pattern continuing as each successive component explains less variation than the one preceding it. Researchers generally hope that the first few components will account for the vast majority of variation within the sample, as the goal of applying PCA to a multivariate data set is generally to simplify and reduce the dimensionality of the data.

The percentage value for the variation accounted for by each component is represented by an eigenvalue and is equal to the sum of the squared factor scores for that particular component (Abdi and Williams, 2010). The eigenvectors then explain to what extent each individual variable, such as a measurement or landmark coordinate, is responsible for explaining the variation along each axis in terms of defining its length and orientation.

By assigning coordinates to the specimens for each axis of variation, one can produce a scattergram of the data (component one versus component two, and so on). Most researchers are generally interested in identifying any clustering or grouping of specimens. In other words, which specimens are most similar or different to one another and how can we describe these affinities? By assessing the position of each specimen relative to one another along each axis, and then examining which variables have the highest eigenvector loading along that axis, one can identify overall trends of variation within the data set.

*Euclidean/Procrustes distance matrix analysis*

Euclidean distance matrix analysis is a matrix composed of all interlandmark distances, which ultimately allows one to compare pairs of objects. Euclidean distance is based on Pythagoras' theorem, the geometric proof stating that the square of the hypotenuse of a right triangle is equal to the sum of squares for the remaining two sides. This can be extended to state that the squared length of a vector is the sum of the squares of its coordinates and the squared distance between two vectors is the sum of squared differences between their individual coordinates.

In the present study I used 3D Procrustes coordinates to create matrices based on Euclidean distance. When using Procrustes landmark coordinates as variables in which size, orientation, and location are controlled for, as in the present study, the product can be referred to as a Procrustes distance matrix with reference to Procrustes shape space. By quantifying distances between the homologous landmark coordinates for each

specimen, one can identify which individuals (or species) are most similar, and which are different based on this overall shape-based distance. The present study used distance matrices to compare distances within- and between- groups of specimens, as well as to compare distances between the regression coefficients for each species.

### 3.2 Reconstruction of the MH1 cranium

A reconstruction of the MH1 cranium was carried out with the goal of correcting for distortion in the cranium and producing a more complete virtual model of the *Au. sediba* skull. Rapidform XOR3 64. Build version 3.1.1.1 ® software was employed in this reconstruction. Rapidform XOR3 64. Build version 3.1.1.1 ® is a specially designed, reverse engineering software that allows for the refinement and processing of 3D models. The original 3D model of the MH1 cranium employed in this reconstruction was created using synchrotron scan data obtained at the European Synchrotron Radiation Facility (ESRF) located in Grenoble, France. The synchrotron data was subsequently decimated and segmented using Avizo 6.3® software, resulting in a 3D virtual rendering of the MH1 cranium, excluding the encasing breccia. This allows for the collection of landmark data in areas that were previously obscured by breccia, such as the palate.

Following an initial examination of an unaltered scan of the MH1 cranium, it was readily apparent to the author that one must first correct for deformation in the fossil prior to developmental simulation, as distortion becomes exaggerated when applying vectors to the specimen via thin-plate spline analysis. This is also crucial for all shape-based analyses aimed at addressing the morphological similarities of the fossil.

When examining the juvenile cranium, several preservation issues concerning the integrity of the fossil are readily apparent (Fig. 1a). The most prominent among these is a large crack, originating at the left supraorbital torus that runs postero-medially across the frontal, widening as it continues to bregma where the crack shows a maximum breadth of approximately seven millimeters (Fig. 1a). An additional crack affecting landmark placement extends from the supero-medial margin of the right orbit, inferomedially across the frontal process of the maxilla, breaking across the nasal bridge. Best viewed from frontal aspect, the crack obscures the right frontomaxillary suture and laterally displaces the inferior portion of both nasals.


**Figure 1:** a) Unreconstructed MH1 cranium frontal and lateral aspect. b) Reconstructed MH1 cranium from frontal and lateral aspect.

As discussed above, the large crack extending across the frontal has resulted in the displacement of the left portion of the frontal bone. The displacement extends laterally from above the left orbit to the articulation of the frontal with the zygomatic bone along the frontozygomatic suture (Fig. 1a). The zygomatic is displaced postero-inferiorly, disarticulating the bone from the zygomatic process of the temporal and the zygomatic process of the frontal. This distortion can also be noted from the frontal aspect when examining the inferior margin of the left orbit. Zygoorbitale is displaced superiorly as a result of this displacement. Correcting for the above cracks and

displacements was the focus of the present reconstruction. An additional goal was to produce a more complete calvaria by reflecting the preserved portions of the left parietal and temporal bones onto the right side.

The 3D model of the MH1 cranium was first imported into Rapidform®, and all adjustments were conducted in mesh mode. It was decided that the most efficient and effective way to account for cracks and displacements was by selecting the affected areas that required adjustment, copying and pasting these regions into a separate window, and then re-aligning the selected area with the original model. The selected areas were reoriented using the scan tools property and align between scan data. Using this tool, one selects a reference scan and a moving scan. The scans are then aligned in accordance with selected analogous points between the reference and moving scan that serve to knit the scans together (Fig. 2).

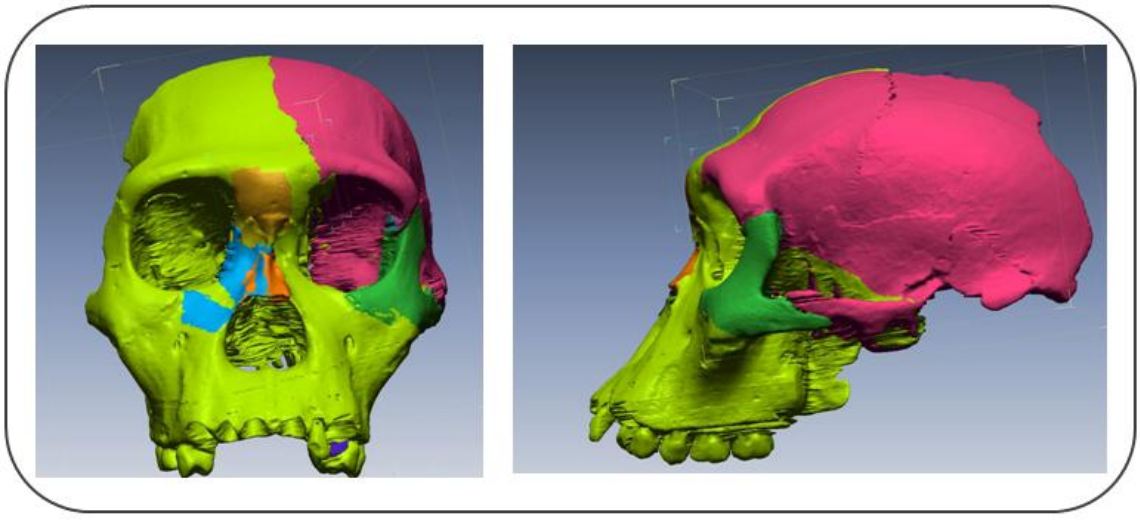

**Figure 2:** Frontal and lateral view of MH1 reconstruction in progress.

To correct for the large crack across the frontal bone, I first selected the preserved portions of the frontal, parietal, sphenoid, and temporal bones extending to the left of the crack. These were then copied/pasted into a separate window and selected as the moving scan to align with the remaining portion of the cranium using the "align between scan data" tool. Once the crack had been corrected for, I was then able to move and realign the zygomatic using the same process, in which the zygomatic bone was removed and then rearticulated with the zygomaticotemporal and zygomaticofrontal sutures. The portion of the nasal bones inferior to the crack were additionally removed and realigned using the same process as the zygomatic and frontal bones.

The mirror tool was used to correct for the distortion along the nasal bridge, by reflecting the left side of the superior portion of the nasal bridge to remove the crack across the frontomaxillary suture. After correcting for displacement and distortion in the cranium, the mirror tool was used to reflect the left half of the calvaria posterior to the coronal suture to produce a more complete calvaria (Fig.3).

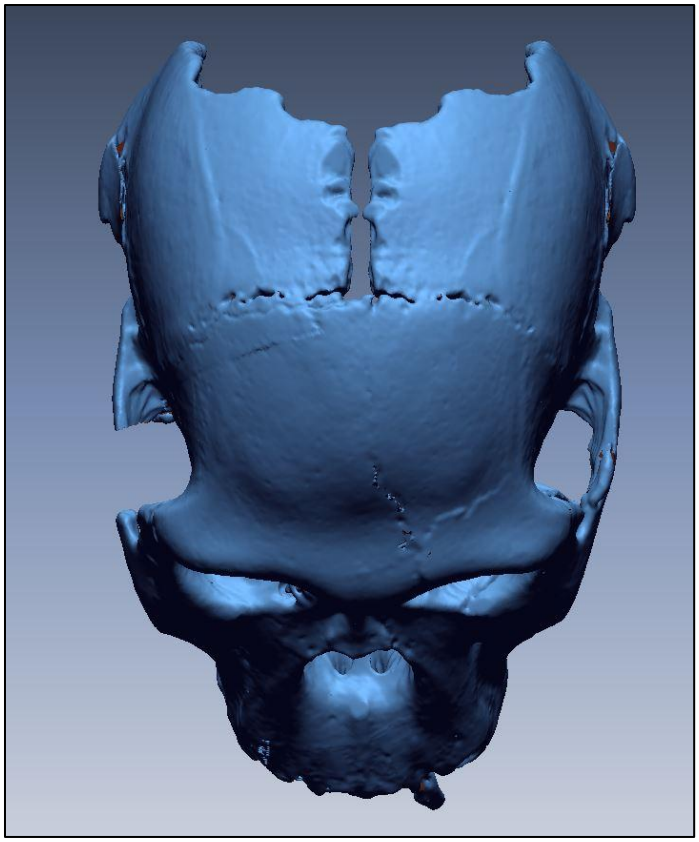

**Figure 3:** Superior view of MH1 with reflection of left parietal

As a final step in the reconstruction, the scans from the corrected model were then merged into a single scan and the resulting model was run through Global Remesh. This command regenerates the mesh structure with removed defects in accordance with the model's curvature flow. In other words, it essentially creates a new mesh on top of the existing mesh, while preserving definition and resolution. The final, reconstructed MH1 cranium is illustrated in Figure 1b as compared the original, unrepaired cranium.

## 3.3 Materials

**Sample**

The hominoid sample used in this study is listed in Tables 1-3, and is comprised of chimpanzees (*P. troglodytes*), gorillas (*G. gorilla gorilla*), and modern humans (*H. sapiens*). A summary total for each group is provided in Table 1, while lists of all individual specimens are provided in Tables 2-3. All apes were collected from the Cleveland Museum of Natural History, which houses the largest collection of African apes in the world. Records for chimpanzees indicate that specimens were collected in Ebolwa, Cameroon, as well as Abong Mbong, French Cameroons and Abong Mbong, Djaposten, Cameroons, West A, with the exception of three specimens for which no geographic data is available (B-1056, B-1435, and B-346). The records for the gorilla crania used in the comparative sample indicate that specimens were collected in French West Africa, French Congo, Ebolwa, Cameroon, Abong Mbong, French Cameroons, and Abong Mbong, Djaposten, Cameroons, West A. Both chimpanzee and gorilla crania were sexed using skeletal remains.

The human sample included primarily cadaver crania obtained from the Raymond A. Dart Collection of Human Skeletons, although several well preserved archaeological crania were included as well from both the Raymond A. Dart Collection of Human Skeletons and the Cleveland Museum of Natural History. Archaeological crania were included as the crania had not been sawed in half during skeletal preparation, therefore allowing for easier landmark-placement. The two archaeological specimens from the Cleveland Museum of Natural History, 0.202 and 0.239, are of

Egyptian and Eskimo ethnicity respectively. Unfortunately, the provenience for these two specimens is not precisely known, although it is known that the Eskimo specimen, 0.239, is from Nunavik Island.

The Raymond A. Dart Collection of Human Skeletons is housed at the School of Anatomical Sciences at the University of the Witwatersrand in Johannesburg, South Africa. The skeletons comprising the Raymond A. Dart Collection of Human Skeletons are primarily of regional, or southern African origin (76%), with cadavers collected from the 1920s until present (Dayal et al., 2009). Specimens used in my comparative sample from the Raymond A. Dart Collection from cadavers were labeled as belonging to the following ethnicities (see Dayal et al., 2009): Shangaan, San (Bushmen), Xhosa, Zulu, Swazi, Pondo, Tswana, Ndebele, Sotho, European (White South African), Mixed-race ('Coloured'), and Pedi. In addition, three specimens were included for which the ethnicity was not stated, indicating that the individual was a black South African of an unstipulated population group. With regard to the archaeological specimens included in my sample, specimen A.44 and A.55 are designated as a San (Bushmen) and European, respectively, although the provenience is not known for either specimen. However, the juvenile archaeological specimen, A.327, does have provenience, coming from Pietersburg Distr, Jacobsdale. This specimen is designated as a 12 year old male San (Bushmen). Specimens with obvious pathologies or abnormalities, such as premature suture closure or acute alveolar absorption, were excluded from the study sample.

Both ape and human specimens were assigned to developmental categories based on dental eruption sequence. Juveniles were judged to be of the same developmental age

as MH1, and therefore suitable for inclusion within the study, if the second molars were erupted and in occlusion (M2-stage) while the third molars had not yet erupted. Specimens were designated adults if the third molars were erupted and in occlusion (M3-stage). Both males and females were sampled for parity.

The hominin fossil sample used in geometric morphometric comparative analyses (Table 4) included a sample of non-robust australopith and early *Homo* crania from five species: *Au. sediba* (MH1), *Au. africanus* (Sts 5, Sts 71, Stw 53), *H. habilis* (OH 24, KNM-ER 1813), *H. rudolfensis* (KNM-ER 1470), and *H. erectus* (D2700, KNM-WT 15000, KNM-ER 3733). It should be noted that while the author considers Stw 53 to represent *Au. africanus*, many would object to this classification, as discussed in section 2.4 of this manuscript. Laser scans of Sts 5 and Sts 71 were collected from original fossil material at the Ditsong Museum of Natural History in Pretoria, South Africa. A laser scan of the Clarke (1985) reconstruction was used for the Stw 53 *Au. africanus* cranium. The original OH 24 fossil was scanned at the National Museum of Tanzania in Dar es Salaam, Tanzania. Scans from the Dmanisi and Kenyan fossil material were obtained from high-quality casts located at Harvard University, as the original fossil material was not available.

**Data collection**

The ontogenetic sample for chimpanzees, gorillas, humans, and fossil hominin crania were collected using a NextEngine 3D laser scanner®. The NextEngine 3D scanner® has a 0.005 inch accuracy and is easily portable, making it convenient for

travel. The NextEngine 3D laser scanner® collects point-cloud data at a speed of 50,000 processed points/sec, collecting information on color as well, and operates in combination with ScanStudio HD Pro version 1.3.2® software. This software scans, aligns, polishes, and fuses the 3D scans to produce a micro-mesh model of the scanned object. The ScanStudio HD Pro version 1.3.2® outputs the PLY file formats that were used for landmark placement and morphological comparisons. Surface scans from multiple perspectives were stitched together and fused manually using Scanstudio HD Pro® software through the selection of homologous points between scans. The final fused scans were later imported into Geomagic® software where they were smoothed and polished using the Mesh Doctor tool. Mesh Doctor provides an automatic polygon mesh improvement tool, which both detects errors in the mesh while also correcting for them.

All holes in the mesh were filled in Geomagic® software to prevent any landmarks or semilandmarks from "falling through" the mesh during landmark placement. This also prevents confusion when applying the morphing function in Landmark Editor (Wiley et al., 2005). These holes were filled by using the "fill holes" tab. I selected holes individually to correct holes in the mesh of hominoid crania. Geomagic® is ideal for this process as it takes into account the curvature of the surface at hand, thus allowing for a seamless transition with the original mesh.

After fusing and polishing the scans, as well as filling any holes that were present, each hominoid scan was subsequently imported into Landmark Editor software (Wiley et al., 2005) where 76 traditional and semilandmarks were placed on the mesh

surface (Figs. 4-6; Table 5). Three semilandmark curves comprised of ten points each were placed along the midsagittal plane between rhinion and bregma, thereby accounting for the curvature of the nasals, supraorbital region and frontal bone. The number and location landmarks were chosen for their repeatability between specimens and representativeness of morphology. These, in turn, further allow for Landmark files for each hominoid species were exported and formatted as text files to be uploaded into to MorphoJ software (Klingenberg, 2011). Here, the combined landmark files for each species were aligned through generalized Procrustes analysis (GPA). GPA minimizes the sum of squared distances between homologous points through translation, rotation, and scaling all specimens to the same centroid size, thereby controlling for the extraneous effects of location, orientation, and size within the sample (Gower, 1975; Rohlf and Slice, 1990). An illustration of the GPA aligned landmarks of *P. troglodytes* is provided in Figure 7.

A subset of 32 landmarks was then used for morphometric comparison of hominin crania with the simulated *Au. sediba* individuals (Fig 8; Table 6). Subsetting was necessary to compare the extant taxa to landmarks obtainable on the fossil specimens selected for analysis. Fossil landmark choice was limited by preserved cranial anatomy. In order to include specimens Sts 71 and KNM-WT 15000, missing landmarks were estimated through the reflection of antimeres.

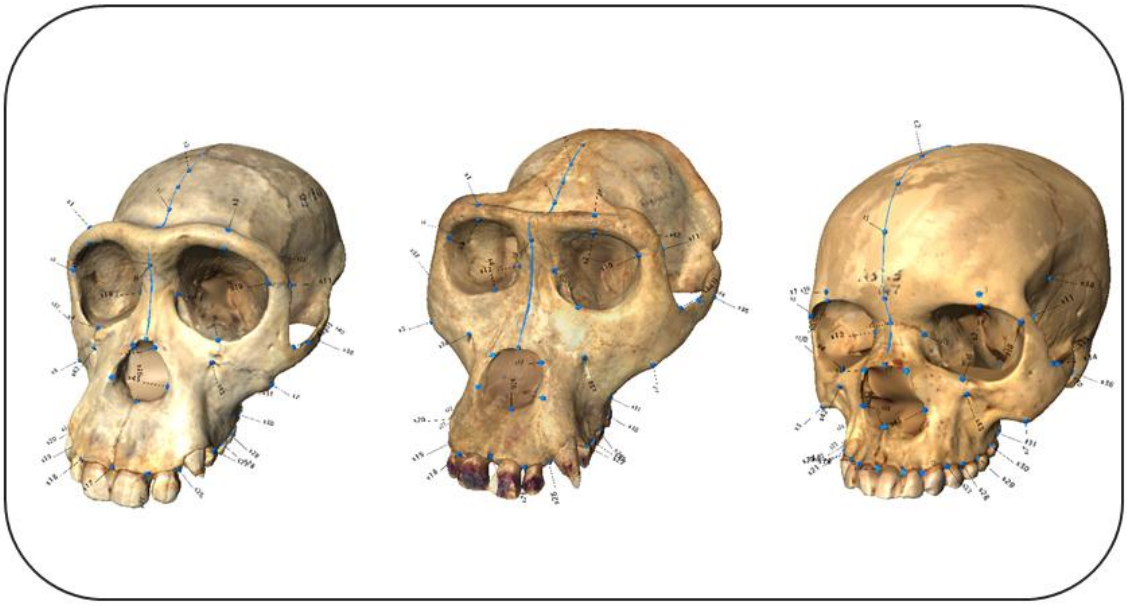

**Figure 4:** Landmark array as visualized on extant hominoids. From left to right: *P. troglodytes*, *G. gorilla*, *H. sapiens.*

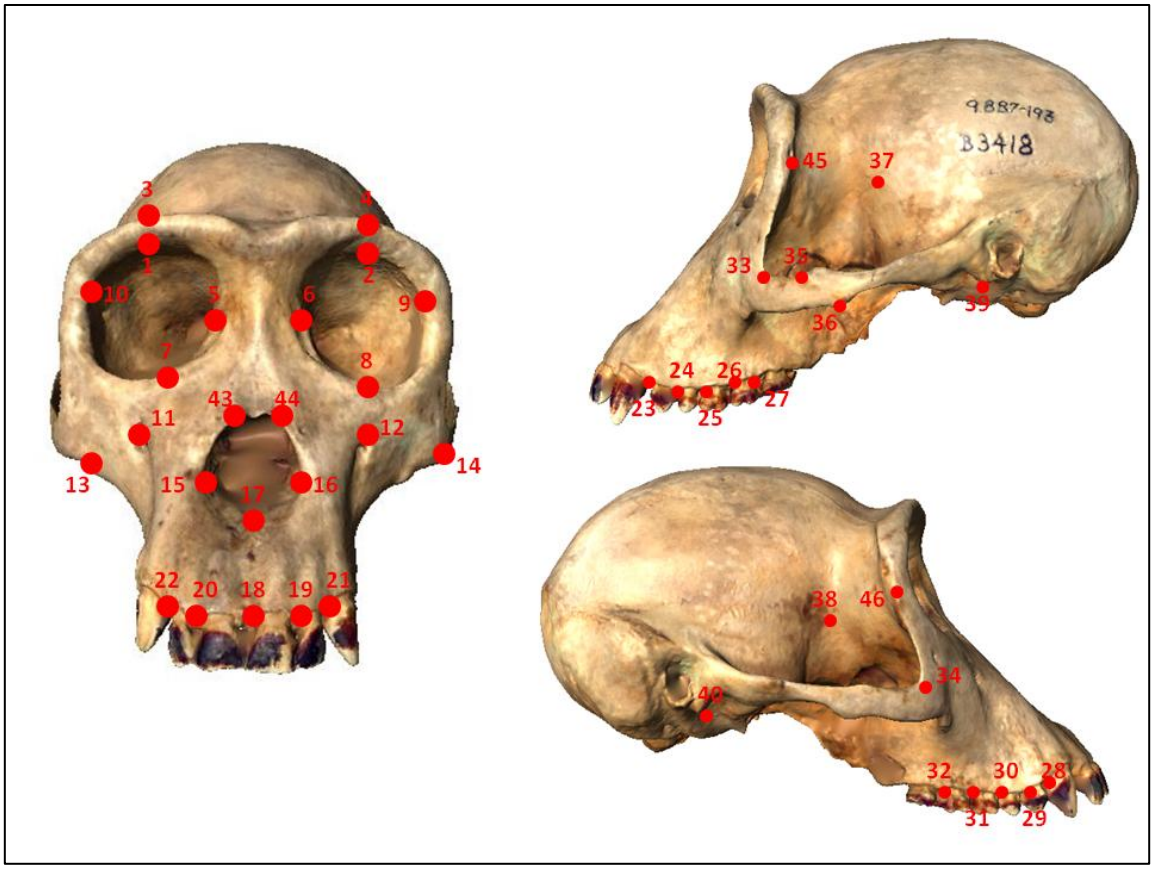


**Figure 5**: Landmarks used in developmental simulation from frontal and lateral aspect. In addition to those pictured here, three curves of 10 equidistant semilandmarks were placed between rhinion and bregma (see Fig. 4). Numbers correspond to definitions in Table 5.

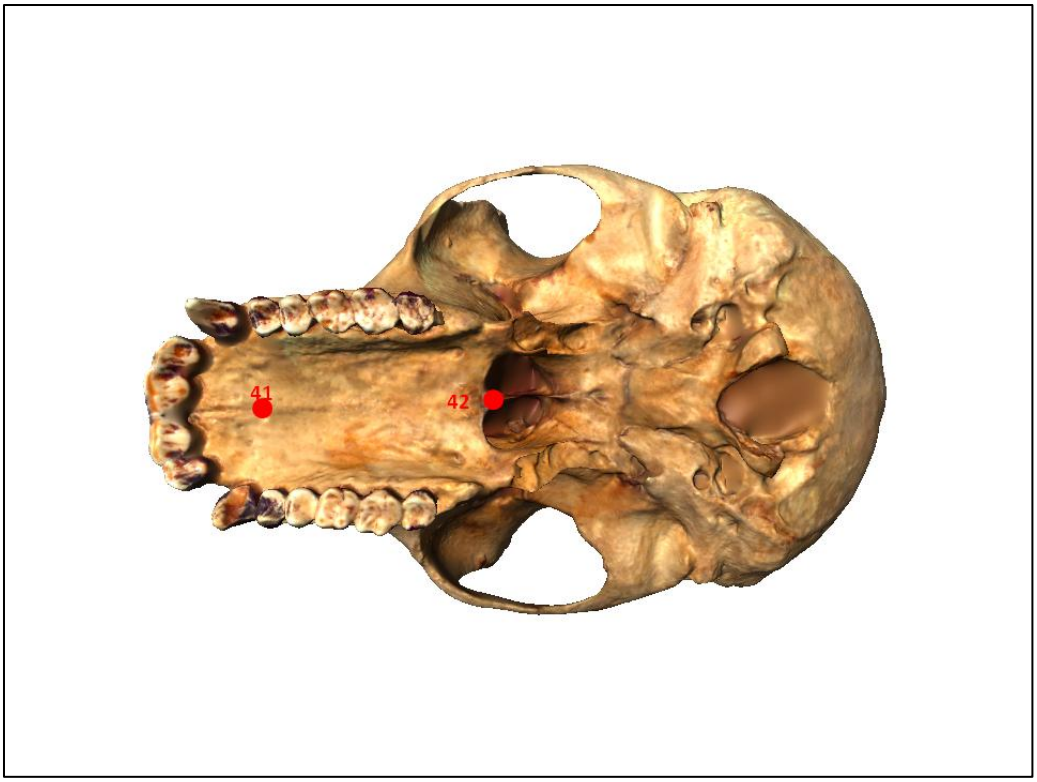


**Figure 6:** Landmarks used in developmental simulation from inferior aspect. Numbers correspond to definitions in Table 5.

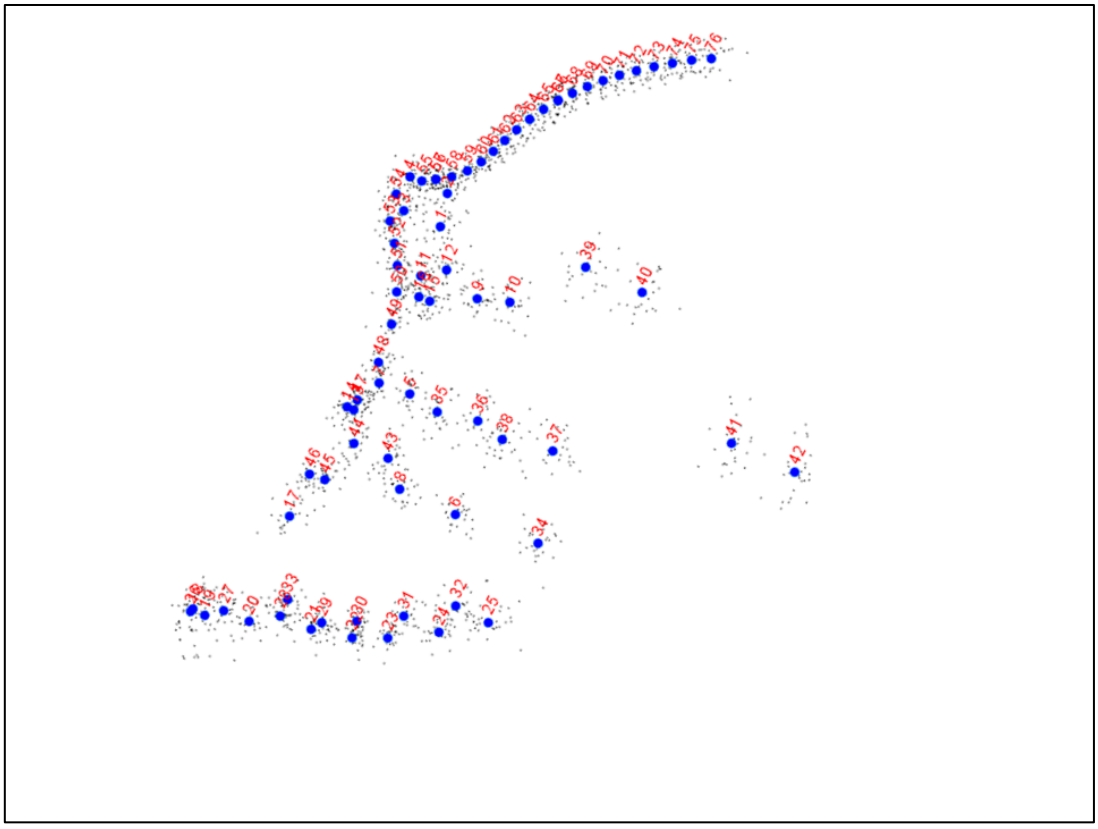

**Figure 7:** Procrustes aligned coordinates of *P. troglodytes*.

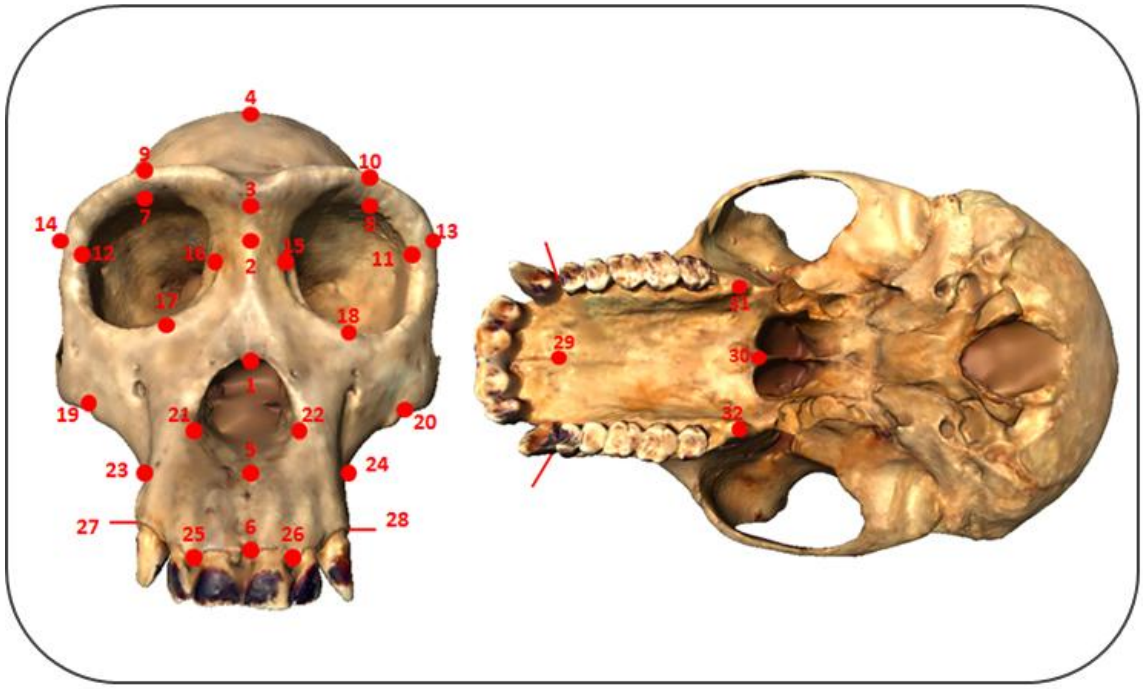


**Figure 8:** Subset of landmarks used for morphometric comparisons. Numbers correspond to definitions in Table 6.

## Data analysis

GPA aligned coordinates for juveniles and adults of each hominoid species were exported from MorphoJ software (Klingenberg, 2011) where they were subsequently imported as a text file into PAST® statistical software. A visual of the GPA aligned coordinates of the *P. troglodytes* sample is provided in Figure 7. Juvenile and adult specimens were separated by dental stage, and a multivariate regression was carried out between the M2-stage juveniles and M3-stage adults of each species. Male and female juveniles were pooled together, while adults were separated by sex. The slope of this regression (i.e. the regression coefficients) was then applied to the Procrustes-aligned

coordinates of the juvenile MH1 cranium to provide the estimated adult *Au. sediba* coordinates.

These estimated adult coordinates for each sex and species were uploaded into Landmark editor software (Wiley et al., 2005). After assigning correspondences between landmarks, the synchrotron scan of the MH1 cranium was then morphed into these simulated adult coordinates via thin-plate spline analysis using the morphing function to provide a 3D rendering of the estimated adult morphology of the MH1 cranium. In total, six simulated adult MH1 crania were produced using extant hominoid developmental vectors, one male and one female from each of the three extant species employed in this analysis (Figs 9-10).

After the developmental simulations were completed, the goal was then to place these simulated adult *Au. sediba* crania in a broader comparative context with other non-robust australopith and early *Homo* fossil crania. After selecting landmarks and aligning the fossil hominins through GPA, morphological variation within the sample was assessed through the application of PCA and Procrustes distance matrices to the data set. These multivariate analyses were chosen for their ability to identify and describe variation and morphological affinities within the fossil sample, as well as quantify the distances within and between taxa.

Two principal component analyses were conducted on the data set, one including chimpanzees and modern humans (Figs 11-13; Table 7) and one including only fossil specimens (Figs 14-18; Table 8). The second PCA was conducted to control for the potential influence of the extant species on the distribution of hominins along the major

axis of variation. A minimum spanning tree was also included to allow for visual assessment of specimen proximity throughout principal components space (Fig 16).

Procrustes distance matrices were calculated for the GPA aligned data set (Tables 9-10). The first Procrustes distance matrix (Table 9) was utilized to assess the total variation present both within- and between- taxa, including the extant species *P. troglodytes* and *H. sapiens*. The average within-group distance was calculated for each species. This allows one to assess whether the total degree of variation present within the *Au. sediba* sample of simulated adults exceeds that of extant hominoids; these averages were then compared between groups to assess overall similarities or differences between taxa.

A second Procrustes distance matrix was also used to compare the regression coefficients of the male and female developmental vectors that were applied to the MH1 cranium (Table 10). This, in turn, allows one to recognize any major dissimilarities between the developmental vectors of each extant hominoid species that was utilized in developmental simulation of the *Au. sediba* cranium. In other words, I applied this test to the data set to assess whether or not any single sex or species develops in a recognizably different pattern than that of other species employed. I was then able to interpret how these differences in developmental trajectories, if present, may potentially influence the results obtained through simulation. This test was considered to be especially important given the considerably divergent life history traits of the species utilized in the present study. The original MH1 coordinates and all simulated adult coordinates used for the above morphometric comparisons are provided in Tables 11-13.

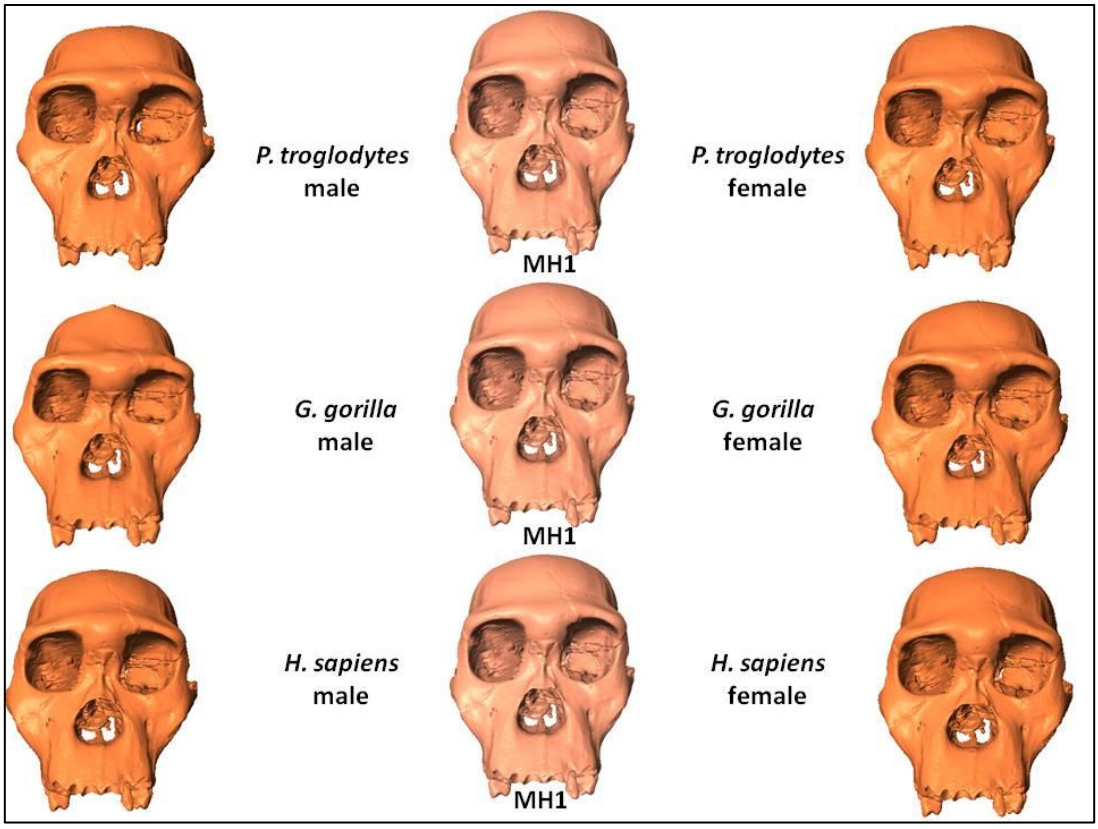


**Figure 9:** Visualizations of hominoid developmental trajectories from frontal perspective

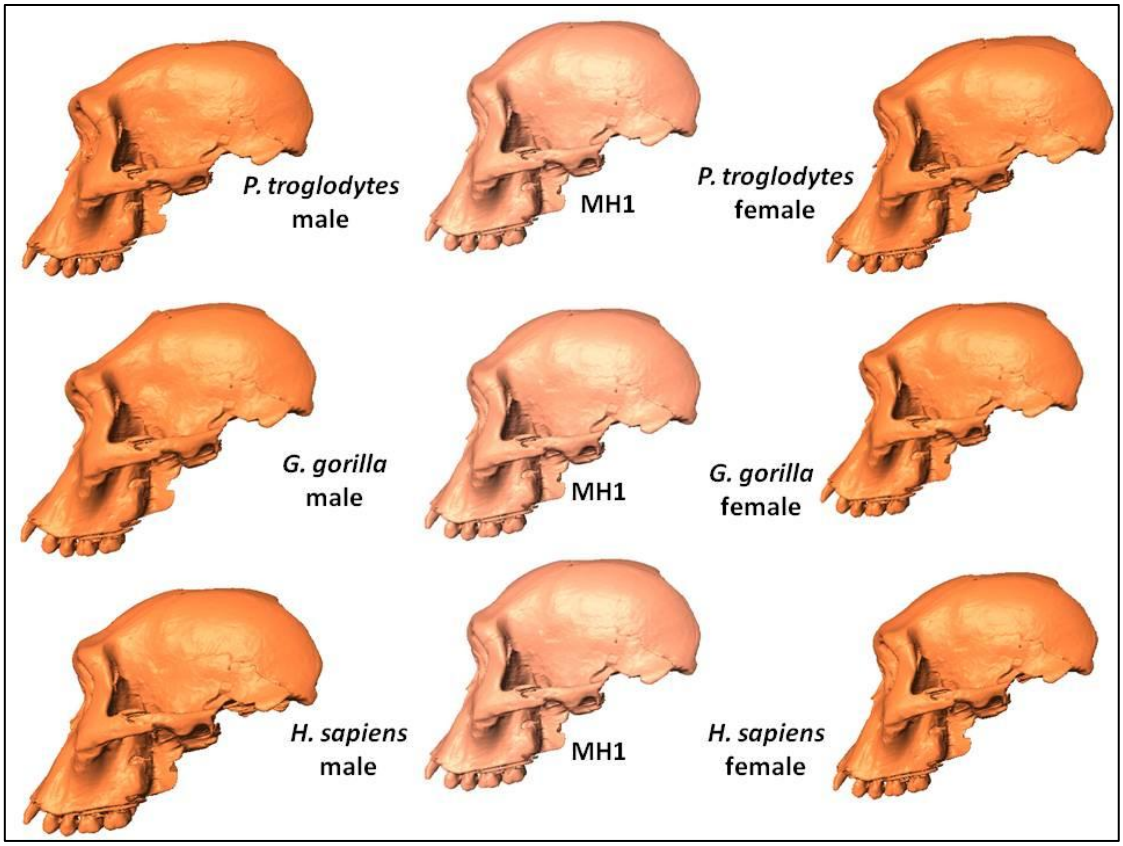


**Figure 10:** Visualizations of hominoid developmental trajectories from lateral perspective

# 4. RESULTS

## 4.1 Description of simulated adult *Au. sediba* crania

The following subsection provides a qualitative description of each simulated adult *Au. sediba* cranium produced from the chimpanzee, human, and gorilla developmental vectors. In general, male simulated adults differed more greatly from the original MH1 cranium when compared to their female counterparts. This is in connection with the development of masculine features following the onset of puberty. The adults simulated from the gorilla developmental vector were shown to vary most greatly from the original juvenile form, while humans were shown to differ the least. Frontal views of all 3D renderings of simulated crania are illustrated in Figure 9, while lateral views simulated crania are illustrated in Figure 10.

### ***P. troglodytes* developmental vectors**

*Male chimpanzee developmental vector*

When examining the simulated adult MH1 generated using the male chimpanzee developmental vector, the overall nature of morphological change is rather subtle. When studying the cranium from frontal perspective, one can observe a straightening of the zygomaticoalveolar crest, as it ascends at a steeper angle from its origin at the malar root towards the zygomatic prominence. There is a slight thickening of the supraorbital torus, creating a more masculine appearance; further, the slope of the frontal bone is somewhat flattened compared to the original, juvenile cranium.

When viewed from lateral perspective, the differences between the original and simulated adult MH1 cranium become more marked. One can see increased facial prognathism compared to the original MH1 cranium. Also, there is a slight increase in the transverse bending across the face, as observed in the angle of the lateral orbit as well as in the bending across the nasal bridge. Overall, the face is slightly more rugged in its general appearance when compared directly to the juvenile MH1, indicating the development of masculine features associated with puberty.

*Female chimpanzee developmental vector*

Very little change is recognizable between the juvenile MH1 cranium and the simulated adult when applying the female chimpanzee developmental vector. One does not observe the thickening in the supraorbital torus, as seen in the male chimpanzee developmental vector; however, some flattening of the frontal bone is still observed for the female chimpanzee vector. Additionally, one continues to see a slight increase in facial prognathism when viewed from lateral perspective, although the increased degree of transverse bending across the face is no longer noticeable when using the female chimpanzee pattern of development.

## ***G. gorilla* developmental vectors**

*Male gorilla developmental vector*

By far the most dramatic morphological changes are observed when applying the male gorilla developmental vector. When viewed from frontal perspective, the block-

like glabellar region is larger and considerably more prominent, over-hanging the nasal bridge. One can also see considerable deepening of the supratoral sulcus. This feature is made all the more prominent by the presence of a crest that arises from this gutter-like supratoral sulcus to form what resembles a sagittal crest near bregma. The supraorbital torus is also thickened in this virtual rendering. The zygomatic prominence flares outwards in the lateral direction.

When viewed from lateral perspective, one notices a dramatic increase in transverse bending across the face, made more prominent by the marked facial prognathism. The frontal process of the zygomatic is also noticeably thicker compared to the original MH1 cranium. Overall, this developmental vector was clearly influenced by the substantial development of secondary sexual characteristics responsible for the marked dimorphism between male and female gorillas.

*Female gorilla developmental vector*

The changes observed for the when applying the male gorilla vector of developmental are largely diminished when using females. One does continue to see some increased development of the glabellar region; however, no cranial cresting is present for the female gorilla developmental vector, nor does one see the marked dishing of the supratoral sulcus. The transverse bending across the face remains noticeable, along with the increased facial prognathism. However, the rugged, masculine appearance is absent. None of these results are terribly surprising considering the widely recognized sexual dimorphism present in this extant hominoid species.

## ***H. sapiens* growth vector**

*Male human developmental vector*

We see the smallest degree of morphological change between second and third molar eruption when applying the human developmental vector, regardless of sex. Shape-based differences are difficult to identify when directly comparing MH1 with the simulated adult *Au. sediba* cranium produced from the male human developmental vector. When viewed from frontal perspective, one may notice a slight increase in the angle the superior orbital margin as it approaches glabella. However, there is no noticeable change in either the amount of facial prognathism, nor the degree of transverse bending across the face. We also do not observe any considerable development of the brow-ridge, as described for both the male chimpanzee and gorilla vectors.

*Female human developmental* vector

The changes observed between the original MH1 juvenile cranium and the simulated adult *Au. sediba* cranium are even more minimal when using the female human developmental vector. The morphology of the supraorbital torus becomes thinner and more "delicate" in the female developmental vector. Additionally, the shape of the nasal aperture is more rounded as compared to the original MH1 cranium.

## 4.2 Multivariate comparisons

**Principal components analysis including extant hominoids**

Principal components analysis (PCA) of covariances was conducted on the Procrustes shape coordinates using a subset of 32 landmarks (Fig 7; Table 6) collected from adult chimpanzees and modern humans (Tables 1-3), as well as the hominin fossil sample of *Au. africanus* and early *Homo* crania (Table 4). The position of specimens along the major shape axes, for both extant and fossil specimens, as well as the simulated adult *Au. sediba* crania are illustrated in Figures 12-13. The eigenvalues for this PCA are illustrated in Figure 11, with the exact percentages of variation provided in Table 7. The first axis of variation is primarily driven by length and orientation of the frontal bone. The second component was also strongly influenced by frontal bone morphology, as well as changes in the cheek morphology, with specimens separated based on the overall gracility or robusticity of the zygomatic bone.

All six simulated adult *Au. sediba* crania, whether created using male or female growth trajectories from chimpanzees, gorillas, and humans, fall out together along both axes with the original, juvenile MH1 cranium in a clean grouping relative to other hominoid species in the analysis. One can immediately notice, when examining the distribution of the fossil sample as observed along components 1 and 2 in Figure 12 that all simulated adult *Au. sediba* crania plot together along both axes, with the original MH1 cranium. Further, all early *Homo* crania tend to cluster together, with the exception of OH 24. One oddity for this distribution of specimens along the first and second components was the position of KNM-ER 1470, which plotted most closely to

*Au. africanus* specimen Sts 5. When directly comparing these specimens through visual examination, few morphological similarities exist. However, this proximity vanishes when we examine the third principal component, wherein KNM-ER 1470 plots as a discrete outlier (Figure 13). While cheek morphology is also an important contributer to specimen distribution along the third component, overall facial prognathism is an even stronger determinant. In addition, considering component 2 versus component 3 (Figure 13) KNM-ER 1813, OH24, and the Dmanisi specimen D2700 are separated from the *H. erectus* crania KNM-WT 15000 and KNM-ER 3733. The early *Homo* crania now plot near the cluster of simulated *Au. sediba* crania. One outlier to this latter cluster is the *Au. sediba* cranium generated using a male gorilla developmental vector, which now plots nearest the Stw 53 and Sts 5 crania. This result is not entirely surprising, however, given that one observes the greatest degree of morphological change when applying this vector. Of perhaps more interest is the fact that a male chimpanzee developmental trajectory makes MH1 appear more similar to early *Homo* and modern humans in this test.

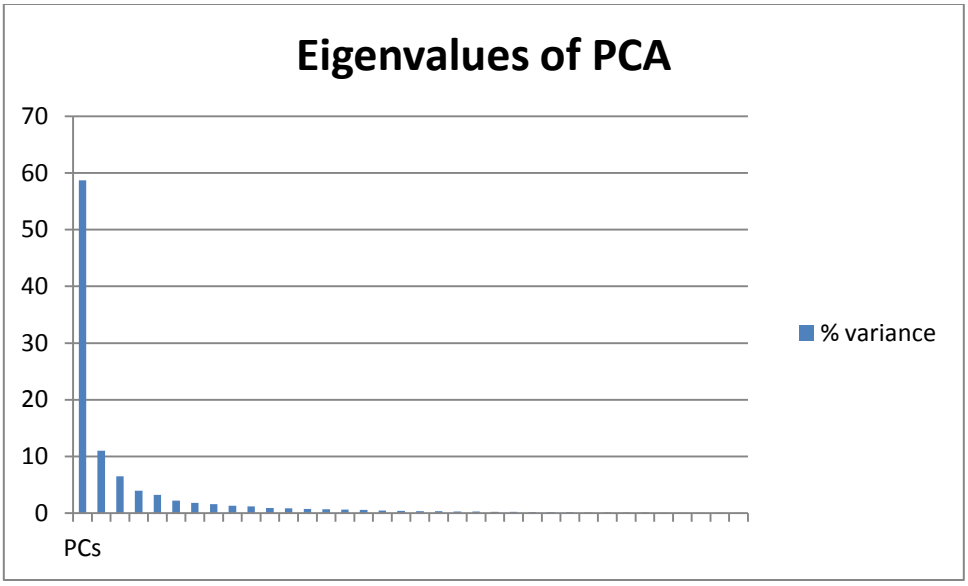


**Figure 11:** Eigenvalues for principal components analysis of Figures 12-13.

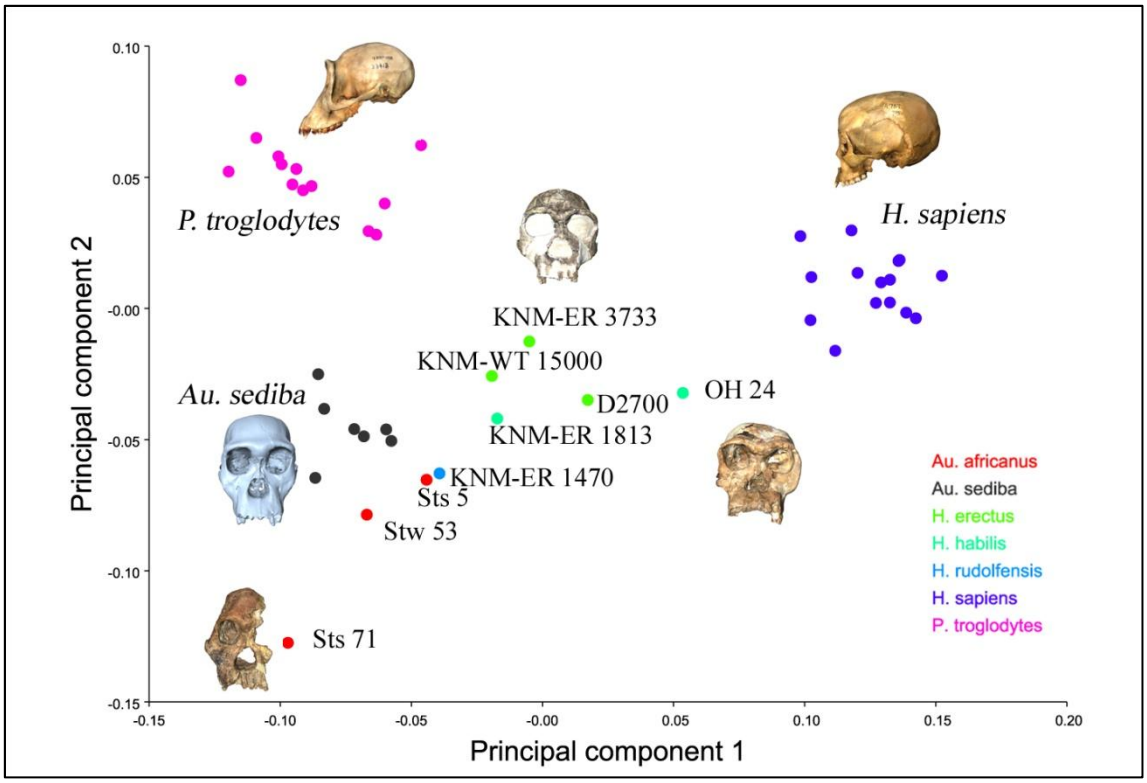


**Figure 12:** A) Principal component 1 (58.7% of variance) versus principal component 2 (11% or variance). B) Principal component 2 versus principal component 3 (6.5% of variance).

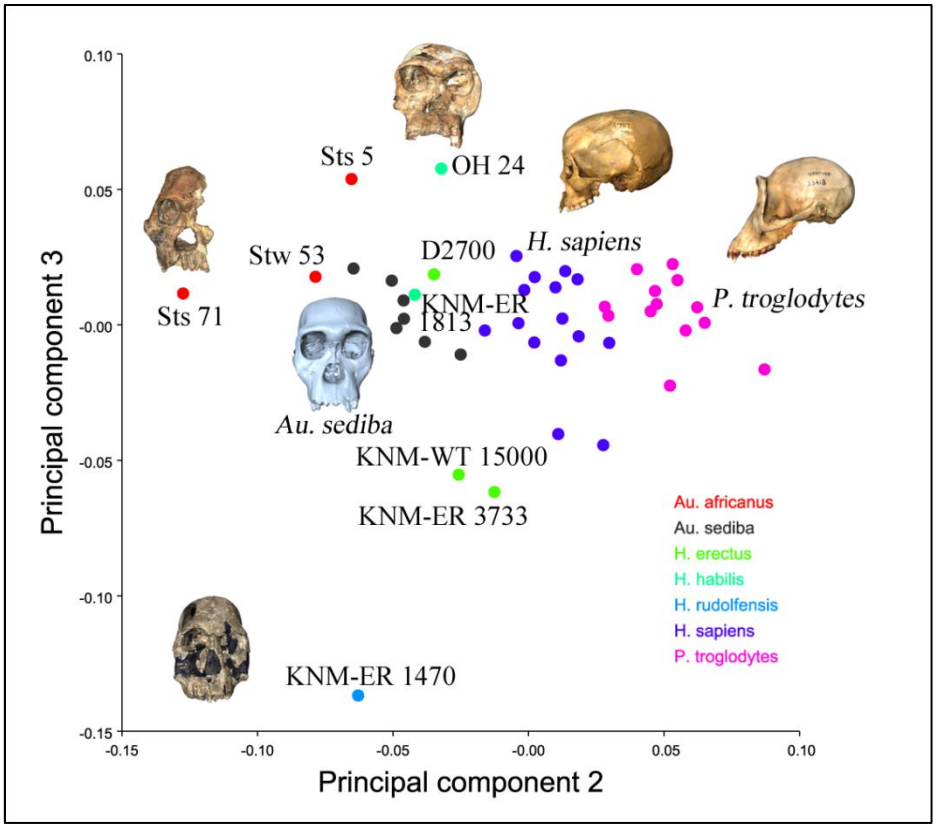


**Figure 13:** Principal component 2 versus principal component 3 (6.5% of variance).

## Principal components analysis using only fossil specimens

One consideration with regard to the prior PCA is the possible influence of extant hominoids with regard to variation along the first principal component axis. In other words, to what extent is the position of the fossil specimens affected by the potential polarizing effects of modern chimpanzees and humans along the major axis of variation? To control for this effect, the present study includes a PCA using only fossil specimens to assess how the distribution of fossil crania changes once these extant crania are removed from the analysis. The results comparing the first through third axes of variation are illustrated in Figures 15-18. Eigenvalues are illutsrated in Figure 14, with

exact percentages of variation provided in Table 8. Figure 16 includes a minimum spanning tree, which serves to link specimens based on the minimum Euclidean distance between them. Therefore, these lines indicate which specimens are separated by the least distance.

Some changes are observed with regard to the distribution of fossils along the first two axes of variation (Fig 15) subsequent to removing the extant hominoids from the analysis. Similar to the PCA including chimpanzees and humans, the first axis of variation is driven by changes in the morphology of the frontal bone and explains 28.3% of the variation, while the second axis explaining 21.7% of the variation is also driven by changes in the morphology of the distal palate, most likely related to the relative degree of facial prognathism among specimens. The zygomatic bone and prosthion were also shown to have high loadings along this axis. When examining specimen distribution along the second component, one can see that specimens are largely separated based on overall facial prognathism, with highly prognathic individuals such as Sts 5 falling at one end of the axis and relatively flat-faced KNM-ER 1470 specimen plotting at the other extreme.

While the *Au. sediba* crania generated using the chimpanzee and modern human developmental vectors continue to plot closely to one another in a very tight cluster, the simulated adults produced from the male and female gorilla developmental vectors showed some dissimilarities relative to other *Au. sediba* specimens. The most noticeable change was that the simulated adult generated from the male gorilla developmental trajectory now plots nearest *Au. africanus* specimen Sts 71. The *Au. sediba* crania

generated using a female gorilla developmental vector plots intermediate to the original MH1 juvenile specimen and Sts 5. Specimen Stw 53 also plots near the clustering of *Au. sediba* specimens. Therefore, the adult *Au. sediba* crania produced from the gorilla developmental trajectory appears to show greater similarities to the *Au. africanus* specimens included in the sample, and Sts 71 in particular.

With regard to the other hominins included in the analysis, one can observe small changes in the distribution of specimens. KNM-ER 1470 is shown to be an outlier along the second axis of variation, widely separated from all other hominins included in the analysis. Interestingly, OH 24 also plots as an outlier, but along the first principal component. Its distance from the other *H. habilis* specimen KNM-ER 1813 suggests that a wide range of morphology is encompassed by these two specimens. *H. erectus* specimens KNM-WT 15000 and KNM-ER 3733 plot nearest to one another, this despite the fact that KNM-WT 15000 is also a juvenile. Early *Homo* specimen KNM-ER 1813 and the Dmanisi specimen D2700 also plot nearest to each other, but are separated from later *H. erectus* along the second principal component. Therefore, while some changes were observed in the overall distribution of the fossil crania, these changes are most strongly reflected in the relative position of adult *Au. sediba* crania produced from the gorilla vectors of development.

As the third principal component also accounts for a substantial amount of the total variation (15.2%), I was interested in examining the fossil distribution along this axis. This third axis of variation was again primarily driven by changes in the frontal bone and palate, although landmarks placed on the nasals and zygomatics also had high

loadings. When comparing principal component 2 versus component 3 (fig 17), all of the *Au. sediba* specimens cluster together. The juvenile specimen D2700 is also shown to plot near this grouping. OH 24 and Sts 5 plot near one another, while KNM-ER 1470 is an outlier along the second component. *H. erectus* specimens KNM-WT 15000 and KNM-ER 3733 continue to plot very closely to one another.

When comparing principal component 1 versus component 3 (Fig 18), the clustering of *Au. sediba* specimens becomes tighter, but again with the exception of the *Au. sediba* adult generated from the male gorilla developmental vector. In this scattergram, D2700 plots nearest KNM-ER 3733 and KNM-WT 15000, while OH 24 is shown to be an outlier. In both scattergrams using the third component, *Au. sediba* was separated from *Au. africanus* individuals along the third axis of variation. However, these plots again illustrate the unique nature of the adult simulated from the male gorilla developmental vector.

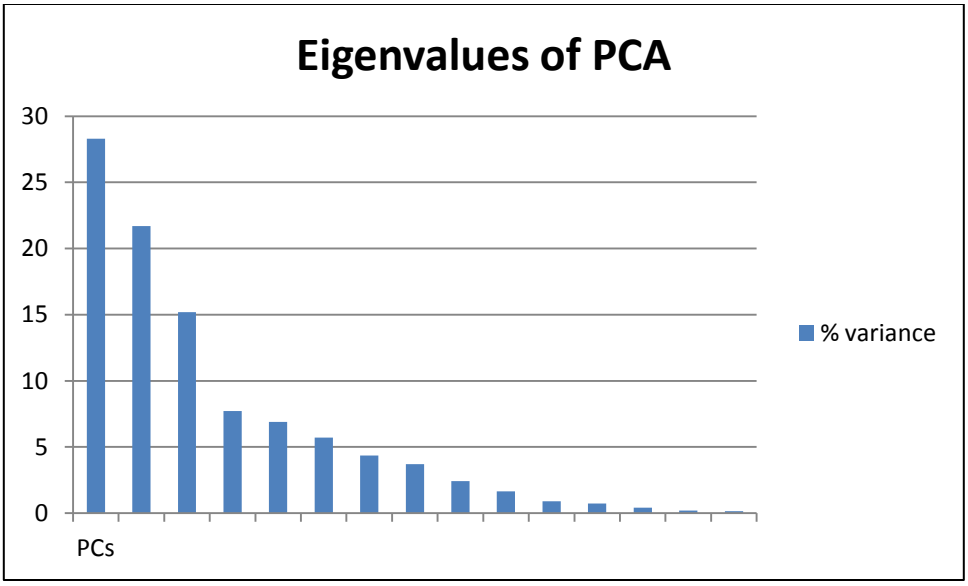


**Figure 14:** Eigenvalues of principal components analysis of Figures 15-18.

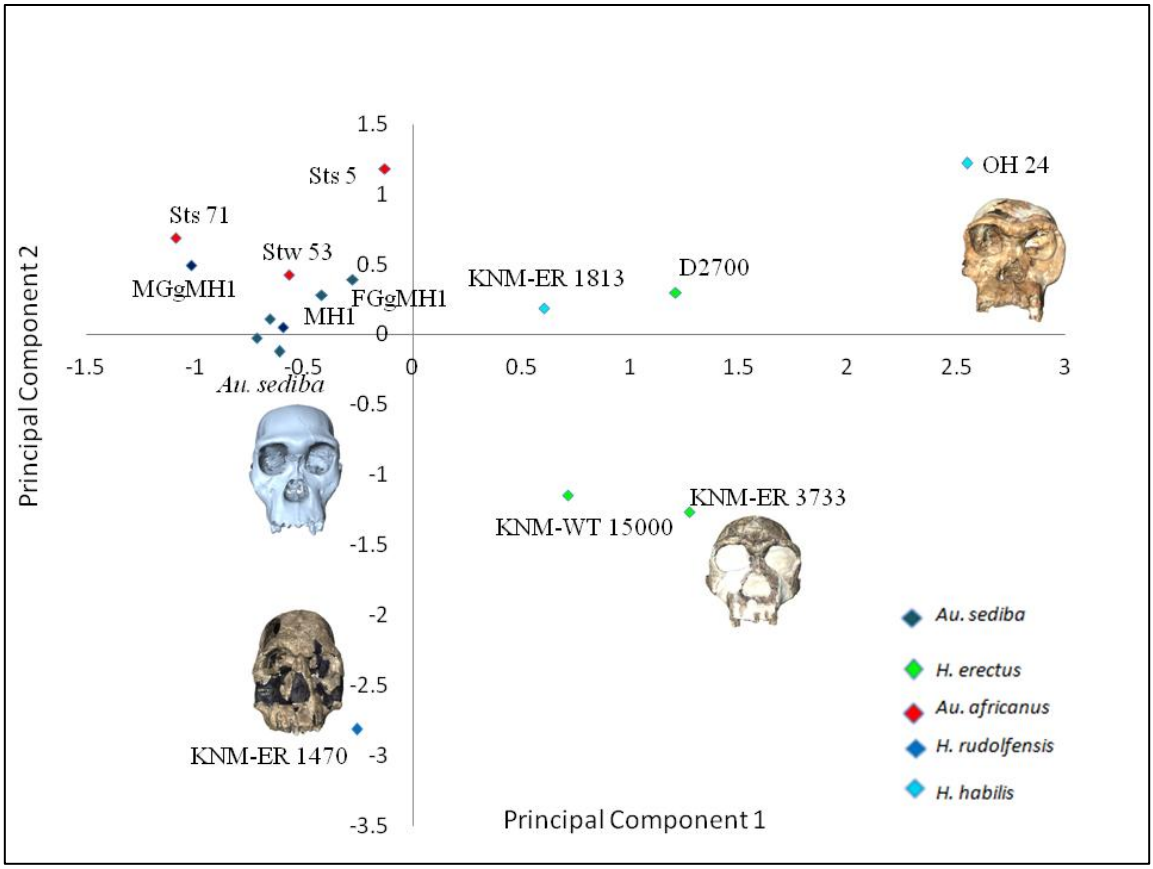


**Figure 15:** Principal component 1(28.3% of variance) versus principal component 2 (21.7% of variance) with no chimpanzees or humans included. MGgMH1 represents the simulated adult generated using the male gorilla developmental vector. FGgMH1represents the simulated adult generated using the female gorilla developmental vector.

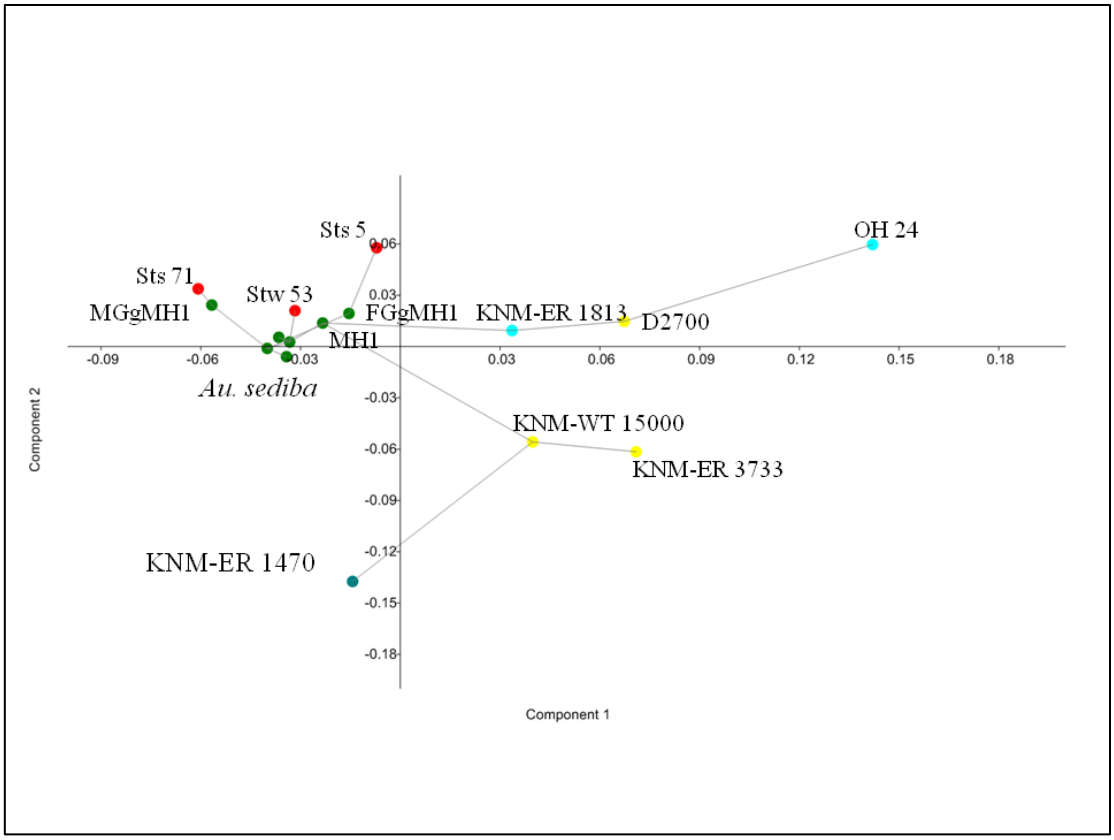


**Figure 16:** Principal components analysis represented in Figure 15 with minimum spanning tree between specimens. MGgMH1 represents the male gorilla developmental vector. FGgMH1 represents the female gorilla developmental vector. MH1 represents the original, juvenile MH1 cranium.

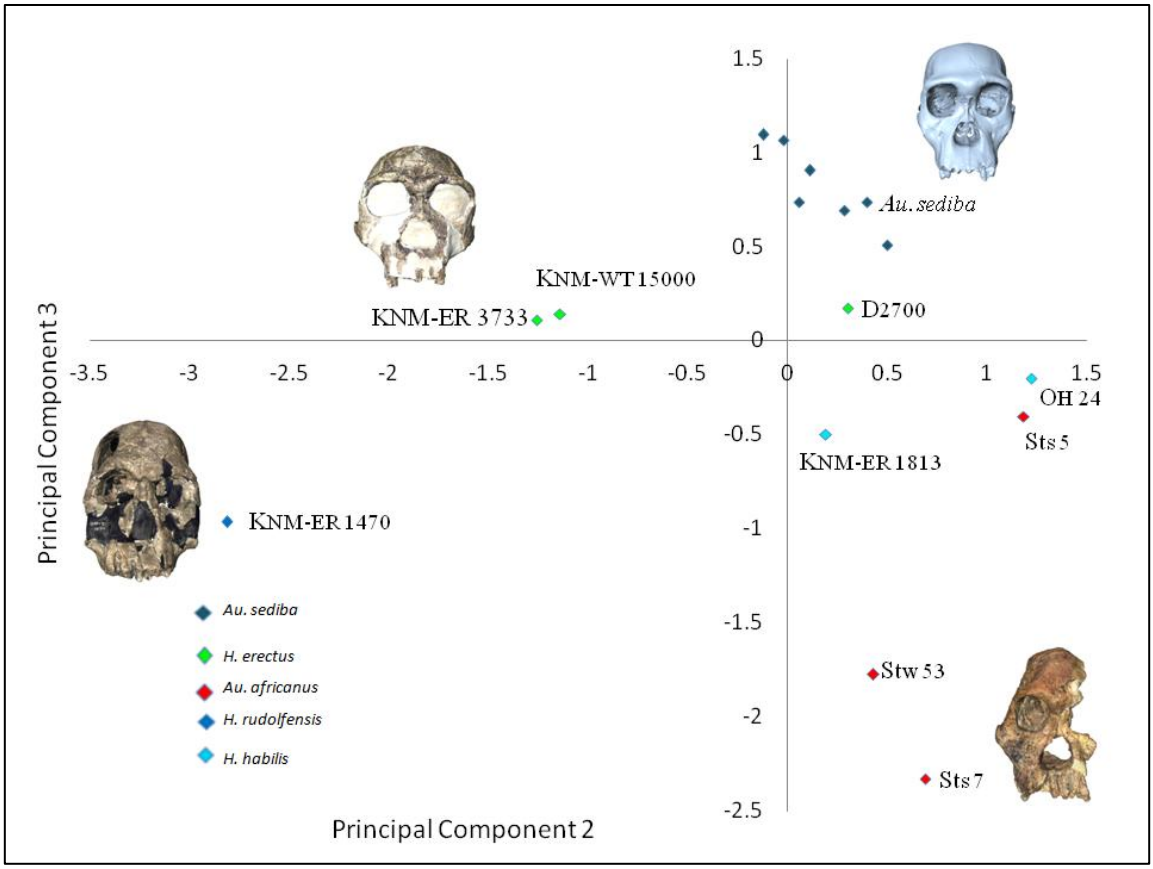


**Figure 17:** Principal component 2 versus principal component 3 (15.2% of variation).

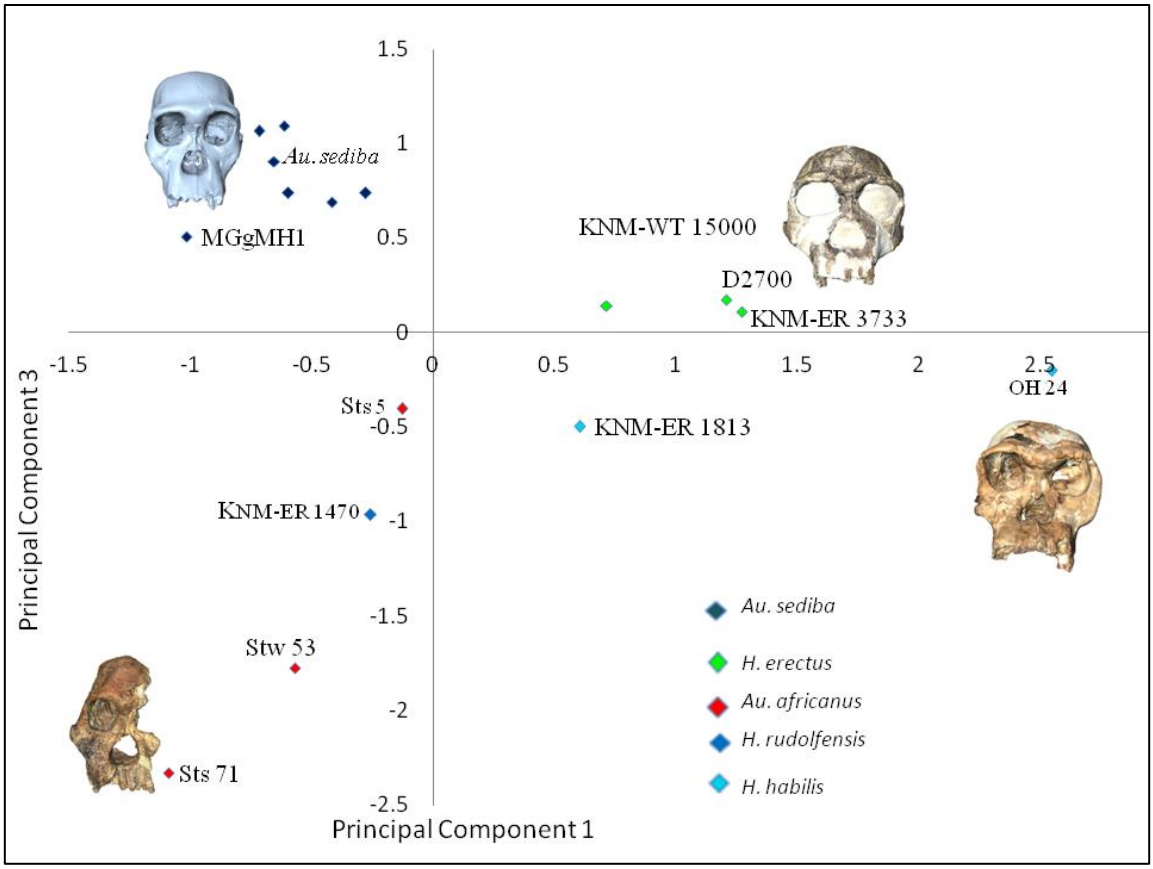


**Figure 18:** Principal component 1 versus principal component 3.

## Procrustes distance matrix analysis within- and between- taxa

Average Procrustes distances both within- and between- taxa were calculated using the same subset of 32 landmarks using Excel software. The resulting matrix is illustrated in Table 9. The purpose of this test was to compare average shape-based distances both within- and among- taxa to determine if the overall distance (i.e. variation) within the *Au. sediba* sample, including all simulated adults and the original juvenile cranium, exceeds that observed in modern hominoid species. One can further compare the average distance between *Au. sediba* and other individual hominin species

to assess group similariteis. The sample of fossil and extant hominoid specimens used in the creation of the Procrustes distance matrix was the same as that used in PCA. As such, an average within-species distance value for *H. rudolfensis* was unavailable, as only a single cranium has been assigned to this species to date.

The most prominent outcome of the Procrustes distance matrix is the average within-group distance for the *Au. sediba* taxon at 0.059. This distance is lower than that observed for the *P. troglodytes* taxon (0.092), as well as that for *H. sapiens* (0.089). Therefore, the within group distance for all generated *Au. sediba* crania, regardless of the developmental vector applied, is well within the range observed for that of extant hominoid species.

When compared to other fossil hominin taxa, *Au. sediba* shows the greatest similarity to *Au. africanus* with a distance of 0.101, followed by *H. erectus* with a distance of 0.112. *Au. sediba* showed the greatest distance when compared to modern *H. sapiens* with a distance of 0.210, followed by *H. rudolfensis* with a value of 0.173. These results further reaffirm Berger et al.'s (2010) interpretation of the morphological similarities of *Au. sediba* as intermediate between *Au. africanus* and early *Homo*, including *H. erectus*.

**Procrustes distance matrix of regression coefficients**

A matrix of distances was calculated using the multivariate regression coefficients calculated from the Procrustes-aligned coordinates (Table 10). These regression coefficients comprised the slope of regression, or developmental vectors, that

were applied to the MH1 cranium to create simulated adults. The Procrustes distance matrix allows for the comparison of the slopes of regression between species to observe to what extent the pattern and degree of developmental change between second and third molar eruption varied between the hominoid species included in the present study.

Generally, distance between slopes of each species were relatively small, with values less than 0.1. The smallest comparative value between vectors was always identified, unsurprisingly, between males and females of the same species. The values were 0.037 between male and female chimpanzees, 0.079 between male and female gorillas, and 0.027 between male and female humans. This indicates that the pattern of developmental change varied the least between male and female humans, reflecting the relatively low degree of sexual dimorphism in modern *H. sapiens*.

The exception to this relatively small variation, however, was the slope of regression for the male gorilla growth vector, with values ranging from 0.12 when compared to the slope of human females, to 0.15 when compared to the slope of male chimpanzees. What this suggests is that the degree of shape change between second and third molar eruption in male gorillas is more extreme than that observed in either humans or chimpanzees. This, in turn, is connected to the marked development of secondary sexual characteristics in the cranium of male gorillas.

The values observed for male chimpanzees ranged from 0.053 when compared to male humans to 0.146 when compared to male gorillas. The relative values were also the same for female chimpanzees, with a value of 0.049 when compared to male humans and a maximum value of 0.142 when compared to male gorillas. The range of values for

male humans ranged from 0.049 when compared to female chimpanzees and 0.126 when compared to male gorillas. Female humans ranged from 0.053 when compared to female chimpanzees and 0.12 when compared to male gorillas. Therefore, the maximum distance for the regression coefficients obtained from both male and female humans and chimpanzees was greatest when compared to the male gorilla developmental vector. This result is in line with the results of the Ackermann and Krovitz (2002) analysis of ontogenetic change, in which they identified significant disparities in growth difference comparisons between gorillas and the other extant species included in their study.

# 5. DISCUSSION

The goal of this study was to test whether or not species specific morphology is established by the eruption of the second molar in extant hominoids, and therefore, whether development of the juvenile type specimen (MH1) is sufficiently complete to allow for reliable phylogenetic analysis of *Au. sediba*. Based upon the results of the qualitative and statistical analyses described above, the null hypothesis of insufficient growth is rejected, and the alternate hypothesis that MH1 had undergone sufficient growth to reflect adult morphology is supported. In other words, development appears to be sufficiently established at the stage of development of MH1 at its age of death to allow for both a species-level diagnosis as well as the reliable comparison of MH1 with other hominin taxa. Qualitative analysis of the simulated adults as visualized through thin-plate splines transformation indicates that the majority of changes expected to occur between second and third molar eruption are related to the development of secondary sexual characteristics. Further, the degree and nature of developmental change associated with the onset of puberty varies among taxa when applied to the MH1 cranium.

Expanding the qualitative comparison of extant developmental vectors, one observed by far the greatest degree of proportional change when applying the male gorilla developmental vector. The simulated adult MH1 cranium produced from the male gorilla vector showed increased development of the supraorbital torus and glabellar region, as well as increased prognathism and transverse bending across the face. These

features also cause it to resemble some specimens assigned to *Au. africanus*, including Sts 71 in particular (Fig. 17). However, this degree of transformation was considerably less when applying the female gorilla developmental vector (Fig 9). Some sex-based morphological changes were also observed when applying the male chimpanzee developmental vector, with similar transformations related to the brow ridge and facial prognathism, although to a lesser degree than that of the male gorilla. Minimal changes were observed, however, when applying the male and female vectors of modern human development between second and third molar eruption.

These results indicate that the developmental changes expected to occur in MH1cranium are indeed related to its age post-puberty and are further dependent upon the relative degree of sexual dimorphism inherent within each extant species. These descriptive observations were supported by the matrix of Procrustes distances of male and female regression coefficients across taxa (Table 10). Based on the results of this matrix comparison, the degree and nature of morphological change differed in male gorillas when compared to chimpanzees and humans of both sexes, as the greatest distance between both male and female humans and chimpanzees results when compared to the regression coefficients of male gorillas. This suggests that perhaps gorillas develop in a different pattern or to a greater extreme between second and third molar eruption than either chimpanzees or humans. However, the greater degree of sexual dimorphism in gorillas is well documented, as described in detail in section 2.7. For these reasons, the author considers the male gorilla developmental vector to be the least

likely to accurately represent the morphological changes set to occur in the *Au. sediba* taxon between second and third molar eruption.

Despite the apparent disparities in the relative development of secondary sexual characteristics, the choice of developmental vector had little impact on the results acquired through the PCA shown in Figure 12, as well as Figures 15-18. In examining the scattergram, all simulated adult *Au. sediba* crania were shown to plot together consistently as a discrete entity, separate from other hominin taxa. This was especially noticeable when comparing the first two principal components (Fig. 12). When comparing sample distribution along principal component two versus principal component three (Fig. 13), the simulated adult *Au. sediba* cranium generated using the male gorilla developmental vector plotted nearest Stw 53, which has been variably argued to represent both *Au. africanus* and early *Homo* as discussed in section 2.4. However, the remaining simulated adults, along with the original MH1 juvenile were shown to cluster nearest specimens assigned to early *Homo*, including *H. habilis* specimen, KNM-ER 1813, and the presumed early *H. erectus* cranium, D2700. In fact, the simulated adult *Au. sediba* cranium created using the male chimpanzee vector was actually shown to plot nearest the modern humans specimens included in the sample. Collectively, the results acquired from the PCA retaining chimpanzees and humans indicates that the *Au. sediba* simulated adults retain their morphological integrity, and distinctiveness when placed in a broader comparative context with other hominin taxa.

This conclusion was further supported in the Procrustes distance matrix analysis comparing average variation within- and between- groups (Table 9). The results of this

distance matrix indicated that the average within-group distance for the simulated *Au. sediba* crania, including the original juvenile cranium, was less than that for extant chimpanzees and modern humans. Therefore, the overall variation within the *Au. sediba* sample is well within the range of living hominoids. This result is in agreement with the output of the PCA discussed above, as well as the conclusion drawn by other researchers that the species diagnostic morphology is established early in ontogeny, prior to first molar eruption (Singleton et al., 2010; McNulty et al., 2006; Ackermann and Krovitz, 2002; Richtsmeier and Walker, 1993). Compared with other fossil hominin taxa, *Au. sediba* was intermediate to its believed ancestor, *Au. africanus*, and later *H. erectus*. This is also in line with the phylogenetic interpretations of *Au. sediba* described in Berger et al. (2010).

However, the statistical results suggest a slightly different conclusion when examining the PCA conducted without the inclusion of chimpanzees and modern humans. Here one observes greater disparities among the sample of *Au. sediba* crania, especially with regard to the models generated using the gorilla developmental vectors (Figs. 15-18). The adult *Au. sediba* crania generated from both male and female human and chimpanzee trajectories illustrated in Figure 15 clustered tightly together as a clean and discrete grouping. However, the original MH1 cranium, as well as the adult model produced from the female gorilla developmental vector, was slightly distanced from the chimpanzee and human simulated *Au. sediba* adults. Sterkfontein specimen, Stw 53, plotted near this cluster as well.

Of particular importance, however, was the position of the *Au. sediba* cranium produced from the male gorilla vector, which was here shown to plot nearest *Au. africanus* specimen Sts 71. And indeed, when directly comparing this simulated adult with the Sts 71 cranium, morphological similarities are clearly noticeable (Fig 19). Similarities are recognizable in the overall development of the glabella, as well as the anterolateral flare of the zygomatic prominence. The shape of the nasal aperture along with the saddle-like nasal region and transverse bending across the face also bear marked resemblance to Sts 71. The overall degree of facial prognathism is also similar to *Au. africanus*. However, the thickening of the frontal process of the zygomatic as well as the brow-ridge development clearly differs from Sts 71. These features, it is believed, are instead related more directly to the nature of development of secondary sexual characteristics in modern gorillas. *Au. africanus* is not known for supraorbital torus development, and in fact this is one of the features said to distinguish *Au. sediba* from earlier *Au. africanus* specimens (Berger et al., 2010).

When including the third axis of variation in scattergrams produced through PCA (Figs 17-18), the sample of *Au. sediba* simulated adults was again shown to cluster together. The exception being the male gorilla developmental vector which was again separated from the remaining individuals when plotting principal component 1 versus principal component 3. This graph again illustrates how this specimen differs in shape space from that of all other simulated adults.

The modern gorilla pattern of growth and development represents the most extreme possibility with regard to sexual dimorphism in hominoids and the related

development of secondary sexual characteristics in the cranium. All currently available evidence concerning sexual dimorphism in the *Au. sediba* taxon indicates that this species was intermediate to the highly dimorphic australopith species, including *Au. afarensis* and *Au. boisei*, and later *H. erectus*. The canine teeth of the presumed male, MH1, are approximately 15% larger than that of the adult female, MH2. MH1 also exhibits larger, more rugose muscle attachment sites throughout the postcranial skeleton, indicating that some degree of sexual dimorphism was present in this species. Greater sample sizes for both male and female representatives of this species are necessary to further our understanding of sexual dimorphism and variability within this taxon. However, no evidence currently exists to suggest that *Au. sediba* would approach the level of dimorphism observed in extant gorillas. For these reasons, it is believed that the gorilla developmental trajectory represents the most extreme and least likely pattern of development for the *Au. sediba* taxon. Rather, the more intermediate chimpanzee represents a more likely trajectory for both the patterning and degree of developmental change in *Au. sediba*.

**Figure 19:** Frontal and lateral comparison of the adult *Au. sediba* cranium generated using the male gorilla developmental vector and *Au. africanus* specimen Sts 71.

# 6. CONCLUSIONS

Upon reviewing the results of the present study, it is reasonable to conclude that the morphological changes expected to occur between second and third molar eruption in the MH1 cranium are unlikely to be substantial enough to alter the current interpretations of this fossil and its morphological affinities as presented in Berger et al. (2010). In other words, had MH1 lived to adulthood, its morphology would look similar enough to its present, juvenile form that we can reliably identify the taxon using this specimen. The developmental changes simulated to occur through geometric morphometrics appear to be strongly related to the onset of puberty and are dependent upon the relative degree of sexual dimorphism inherent in the extant species vector that is applied.

If MH1 is proven to be a male, one can reasonably assume that some further development of masculine features would have occurred as MH1 continued towards adulthood. The supraorbital torus and supratoral sulcus likely would have become more pronounced, combined with a slight increase in facial prognathism. However, the current designation for the Malapa hominins as a unique species separate from *Au. africanus* is unlikely to change unless the degree of sexual dimorphism present within the sample is on a level similar to that of modern gorillas. At present, all currently available evidence indicates that this is highly unlikely and that the level of sexual dimorphism within the Malapa hominin sample is intermediate to that of the highly dimorphic *Au. afarensis* or *Au. boisei* and later *H. erectus*. Further, the total variation

observed within the sample of simulated adults, including the original juvenile cranium (table 8), did not exceed that of modern humans or chimpanzees. This indicates that, regardless of the developmental vector that is applied, the sample of *Au. sediba* crania remains a discrete phenon, separate from other species.

Following upon these analyses, the larger question remains: how do the results of this study impact our understanding of *Au. sediba* and its broader role in the ancestry of the genus *Homo*? Generally, the results reported here indicate that the morphological traits believed to align *Au. sediba* with later representatives of the genus *Homo* are unlikely to change by any significant degree. Craniofacial features such as the supraorbital torus and sulcus, limited post-orbital constriction, squared upper facial profile, and gracile zygomatics with limited lateral flaring did not change by any large degree in the chimpanzee or human developmental vectors. This is especially true with regard to all simulated adults resulting from the application of female developmental vectors. The mosaic morphology and intermediate traits, aligning MH1 with both *Australopithecus* and the genus *Homo* remain present throughout the remaining period of development between second and third molar eruption.

Likewise, the morphological characters that led Berger et al. (2010) to classify *Au. sediba* within the genus *Australopithecus* are observable in the steep zygomaticoalveolar crest and large and block-like glabellar prominence. Further, as MH1 had achieved 95% of its estimated cranial capacity at age of death (Berger et al., 2010), the limited brain size would have remained within the range of *Australopithecus*. As such, the results of this study do not indicate that a reclassification of the Malapa

hominins to the genus *Homo* is needed, as some commentators have suggested (Balter, 2010).

Additional conclusions resulting from this study relate to the critical importance of separating developmental vectors by sex when practicing developmental simulation through geometric morphometrics. While the assignment of fossil crania to male or female sex is typically uncertain, lacking pelvic remains, a tremendous amount of morphological variation would have been obscured had male and female adults been pooled in a multivariate regression. The slope of change likely would have been reduced, and the considerable influence of secondary sexual characteristics on the simulated adult forms would have been blurred. These variations between sexes are viewed as especially vital to the present study given the period of developmental change under question. As such, it is the strong recommendation of the author that all studies involving developmental simulation separate vectors by sex when possible.

To summarize, the results of this study highlight the practicality and importance of 3D geometric morphometric tools for investigating questions of ontogeny and developmental change in the hominin fossil record. The visualizations produced through this analysis allowed for detailed qualitative analysis of simulated 3D forms, as well as quantitative comparison of the virtual adult crania in the broader context of the hominin fossil record. Sexual dimorphism and puberty can have a significant impact on morphology between second and third molar eruption; however, barring dimorphism to the level of extant gorillas, subsequent developmental changes for the MH1 individual are unlikely to impact the hypotheses or species designation for the Malapa hominins as

presented by Berger et al. (2010). The comparative analyses presented here indicate that male gorillas develop in a different pattern and to a greater extent than either humans or chimpanzees during puberty. In conclusion, the degree and nature of morphological change expected to occur between MH1's current stage of development and full adulthood would not significantly alter our current understanding of its morphological affinities as intermediate to *Au. africanus* and later representatives of the genus *Homo*.

# REFERENCES


Abdi, H, Williams, LJ. 2010. Principal component analysis. Wiley Interdiscip Rev Comput Stat 2: 1-45.

Ackermann, RR, Krovitz, GE. 2002. Common patterns of facial ontogeny in the hominid lineage. Anat Rec 269: 142-147.

Adams, DC, Rohlf, JF, Slice, DE. 2004. Geometric morphometrics: ten years of progress following the 'revolution'. Ital J Zool 71: 5-16.

Ahern, JCM. 1998. Underestimating intraspecific variation: the problem with excluding Sts 19 from *Australopithecus africanus*. Am J Phys Anthropol 105: 461-480.

Alexeev, V. 1986. The origin of the human race. Moscow: Progress.

Asfaw, B, White, T, Lovejoy, O, Latimer, B, Simpson, S, Suwa, G. 1999. *Australopithecus garhi*: a new species of early hominid from Ethiopia. Science 284: 629-635.

Balter, M. 2010. Candidate human ancestor for South Africa sparks praise and debate. Science 328: 154-155.

Bamford, MK, Neumann, FH, Pereira, LM, Scott, L, Dirks, PHGM, Berger, LR. 2010. Botanical remains from a coprolite from the Pleistocene hominin site of Malapa, Sterkfontein Valley, South Africa. Palaeont Afr 45: 23-28.

Bastir, M, Rosas, A. 2004. Comparative ontogeny in humans and chimpanzees: similarities, differences and paradoxes in postnatal growth and development of the skull. Ann Anat 186: 503-509.

Bastir, M, O'Higgins, P, Rosas, A. 2007. Facial ontogeny in Neanderthals and modern humans. Proc Biol Sci 274: 1125-1132.

Beltzer, C, Ring, U. 1995. Sedimentology of the Malawi Rift: facies and stratigraphy of the Chiwondo Beds, northern Malawi. J Hum Evol 28: 23-35.

Berger, LR., de Ruiter, DJ, Churchill, SE, Schmid, P, Carlson, KJ, Dirks, PHGM, Kibii, JM. 2010. *Australopithecus sediba*: a new species of Homo-like australopith from South Africa. Science 328: 195-204.

Blumenschine, RJ, Peters, CR, Masao, FT, Clarke, RJ, Deino, AL, Hay, RL, Swisher, CC, Stanistreet, IG, Ashley, GM, McHenry, LJ, Sikes, NE, van der Merwe, NJ, Tactikos, JC, Cushing, AE, Deocampo, DM, Njau, JK, Eberg, JI. 2003. Late Pliocene *Homo* and hominid land use from western Olduvai Gorge, Tanzania. Science 299: 1217-1221.

Boesch, C, Boesch-Ackermann, H. 2000. The chimpanzees of the Taï Forest: behavioral ecology and evolution. New York: Oxford University Press.

Bookstein, FL. 1991. Morphometric tools for landmark data: geometry and biology. Cambridge: Cambridge University Press.

Brace, CL. 1972. Sexual dimorphism in human evolution. Yearb Phys Anthropol 16: 31-49.

Bromage, TG, Dean, CM. 1985. Re-evaluation of the age at death of immature fossil hominids. Nature. 317: 525-527.

Bromage, TG, Schrenk, F, Zonnvel, FW. 1995. Paleoanthropology of the Malawi Rift: an early hominid mandible from the Chiwondo beds, northern Malawi. J Hum Evol 28: 71-108.

Broom, R, Robinson, JT, Schepers, G. 1950. The Sterkfontein ape-man *Plesianthropus transvaalensis*. Transvaal Museum Memoir 4, Pretoria.

Brunet, M, Guy, F, Pilbeam, D, Taisso, M, Likius, A, Ahounta, D, Beauvilain, A, Blondel, C, Bocherens, H, Boisserie, JF, De Bonis, L, Coppens, Y, Dejax, J, Denys, C, Duringer, P, Eisenmann, V, Fanone, G, Fronty, P, Geraads, D, Lehmann, T, Lihoreau, F, Louchart, A, Mahamat, A, Merceron, G, Mouchelin, G, Otero, O, Campomanes, PP, Ponce de Leon, M, Rage, JC, Sapanet, M, Schuster, M, Sudre, J, Tassy, P, Valentin, X, Vignaud, P, Viriot, L, Zazzo, A, Zollikofer, C. 2002. A new hominid from the upper Miocene of Chad, Central Africa. Nature 418: 145-151.

Buikstra, JE, Ubelaker, DH, editors. 1994. Standards for Data Collection from Human Skeletal Remains. Arkansas Archaeological Survey Research Series No 44.

Campbell, NA, Atchley, WR. 1981. The geometry of canonical variate analysis. Syst Zool 30: 268-280.

Carlson, KJ, Stout, D, Jashashvili, de Ruiter, DJ, Tafforeau, P, Carlson, K, Berger, LR. 2011. The endocast of MH1, *Australopithecus sediba*. Science 333: 1402-1407.

Chamberlain, AT, Wood, BA. 1987. Early hominid phylogeny. J Hum Evol 16: 119-133.

Cherry, M. 2010. Claim over 'human ancestor' sparks furore. Nature doi:10.1038/news.2010.171.

Clark, WE Le Gross. 1947. Observations on the anatomy of the fossil Australopithecinae. J Anat 81: 300-333.

Clarke, RJ. 1977. A juvenile cranium and some adult teeth of early *Homo* from Swartkrans, Transvaal. S Afr J Sci 73: 46-49.

Clarke, RJ. 1985. *Australopithecus* and early *Homo* in southern Africa. In: Delson, E, editor. Ancestors: the hard evidence. New York: Alan R. Liss, Inc. p 171-177.

Clarke, RJ. 2008. Latest information on Sterkfontein's *Australopithecus* skeleton and a new look at *Australopithecus*. S Afr J Sci 104: 443-449.

Cobb, SN, O'Higgins, P. 2004. Hominins do not share a common postnatal facial ontogenetic shape trajectory. J Exp Zool 302: 302-321.

Copeland, SR, Sponheimer, M, de Ruiter, DJ, Lee-Thorp, J, Codron, D, le Roux, PJ, Vaughan, G, Richards, MP. 2011. Strontium isotope evidence for landscape use by early hominins. Nature 474: 76-79.

Cronin, JE, Boaz, NT, Stringer, CB, Rak, Y. 1981. Tempo and mode in hominid evolution. Nature 292: 113-122.

Curnoe, D. 2010. A review of early *Homo* in southern Africa focusing on cranial, mandibular and dental remains, with the description of a new species (*Homo gautengensis* sp nov.) Homo 61: 151-177.

Curnoe, D, Tobias, PV. 2006. Description, new reconstruction, comparative anatomy, and classification of the Sterkfontein Stw 53 cranium, with discussions about the taxonomy of other southern African early *Homo* remains. J Hum Evol 50: 36-77.

Dart, RA. 1925. *Australopithecus africanus*: the man-ape of South Africa. Nature. 115:195-199.

Dayal, MR, Kegley, ADT, Štrkalj, G, Bidmos, MA, Kuykendall, KL. 2009. The history and composition of the Raymond A. Dart collection of human skeletons at the University of the Witwatersrand, Johannesburg, South Africa. Am J Phys Anthopol 140: 324-335.

Dean, MC, Lucas, VS. 2009. Dental and skeletal growth in early fossil hominins. Ann Hum Biol 36: 545-561.

Dean, MC, Wood, BA. 1982. Basicranial anatomy of Plio-Pleistocene hominids from East and South Africa. Am J Phys Anthropol 59: 157-174.

Delson, E, Eldredge, N, Tattersall, I. 1977. Reconstruction of hominid phylogeny: a testable framework based on cladistic analysis. J Hum Evol 6: 263-278.

de Ruiter, DJ, Carlson, KB, Churchill, SE, Carlson, KJ, Tafforeau, P, Berger, LR. The skull of *Australopithecus sediba*. Science. In preparation.

de Ruiter, DJ, Churchill, SE, Berger, LR. 2013a. *Australopithecus sediba* from Malapa, South Africa. In: Reed, KE, Fleagle, JG, Leakey, RE, editors. The paleobiology of *Australopithecus*: vertebrate paleobiology and paleoanthropology series. Netherlands: Springer. p 147-160.

de Ruiter, DJ, DeWitt, TJ, Carlson, KB, Brophy, JK, Schroeder, L, Ackermann, RR, Churchill, SE, Berger, LR. 2013b. Mandibular remains support taxonomic validity of *Australopithecus sediba*. Science. 340: 1232997-1-4.

Dirks, PHGM, Kibii, JM, Kuhn, B, Steininger, C, Churchill, SE, Kramers, JD, Pickering, R, Farber, DL, Mériaux, A, Herries, AIR, King, GCP, Berger, LR. 2010. Geological setting and age of *Australopithecus sediba* from southern Africa. Science 328: 205-208.

Dixson, AF. 2009. Sexual selection and the origins of human mating systems. Oxford: Oxford University Press.

Eldredge, N, Tattersall, I. 1975. Evolutionary models, phylogenetic reconstruction, and another look at hominid phylogeny. In: Szalay, F.S., editor. Approaches to primate paleobiology: contributions to primatology, vol. 5. New York: Karger. p. 218-242.

Ferring, R, Oms, O, Agustí, J, Berna, F, Nioradze, M, Shelia, T, Tappen, M, Vekua, A, Zhvania, D, Lordkipanidze, D. 2011. Earliest human occupations at Dmanisi (Georgian Caucasus) dated to 1.85-1.78 Ma. Proc Natl Acad Sci 108: 10432-10436.

Galdikas, BMF, Wood, JW. 1990. Birth spacing patterns in humans and apes. Am J Phys Anthropol 83: 185-191.

Gibbons A. 2001. Studying humans--and their cousins and parasites. Science 292: 627-629.

Glantz, MM, Athreya, S, Ritzman, T. 2009. Is Central Asia the eastern outpost of the Neandertal range? A reassessment of the Teshik-Tash child. Am J Phys Anthropol 138: 45-61.

Gordon, AD, Green, DJ, Richmond, BG. 2008. Strong postcranial size dimorphism in *Australopithecus afarensis*: results from two new resampling methods for multivariate data sets with missing data. Am J Phys Anthropol 135: 311-328.

Gower, JC. 1975. Generalized Procrustes analysis. Psychometrika 40: 33-51.

Greenfield, LO. 1992. Origin of the human canine: a new solution to an old enigma. Yearb Phys Anthropol 35: 153-185.

Gremitsky, MA. 1949. The skull of the Neandertal child from the cave of Teshik-Tash, southern Uzbekistan. In: Gremiatsky, MA, Nesturkh, MF, editors. Teshik Tash: Paleolithic man. Moscow: Moscow State University. p 137-182.

Gunz, P, Bulygina, E. 2012. The Mousterian child from Teshik-Tash is a Neanderthal: a geometric morphometric study of the frontal bone. Am J Phys Anthropol 149: 365-379.

Gunz, P, Neubauer, S, Maureille, B, Hublin, JJ. 2010. Brain development after birth differs between Neanderthals and modern humans. Curr Biol 20: 921-922.

Gunz, P, Neubauer, S, Golovanova, L, Doronichev, V, Maureille, B, Hublin, JJ. 2012. A uniquely modern human pattern of endocranial development. Insights from a new cranial reconstruction of the Neandertal newborn from Mezmaiskaya. J Hum Evol 62: 300-313.

Gustafsson, A, Lindensfors, P. 2004. Human size evolution: no evolutionary relationship between male and female stature. J Hum Evol 47: 253-266.

Harcourt, AH, Fossey, D, Stewart, KJ, Watts, DP. 1980. Reproduction in wild gorillas and some comparisons with chimpanzees. J Reprod Fertil Suppl. S 28: 59-60.

Harmon, EH. 2006. Size and shape of *Australopithecus afarensis* proximal femora. J Hum Evol 51: 217-227.

Henry, AG, Ungar, PS, Passey, BH, Sponheimer, M, Rossouw, L, Bamford, M, Sandberg, P, de Ruiter, DJ, Berger, LR. 2012. The diet of *Australopithecus sediba*. Nature 487: 90-93.

Herries, IR, Shaw, J. 2011. Palaeomagnetic analysis of the Sterkfontein palaeocave deposits: Implications for the age of the hominin fossils and stone tool industries. J Hum Evol 60: 523.

Hill, A, Ward, S, Deino, A, Curtis, G, Drake, R. 1992. Earliest *Homo*. Nature 355: 719-722.

Howell, FC. 1978. Hominidae. In: Maglio, VJ, Cooke, HSB, editors. Evolution of African mammals. Cambridge: Harvard University Press. p 152–248.

Howell, FC, Haesaerts, P, de Heinzelin, J. 1987. Depositional environments, archaeological occurrences and hominids from Members E and F of the shungura Formation (Omo basin, Ethiopia). J Hum Evol 16: 665.

Hublin, JJ. 2009. The origin of Neandertals. Proc Natl Acad Sci USA 106: 16022-16027.

Hublin, JJ. 2014. Paleoanthropology: *Homo erectus* and the limits of a paleontological species. Curr Biol 24: 82-84.

Hughes, AR, Tobias, PV. 1977. A fossil skull probably of the genus *Homo* from Sterkfontein, Transvaal. Nature 265: 310-312.

Jelinek, J, Dupree, L, Gallus, A, Gams, H, Narr, KJ, Poulianos, AN, Sackett, JR, Schott, L, Suchy, J, Yakimov, VP. 1969. Neanderthal Man and the *Homo sapiens* in Central and Eastern Europe. Curr Anthropol 10: 475-503.

Johanson, DC, White, TD. 1979. A systematic assessment of early African hominids. Science 203: 321-330.

Jungers, WL, Stern, JT. 1983. Body proportions, skeletal allometry and locomotion in the Hadar hominids: a reply to Wolpoff. J Hum Evol 12: 673-684.

Kharitonov, V. 2009. Age status of the Neanderthal child from Teshik-Tash in relation to its position within the Neanderthal clade. In: International conference "Man and its social and biological environment." p 10-19.

Kibii, JM, Churchill, SE, Schmid, P, Carlson, KJ, Reed, ND, de Ruiter, DJ, Berger, LR. 2011. A partial pelvis of *Australopithecus sediba*. Science 333: 1407-1411.

Kimbel, WH. 2009. The origin of *Homo*. In: Grine, FE, Fleagle, JG, Leakey, REF, editors. The First Humans: origin and early evolution of the genus *Homo*. New York: Springer. p 31-37.

Kimbel, WH. 2013. Hesitation on hominin history. Nature 497: 573-574.

Kimbel, WH, Delezene, LK. 2009. "Lucy" redux: a review of research on *Australopithecus afarensis.* Yearb Phys Anthropol. 52: 2-48.

Kimbel, WH, Rak, Y. 1993. The importance of species taxa in paleoanthropology and an argument for the phylogenetic concept of the species category. In: Kimbel, WH, Martin, LB, editors. Species, Species Concepts, and Primate Evolution. New York: Plenum. p 461-484.

Kimbel, WH, Johanson, DC, Rak, Y. 1997. Systematic assessment of a maxilla of *Homo* from Hadar, Ethiopia. Am J Phys Anthropol 103: 235-262.

Kimbel, WH, Walter, RC, Johanson, DC, Reed, KE, Aronson, JL, Assefa, Z, Marean, CW, Eck, GG, Bobe, R, Hovers, E, Rak, Y, Vondra, C, Yemane, T, York, D, Chen, Y, Evensen, NM, Smith, PE. 1996. Late Pliocene *Homo* and Oldowan tools from the Hadar Formation (Kada Hadar Member), Ethiopia. J Hum Evol 31: 549-561.

Kivell, TL, Kibii, JM, Churchill, SE, Schmid, P, Berger, LR. 2011. *Australopithecus sediba* hand demonstrates mosaic evolution of locomotor and manipulative abilities. Science 333: 1411-1417.

Klingenberg, CP. 2011. MorphoJ: an integrated software program for geometric morphometrics. Mol Ecol Resour 11: 353-357.

Kuhn, BF, Werdelin, L, Hartstone-Rose, A, Lacruz, RS, Berger, LR. 2011. Carnivoran remains from the Malapa hominin site, South Africa. PLoS One 6: e26940.

Kuman, K, Clarke, RJ. 2000. Stratigraphy, artefact industries and hominid association for Sterkfontein, Member 5. J Hum Evol 38: 827-847.

Leakey, LSB, Tobias, PV, Napier, JR. 1964. A new species of the genus *Homo* from Olduvai Gorge. Nature 202: 7-9.

Leakey, ME, Spoor, F, Brown, FH, Gathogo, PN, Kiarie, C, Leakey, LM, McDougall, I. 2001. New hominin genus from eastern Africa shows diverse middle Pliocene lineages. Nature 410: 433-440.

Leakey, MG, Spoor, F, Dean, MC, Feibel, CS, Antón, SC, Kiarie, C, Leakey, LN. 2012. New fossils from Koobi Fora in northern Kenya confirm taxonomic diversity in early *Homo*. Nature 488: 201-204.

Leakey, REF. 1973. Evidence for an advanced Plio-Pleistocene hominid from East Rudolf, Kenya. Nature 242: 447-450.

Le Cabec, A, Tafforeau, P, Smith, TM, Carlson, KJ, Berger, LR. 2014. Dental development of the *Australopithecus sediba* juvenile MH1 determined from synchrotron virtual paleobiology. Am J Phys Anthropol S58: 166.

Leutenegger, W, Kelly, JT. 1977. Relationship of sexual dimorphism in canine size and body size to social, behavioral, and ecological correlates in anthropoid primates. Primates 18: 117-136.

Lockwood, CA. 1999. Sexual dimorphism in the face of *Australopithecus africanus*. J Hum Evol 31: 537-548.

Lockwood, CA, Kimbel, WH, Lynch, J. 2002. Temporal bone morphology and earliest *Homo*. Am J Phys Anthropol S34: 102.

Lockwood, CA, Richmond, BG, Jungers, WL, Kimbel, WH. 1996. Randomization procedures and sexual dimorphism in *Australopithecus afarensis*. J Hum Evol 39: 23-55.

Lordkipanidze, D, Ponce de León, MS, Margvelashvili, A, Rak, Y, Rightmire, GP, Vekua, A, Zollikofer, CPE. 2013. A complete skull from Dmanisi, Georgia, and the evolutionary biology of early *Homo*. Science 342: 326-331.

Lordkipanidze, D, Vekua, A, Ferring, R, Rightmire, GP, Zollikofer, CPE, Ponce de León, MS, Agusti, J, Kiladze, G, Mouskhelishvili, A, Medea, N, Tappen, M. 2006. A fourth hominin skull from Dmanisi, Georgia. Anat Rec 288: 1146-1157.

Martyn, J. 1967. Pleistocene deposits and new fossil localities in Kenya. Nature 215: 476-479.

McHenry, HM. 1991. Sexual dimorphism in *Australopithecus afarensis*. J Hum Evol 20: 21-32.

McHenry, HM, Coffing, K. 2000. *Australopithecus* to *Homo*: transformations in body and mind. Annu Rev Anthropol 29: 125-146.

McNulty, KP, Frost, SR, Strait, DS. 2006. Examining affinities of the Taung child by developmental simulation. J Hum Evol 51: 274-296.

Mitteroecker, P, Gunz, P, Bernhard, M, Schaefer, K, Bookestein, FL. 2004. Comparison of cranial ontogenetic trajectories among great apes and human. J Hum Evol 46: 679-798.

Moggi-Cecchi, J, Tobias, PV, Beynon, AD. 1998. The mixed dentition and associated skull fragments of a juvenile fossil hominid from Sterkfontein, South Africa. Am J Phys Anthropol 106: 425-465.

Nelson, E, Rolian, C, Cashmore, L, Shultz, S. 2011. Digit ratios predict polygyny in early apes, *Ardipithecus*, Neanderthals and early modern humans but not in *Australopithecus*. Philos Trans R Soc Lond, B 278: 1556-1563.

Neubauer, S, Gunz, P, Hublin, J. 2010. Endocranial shape changes during growth in chimpanzees: a morphometric analysis of unique and shared aspects. J Hum Evol 59: 555-566.

O'Higgins, P. 2000a. Quantitative Approaches to the Study of Craniofacial Growth and Evolution: Advances in Morphometric Techniques: Development, Growth and Evolution. San Diego: Academic Press.

O'Higgins, P. 2000b. The study of morphological variation in the hominid fossil record: biology, landmarks and geometry. J Anat 197: 103–120.

Okladnikov, AP. 1949. Investigations of the Mousterian site and the Neanderthal burial at the Teshik-Tash grotto, South Uzbekistan (Central Asia). In Gremiatsky MA, Nesturkh, MF, editors. Teshik Tash: paleolithic man: Moscow: Moscow State University. p 7-85.

Olivier, G. 1976. The stature of Australopithecines. J Hum Evol 5:529-534.

Parnell, RJ. 2002. Group size and structure in western lowland gorillas (*Gorilla gorilla gorilla*) at Mbeli Bai, Republic of Congo. Am J Primatol. 56: 193-206.

Pickering, R, Kramers, JD. 2010. Re-appraisal of the stratigraphy and determination of new U-Pb dates for the Sterkfontein hominin site, South Africa. J Hum Evol 59: 70.

Pickering, R, Dirks, PHGM, Jinnah, Z, de Ruiter, DJ, Churchill, SE, Herries, AIR., Woodhead, JD, Hellstrom, JC, Berger, LR. 2011. *Australopithecus sediba* at 1.977 Ma and implications for the origin of the genus *Homo*. Science 333: 1421-1423.

Plavcan JM. 1999. Mating systems, intrasexual competition and sexual dimorphism in primates. In: Lee, PC, editor. Comparative Primate Sociology. United Kingdom: Cambridge University Press. p 241-260.

Plavcan, JM. 2012. Sexual size dimorphism, canine dimorphism, and male-male competition in primates: where do humans fit in? Hum Nat 23: 45-67.

Plavcan, JM, Ward, CV, Paulus, FL. 2009. Estimating canine tooth crown height in early *Australopithecus*. J Hum Evol 57: 2-10.

Ponce de León, MS, Zollikofer, CPE. 2001. Neanderthal cranial ontogeny and its implications for late hominid diversity. Nature 412:534–538.

Prat, S, Brugal, JP, Tiercelin, JJ, Barrat, JA, Bohn, M, Delagnes, A, Harmand, S, Kimeu, K, Kibunjia, M, Texier, PJ, Roche, H. 2005. First occurrence of early *Homo* in the Nachukui Formation (West Turkana, Kenya) at 2.3-2.4 Myr. J Hum Evol 49: 230-240.

Puts, DA. 2010. Beauty and the beast: mechanisms of sexual selection in humans. Evol Hum Behav. 31: 157-175.

Rak, Y. 1983. The australopithecine face. New York: Academic Press.

Reno, PL, McCollum, MA, Meindl, RS, Lovejoy, CO. 2010. An enlarged postcranial sample confirms *Australopithecus afarensis* dimorphism was similar to modern humans. Philos Trans R Soc Lond, B 365: 3355-3363.

Reno, PL, Meindl, RS, McCollum, MA, Lovejoy, CO. 2003. Sexual dimorphism in *Australopithecus afarensis* was similar to that of modern humans. Proc Natl Acad Sci 100: 9404-9409.

Richmond, BG, Jungers, WL. 1995. Size variation and sexual dimorphism in *Australopithecus afarensis* and living hominoids. J Hum Evol 29: 229-245.

Richtsmeier JT, Walker A. 1993. A morphometric study of facial growth. In: Walker, A, Leakey, R, editors. The Nariokotome *Homo erectus* skeleton. Cambridge: Harvard University Press. p 391–410.

Richtsmeier, JT, Cheverud, JM., Lele, S. 1992. Advances in anthropological morphometrics. Annu Rev Anthropol 21: 283-305

Robinson, JT. 1965. *Homo 'habilis'* and the australopithecines. Nature 205:121-124

Robinson, JT. 1966. The distinctiveness of *Homo habilis*. Nature 209: 957-960.

Rohlf, FJ, Slice, D. 1990. Extensions of the Procrustes method for the optimal superimposition of landmarks. Syst Zool 39: 40-59.

Rosas, A. 2001. Occurrence of Neanderthal features in mandibles from the Atapuerca-SH site. Am J Phys Anthropol 114: 74-91.

Schmid, P, Churchill, SE, Nalla, S, Weissen, E, Carlson, KJ, de Ruiter, DJ, Berger, LR. 2013. Mosaic morphology in the thorax of *Australopithecus sediba*. Science 340: 1234598-1-5.

Schrenk, F, Bromage, TG, Betzler, CG, Ring, U, Juwayeyi, YM. 1993. Oldest *Homo* and Pliocene biogeography of the Malawi Rift. Nature 365: 833-836.

Schwartz, JH, Tattersall, I, Chi, Z. 2014. Comment on "A complete skull from Dmanisi, Georgia, and the evolutionary biology of early *Homo*". Science 344: 1250056-360a.

Scott, JE, Stroik, LK. 2006. Bootstrap tests of significance and the case for humanlike skeletal-size dimorphism in *Australopithecus afarensis*. J Hum Evol. 51: 422-428.

Sefcek, JA, Brumbach, BH, Vasquez, G, Miller, GF. 2006. The evolutionary psychology of human mate choice: how ecology, genes, fertility, and fashion influence

mating behavior. In: Knauth, M, editor. Handbook of the evolution of human sexuality. Binghampton: Haworth Press. p 125-182.

Shea, BT. 1985. The ontogeny of sexual dimorphism in the African apes. Am J Primatol. 8: 183-188.

Shennan, S. 1997. Quantifying archaeology. Second edition. Iowa City: University of Iowa Press.

Simpson, SW, Quade, J, Levin, NE, Butler, R, Dupont-Nivet, G, Everett, M, Semaw, S. 2008. A female *Homo erectus* pelvis from Gona, Ethiopia. Science 322: 1089-1092.

Singleton, M. 2012. Postnatal cranial development in papionin primates: an alternative model for hominin evolutionary development. Evol Biol 39: 499-520.

Singleton, M, Mcnulty, KP, Frost, SR, Soderberg, J, and Guthrie, EM. 2010. Bringing up baby: developmental simulation of the adult cranial morphology of *Rungwecebus kipunji*. Anat Rec 293: 388-401.

Skelton, RR, McHenry, HM. 1992. Evolutionary relationships among early hominids. J Hum Evol 23: 309-349.

Skelton, RR, McHenry, HM, Drawhorn, GM. 1986. Phylogenetic analysis of early hominids. Curr Anthropol 27: 21-43.

Slice, DE. 2007. Geometric Morphometrics. Annu Rev Anthropol 36: 261-281.

Smith, RJ, Jungers, WL. 1997. Body mass in comparative primatology. J Hum Evol 32: 523-559.

Spoor, F. 2011. Malapa and the genus *Homo*. Nature 478: 44-45.

Spoor, F. 2013. Small-brained and big-mouthed. Nature 502: 452-453.

Stefan, VH, Trinkaus, E. 1998. Discrete trait and dental morphometric affinities of the Tabun 2 mandible. J Hum Evol 34: 443-468.

Strait, DS, Grine, FE. 2004. Inferring hominoid and early hominid phylogeny using craniodental characters: the role of fossil taxa. J Hum Evol 47: 399-452.

Strait, DS, Grine, FE, Moniz, MA. 1997. A reappraisal of early hominid phylogeny. J Hum Evol 32: 17-82.

Suwa, G, White, TD, Howell, FC. 1996. Mandibular postcanine dentition from the Shungura Formation, Ethiopia: Crown morphology, taxonomic allocations, and Plio-Pleistocene hominid evolution. Am J Phys Anthropol 101: 247.

Thompson D'AW. 1917. On growth and form. Cambridge: Cambridge University Press.

Tobias, PV. 1966. The distinctiveness of *Homo habilis*. Nature 209: 953-957.

Tobias, PV. 1967a. The cranium and maxillary dentition *of Australopithecus (Zinjanthropus) boisei.* Olduvai Gorge, Volume 2. Cambridge: Cambridge University Press.

Tobias, PV. 1967b. Pleistocene deposits and new fossil localities in Kenya. Nature 215: 479-480.

Tobias, PV. 1971. The brain in hominid evolution. New York: Columbia University Press.

Tobias, PV. 1980. *Australopithecus afarensis* and *A. africanus*: critique and an alternative hypothesis. Palaeont Afr 23: 1-17.

Tobias, PV. 1991. Olduvai Gorge, Volume 4: the skulls, endocasts and teeth of *Homo habilis*. New York: Cambridge University Press.

Trinkaus, E. 2003. Neandertal faces were not long: modern human faces are short. Proc Natl Acad Sci USA 100: 8142-8145.

Trinkaus, E. 2006. Modern human versus Neandertal evolutionary distinctiveness. Curr Anthropol 47: 597-620.

Vlcek, E. 1991. Fossil man in central-Europe. Anthropologie 95:409-472.

Ward, CV, Plavcan, JM, Manthi, FK. 2010. Anterior dental evolution in the *Australopithecus anamensis-afarensis* lineage. Philos Trans R Soc Lond, B 365: 3333-3344.

Weidenreich, F. 1945. The Paleolithic child from the Teshik-Tash Cave in southern Uzbekistan (Central Asia). Am J Phys Anthropol 3: 151-163.

White, TD. 1995. African omnivores: global climatic change and Plio-pleistocene hominids and suids. In: Vrba, ES, Denton, GH, Partridge, TC, Burckle, LH, editors. Paleoclimate and evolution with emphasis on human origins. New Haven, CT: Yale University Press. p 369-384.

White, T. 2003. Early hominids---diversity or distortion? Science 299: 1994-1997.

White, T, Folkens, PA. 2000. Human osteology, second edition. San Diego: Academic.

White, TD, Asfaw, B, Beyene, Y, Haile-Selassie, Y, Lovejoy, CO, Suwa, G, WoldeGabriel, G. 2009. *Ardipithecus ramidus* and the paleobiology of early hominids. Science 326: 75-86.

Wiley, DF, Amenta, N, Alcantara, DA, Ghosh, D, Kil, YJ, Delson, E, Harcourt-Smith, W, St. John, K, Rohlf, JF, Hamann, B. 2005. Evolutionary Morphing. 16th IEEE Visualization. 431-438.

Williams, SA, Ostrofsky, KR, Frater, N, Churchill, SE, Schmid, P, Berger, LR. 2013. The vertebral column of *Australopithecus sediba*. Science 340: 1232996-1-5.

Wolpoff, MH. 1976. Some aspects of the evolution of early hominid sexual dimorphism. Curr Anthropol. 17: 579-606.

Wolpoff, M, Mannheim, B, Mann, A, Hawks, J, Caspari, R, Rosenberg, K, Frayer, D, Gill, K, Clark, G. 2004. Why not the Neandertals? World Archaeol 36: 527-456.

Wood, B. 1991. Koobi Fora Research Project. Volume 4: Hominid Cranial Remains. Oxford: Clarendon Press.

Wood, BA. 1987. Who is the 'real' *Homo habilis*. Nature 327: 187-188.

Wood, BA. 1992. Origin and evolution of the genus *Homo*. Nature 355: 783-790.

Wood, B, Collard, M. 1999a. The human genus. Science 284: 65-71.

Wood, B, Collard, M. 1999b. The changing face of the genus *Homo*. Evol Anthropol 8: 195-207

Wood, B, Harrison, T. 2011. The evolutionary context of the first hominins. Nature 470: 347-352.

Zipfel, B, DeSilva, JM, Kidd, RS, Carlson, KJ, Churchill, SE, Berger, LR. 2011. The foot and ankle of *Australopithecus sediba*. Science 333: 1417-1420.

APPENDIX

TABLES

**Table 1:** Summary total of ontogenetic sample for *P. troglodytes*, *G. gorilla*, and *H. sapiens*.

| | **M2-Juveniles** | **M3-Males** | **M3-Females** |
|---|---|---|---|
| ***P. troglodytes*** | 13 | 6 | 7 |
| ***G. gorilla*** | 15 | 6 | 4 |
| ***H. sapiens*** | 8 | 16 | 11 |

**Table 2:** Ontogenetic sample collected from Cleveland Museum of Natural History.

| | **Cleveland Museum of Natural History** | | | |
|---|---|---|---|---|
| | **M3 erupted** | **Sex** | **M3 unerupted** | **Sex** |
| ***Pan troglodytes*** | B-1056 | Male | B-1435 | Female |
| | B-1722 | Male | B-1702 | Female |
| | B-1739 | Male | B-1705 | Female |
| | B-1741 | Female | B-1715 | Female |
| | B-1747 | Female | B-1742 | Female |
| | B-1843 | Female | B-1750 | Male |
| | B-1882 | Male | B-1767 | Female |
| | B-2027 | Male | B-1771 | Female |
| | B-2748 | Female | B-1800 | Female |

**Table 2** Continued

| | **M3 erupted** | **Sex** | **M3 unerupted** | **Sex** |
|---|---|---|---|---|
| | B-2756 | Female | B-1855 | Male |
| | B-2771 | Female | B-2811 | Male |
| | B-3418 | Female | B-346 | Uncertain |
| | B-3552 | Male | B-3553 | Female |
| ***Gorilla gorilla*** | B-1181 | Male | B-1403 | Male |
| | B-1404 | Male | B-1711 | Male |
| | B-1712 | Male | B-1845 | Male |
| | B-1904 | Male | B-1860 | Male |
| | B-2741 | Male | B-1938 | Male |
| | B-1399 | Female | B-2758 | Male |
| | B-1798 | Female | B-3428 | Male |
| | B-1854 | Female | B-2817 | Female |
| | B-2792 | Male | B-1952 | Female |
| | B-2799 | Female | B-1942 | Female |
| | | | B-1940 | Female |
| | | | B-1928 | Female |
| | | | B-1906 | Female |

**Table 2** Continued

| | **M3 erupted** | **Sex** | **M3 unerupted** | **Sex** |
|---|---|---|---|---|
| ***Homo sapiens*** | 0.202 | Male | | |
| | 0.239 | Male | | |

**Table 3:** Ontogenetic sample collected from Raymond A. Dart collection of human skeletons.

| | **Raymond A. Dart Collection of Human Skeletons** | | | |
|---|---|---|---|---|
| ***Homo sapiens*** | **M3 erupted** | **Sex** | **M3 unerupted** | **Sex** |
| | A58.202 | Male | A680.671 | Male |
| | A44 | Male | A769.787 | Female |
| | A477.543 | Male | A3013.2747 | Male |
| | A744.758 | Male | A2940.4094 | Male |
| | A1424.188 | Male | A1630.2299 | Female |
| | A1498.199 | Male | A3109.4634 | Male |
| | A2073.269 | Male | A327 | Male |
| | A2102.274 | Male | A439.500 | Male |
| | A2103.2746 | Male | | |
| | A1549.2082 | Female | | |
| | A1773.2373 | Male | | |
| | A2183.2928 | Female | | |

**Table 3** Continued

| ***Homo sapiens*** | **M3 erupted** | **Sex** | **M3 unerupted** | **Sex** |
|---|---|---|---|---|
| | A2191.2852 | Female | | |
| | A2648.3496 | Male | | |
| | A56 | Uncertain | | |
| | A519.608 | Female | | |
| | A55 | Uncertain | | |
| | A150-257 | Male | | |
| | A740.870 | Female | | |
| | A745.739 | Female | | |
| | A787-718 | Female | | |
| | A1410.1856 | Female | | |
| | A1418.1869 | Male | | |
| | A3509.5822 | Female | | |
| | A3523,5868 | Female | | |
| | A3699.6555 | Male | | |
| | A3791.6585 | Female | | |

**Table 4:** Hominin fossil sample used for comparative analyses

| **Species** | **Specimens** |
|---|---|
| *Au. sediba* | MH1 |

**Table 4** Continued

| Species | Specimens |
|---|---|
| *Au. africanus* | Sts 5, Sts 71, Stw 53 |
| *H. habilis* | OH 24, KNM-ER 1813 |
| *H. rudolfensis* | KNM-ER 1470 |
| *H. erectus* | D2700, KNM-ER 3733, KNM-WT 15000 |

**Table 5:** Landmark definitions for landmarks used in developmental simulation. In addition to the landmarks listed here, three curves of semilandmarks were added along the mid-sagittal curve between rhinion and bregma, with a density of ten equidistant spaced semi-landmarks each (indicated by red line), making for a total of 76 landmarks.

| Landmark | Landmark definition |
|---|---|
| **1-2** | Mid-torus inferior (right and left) |
| **3-4** | Mid-torus superior (right and left) |
| **5-6** | Dacryon (right and left) |
| **7-8** | Zygoorbitale (right and left) |
| **9-10** | Frontomalare orbitale (left and right) |
| **11-12** | Infraorbital foramen (right and left) |
| **13-14** | Zygomaxillare (right and left) |
| **15-16** | Alare (right and left) |
| **17** | Anterior attachment of nasal septum |
| **18** | Prosthion |
| **19&20** | I1-I2 contact (left and right) |
| **21&22** | I2-Canine contact (left and right) |
| **23&28** | Canine-P3 contact |
| **24&29** | P3-P4 contact |

**Table 5** Continued

| Landmark | Landmark definition |
|---|---|
| **25&30** | P4-M1 contact |
| **26&31** | M1-M2 contact |
| **27&32** | M2-M3 contact |
| **33&34** | Jugale (left and right) |
| **35** | Zygomatico-temporal suture superior |
| **36** | Zygomatico-temporal suture inferior |
| **37-38** | Pterion |
| **39&40** | Inferior-most point of post-glenoid process |
| **41** | Incisivion |
| **42** | Alveolon |
| **43&44** | Inferolateral junction of nasal with maxilla (right and lft) |
| **45&46** | Frontomalare temporale (left and right) |

**Table 6:** Landmarks definitions for subset of landmarks used in morphometric comparison.

| Landmark | Landmark definition |
|---|---|
| **1** | Rhinion |
| **2** | Nasion |
| **3** | Glabella |
| **4** | Bregma |
| **5** | Anterior attachment of nasal septum |
| **6** | Prosthion |

**Table 6** Continued

| **Landmark** | **Landmark definition** |
|---|---|
| **7-8** | Mid-torus inferior (right and left) |
| **9-10** | Mid-torus superior (right and left) |
| **11-12** | Frontomalare orbitale (left and right) |
| **13-14** | Frontomalare temporale (left and right) |
| **15-16** | Dacryon (left and right) |
| **17-18** | Zygoorbitale (right and left) |
| **19-20** | Zygomaxillare (right and left) |
| **21-22** | Alare (right and left) |
| **23-24** | Malar root origin (right and left) |
| **25-26** | I1-I2 contact |
| **27-28** | C-P3 contact |
| **29** | Incisivion |
| **30** | Alveolon |
| **31** | Left distal palate |
| **32** | Right distal palate |

**Table 7:** Eigenvalues of PCA including *P. troglodytes* and *H. sapiens*

| PC | Eigenvalue | % variance |
|---|---|---|
| 1 | 0.010061 | 58.718 |
| 2 | 0.001888 | 11.021 |
| 3 | 0.001112 | 6.4903 |
| 4 | 0.000682 | 3.9795 |
| 5 | 0.000549 | 3.2042 |
| 6 | 0.000375 | 2.186 |
| 7 | 0.000314 | 1.8351 |

**Table 7** Continued

| PC | Eigenvalue | % variance |
|---|---|---|
| 8 | 0.000271 | 1.5798 |
| 9 | 0.000223 | 1.2989 |
| 10 | 0.000205 | 1.1992 |
| 11 | 0.000161 | 0.94205 |
| 12 | 0.000151 | 0.88228 |
| 13 | 0.000126 | 0.73593 |
| 14 | 0.000118 | 0.6899 |
| 15 | 0.000108 | 0.62743 |
| 16 | 9.81E-05 | 0.57283 |
| 17 | 8.21E-05 | 0.47918 |
| 18 | 6.57E-05 | 0.38369 |
| 19 | 6.40E-05 | 0.37347 |
| 20 | 5.70E-05 | 0.33247 |
| 21 | 5.32E-05 | 0.31045 |
| 22 | 5.00E-05 | 0.29205 |
| 23 | 4.17E-05 | 0.24348 |
| 24 | 3.90E-05 | 0.22744 |
| 25 | 3.54E-05 | 0.20666 |
| 26 | 3.35E-05 | 0.19565 |
| 27 | 3.07E-05 | 0.17915 |
| 28 | 2.54E-05 | 0.14818 |
| 29 | 2.21E-05 | 0.12925 |
| 30 | 2.05E-05 | 0.1196 |
| 31 | 1.72E-05 | 0.10024 |
| 32 | 1.50E-05 | 0.087581 |
| 33 | 1.36E-05 | 0.079501 |
| 34 | 1.16E-05 | 0.067732 |
| 35 | 8.82E-06 | 0.051481 |
| 36 | 5.24E-06 | 0.030572 |

**Table 8:** Eigenvalues of PCA including only fossil hominins

| PC | Eigenvalue | % variance |
|---|---|---|
| 1 | 0.003108 | 28.298 |
| 2 | 0.002384 | 21.705 |
| 3 | 0.001667 | 15.181 |
| 4 | 0.000847 | 7.7122 |
| 5 | 0.000756 | 6.8871 |
| 6 | 0.000626 | 5.7017 |
| 7 | 0.000479 | 4.3647 |
| 8 | 0.000406 | 3.6985 |
| 9 | 0.000267 | 2.4336 |
| 10 | 0.00018 | 1.6418 |
| 11 | 9.79E-05 | 0.89101 |
| 12 | 7.92E-05 | 0.72113 |
| 13 | 4.69E-05 | 0.42656 |
| 14 | 2.07E-05 | 0.18879 |
| 15 | 1.64E-05 | 0.14917 |

**Table 9:** Matrix of average Euclidean (i.e. Procrustes distances) between taxa, and average distances within species (highlighted in yellow).

| | *A. afric.* | *A. sediba* | *H. erectus* | *H. habilis* | *H. sapiens* | *P. troglo.* | *H. rudolf.* |
|---|---|---|---|---|---|---|---|
| ***A. africanus*** | 0.145 | | | | | | |
| ***A. sediba*** | 0.101 | 0.059 | | | | | |
| ***H. erectus*** | 0.138 | 0.112 | 0.144 | | | | |
| ***H. habilis*** | 0.137 | 0.138 | 0.098 | 0.163 | | | |
| ***H. sapiens*** | 0.226 | 0.210 | 0.149 | 0.146 | 0.089 | | |
| ***P. troglodytes*** | 0.152 | 0.110 | 0.133 | 0.159 | 0.218 | 0.092 | |
| ***H. rudolfensis*** | 0.188 | 0.173 | 0.158 | 0.208 | 0.236 | 0.200 | --- |

**Table 10:** Matrix of Euclidean distances between multivariate regression coefficients used in adult simulations. Pt= *P. troglodytes*, Gg= *G. gorilla*, Hs= *H. sapiens*. Distances between male and female regression coefficients for the same species are highlighted in yellow.

| | | | | | | |
|---|---|---|---|---|---|---|
| Pt male | | | | | | |
| Pt female | 0.0367 | | | | | |
| Gg male | 0.14602 | 0.1417 | | | | |
| Gg female | 0.0976 | 0.0973 | 0.0789 | | | |
| Hs male | 0.0533 | 0.0488 | 0.1256 | 0.0777 | | |
| Hs female | 0.0577 | 0.0526 | 0.1200 | 0.0766 | 0.0268 | |
| | Pt male | Pt female | Gg male | Gg female | Hs male | Hs female |

**Table 11:** Data for *P. troglodytes* developmental vectors and coordinates for simulated *Au. sediba* adult crania. Lower case "s" stands for semi-landmark coordinate.

| | | **Data for male virtual adult** | | | **Data for female virtual adult** | | |
|---|---|---|---|---|---|---|---|
| **Landmark** | | MH1 | Male Slope | *P. troglodytes* male adult | MH1 | Female Slope | *P. troglodytes* female adult |
| Mid-torus inferior (rt) | x | 0.040001 | 0.001715 | 0.041716 | 0.040001 | 0.001355 | 0.041356 |
| | y | 0.021477 | 0.001363 | 0.022841 | 0.021477 | 0.003749 | 0.025226 |
| | z | -0.06852 | -0.00336 | -0.07188 | -0.06852 | -0.00021 | -0.06873 |
| Mid-torus superior (rt) | x | 0.054336 | 0.002953 | 0.057289 | 0.054336 | 0.001811 | 0.056147 |
| | y | 0.019756 | 0.003125 | 0.022881 | 0.019756 | 0.003526 | 0.023282 |
| | z | -0.07078 | -0.00398 | -0.07476 | -0.07078 | 0.000349 | -0.07043 |
| Mid-torus inferior (lft) | x | 0.040532 | 0.001156 | 0.041688 | 0.040532 | 0.001598 | 0.04213 |
| | y | 0.040087 | 0.003979 | 0.044066 | 0.040087 | 0.002792 | 0.042879 |
| | z | 0.06147 | 0.004009 | 0.065479 | 0.06147 | 0.00126 | 0.062729 |
| Mid-torus superior (lft) | x | 0.053778 | 0.002125 | 0.055903 | 0.053778 | 0.001806 | 0.055584 |
| | y | 0.039314 | 0.003662 | 0.042976 | 0.039314 | 0.004154 | 0.043468 |
| | z | 0.063738 | 0.00457 | 0.068308 | 0.063738 | -7.48E-05 | 0.063663 |
| zygoorbitale (rt) | x | -0.03141 | 0.00928 | -0.02213 | -0.03141 | 0.008359 | -0.02305 |
| | y | -0.00293 | 0.004041 | 0.001112 | -0.00293 | 0.002051 | -0.00088 |
| | z | -0.06279 | 0.010142 | -0.05265 | -0.06279 | 0.00303 | -0.05976 |
| zygomaxillare (rt) | x | -0.06949 | 0.006343 | -0.06315 | -0.06949 | 0.005332 | -0.06416 |
| | y | -0.01954 | 0.005402 | -0.01414 | -0.01954 | 0.000611 | -0.01893 |
| | z | -0.10104 | -0.00117 | -0.10222 | -0.10104 | -0.00074 | -0.10178 |
| zygoorbitale (lft) | x | -0.03448 | 0.010468 | -0.02401 | -0.03448 | 0.009715 | -0.02476 |
| | y | 0.014232 | 0.00069 | 0.014922 | 0.014232 | 0.001604 | 0.015837 |
| | z | 0.046424 | -0.01096 | 0.035464 | 0.046424 | -0.00369 | 0.042733 |
| zygomaxillare (lft) | x | -0.06913 | 0.004852 | -0.06428 | -0.06913 | 0.004235 | -0.0649 |
| | y | 0.003487 | 0.002463 | 0.005949 | 0.003487 | -0.00021 | 0.003279 |
| | z | 0.088425 | 0.000583 | 0.089007 | 0.088425 | 0.000882 | 0.089307 |
| frontomalare orbitale (rt) | x | 0.024014 | 0.001403 | 0.025417 | 0.024014 | 0.00376 | 0.027774 |

**Table 11** Continued

| **Landmark** | | MH1 | Male Slope | *P. troglodytes* male adult | MH1 | Female Slope | *P. troglodytes* female adult |
|---|---|---|---|---|---|---|---|
| | y | -0.0062 | -0.00038 | -0.00658 | -0.0062 | -0.00095 | -0.00716 |
| | z | -0.09604 | -0.00376 | -0.09981 | -0.09604 | -0.00189 | -0.09794 |
| frontomalare temporale (rt) | x | 0.039434 | 0.003262 | 0.042696 | 0.039434 | 0.008762 | 0.048196 |
| | y | -0.01951 | 0.002901 | -0.01661 | -0.01951 | 0.002543 | -0.01696 |
| | z | -0.10215 | -0.0061 | -0.10825 | -0.10215 | -0.00134 | -0.10349 |
| frontomalare orbitale (lft) | x | 0.022353 | 0.00207 | 0.024422 | 0.022353 | 0.004653 | 0.027006 |
| | y | 0.021286 | -0.00053 | 0.02076 | 0.021286 | -0.00113 | 0.020153 |
| | z | 0.089176 | 0.003554 | 0.09273 | 0.089176 | 0.003533 | 0.092709 |
| frontomalare temporale (lft) | x | 0.041595 | 0.002461 | 0.044056 | 0.041595 | 0.006023 | 0.047618 |
| | y | 0.010873 | 0.003249 | 0.014122 | 0.010873 | 0.003452 | 0.014325 |
| | z | 0.101201 | 0.003533 | 0.104734 | 0.101201 | 0.00385 | 0.105051 |
| inferolateral junction of nasal with maxilla (rt) | x | -0.04452 | 0.000882 | -0.04364 | -0.04452 | 0.004719 | -0.0398 |
| | y | 0.019559 | -0.00023 | 0.019333 | 0.019559 | -0.00278 | 0.016774 |
| | z | -0.0244 | 0.0016 | -0.0228 | -0.0244 | 0.002129 | -0.02227 |
| inferolateral junction of nasal with maxilla (lft) | x | -0.04284 | 0.001244 | -0.04159 | -0.04284 | 0.004983 | -0.03785 |
| | y | 0.023497 | 0.000351 | 0.023849 | 0.023497 | -0.00278 | 0.020718 |
| | z | 0.006697 | -0.00144 | 0.005258 | 0.006697 | -0.00133 | 0.005371 |
| dacryon (rt) | x | 0.012151 | 0.002967 | 0.015119 | 0.012151 | 0.004093 | 0.016244 |
| | y | 0.019414 | 0.002918 | 0.022332 | 0.019414 | -0.00256 | 0.016849 |
| | z | -0.02427 | -0.00141 | -0.02568 | -0.02427 | -0.00313 | -0.0274 |
| dacryon (lft) | x | 0.008421 | 0.00346 | 0.011881 | 0.008421 | 0.004946 | 0.013367 |
| | y | 0.027002 | 0.00353 | 0.030532 | 0.027002 | -0.00023 | 0.026773 |
| | z | 0.012626 | 0.000472 | 0.013099 | 0.012626 | 0.005233 | 0.01786 |
| anterior attachment of nasal septum | x | -0.09648 | 0.004036 | -0.09244 | -0.09648 | 0.002285 | -0.09419 |

**Table 11** Continued

| **Landmark** | | MH1 | Male Slope | *P. troglodytes* male adult | MH1 | Female Slope | *P. troglodytes* female adult |
|---|---|---|---|---|---|---|---|
| | y | 0.023717 | -0.00289 | 0.02083 | 0.023717 | -0.0029 | 0.020819 |
| | z | -0.00751 | 0.000586 | -0.00692 | -0.00751 | 0.000531 | -0.00698 |
| prosthion | x | -0.14784 | -0.01235 | -0.16019 | -0.14784 | -0.00862 | -0.15645 |
| | y | 0.041207 | -0.00454 | 0.036664 | 0.041207 | -0.00011 | 0.041099 |
| | z | -0.00979 | -0.00047 | -0.01026 | -0.00979 | -0.00087 | -0.01066 |
| I1-I2 contact (rt) | x | -0.14796 | -0.01063 | -0.1586 | -0.14796 | -0.00817 | -0.15613 |
| | y | 0.035137 | -0.00264 | 0.032496 | 0.035137 | 0.000679 | 0.035816 |
| | z | -0.03358 | 0.0045 | -0.02908 | -0.03358 | 0.002267 | -0.03131 |
| I2-canine contact (rt) | x | -0.14736 | -0.00697 | -0.15433 | -0.14736 | -0.00456 | -0.15192 |
| | y | 0.022948 | -0.00111 | 0.021839 | 0.022948 | 0.001964 | 0.024911 |
| | z | -0.04887 | 0.00037 | -0.0485 | -0.04887 | 0.002027 | -0.04684 |
| Canine-P3 contact (rt) | x | -0.14338 | -0.00302 | -0.14639 | -0.14338 | -0.00266 | -0.14604 |
| | y | 0.007167 | -0.00355 | 0.003619 | 0.007167 | -0.00371 | 0.003456 |
| | z | -0.06359 | -0.00028 | -0.06387 | -0.06359 | 0.00036 | -0.06323 |
| P3-P4 contact (rt) | x | -0.14015 | -0.00071 | -0.14086 | -0.14015 | -0.00239 | -0.14254 |
| | y | -0.01247 | -0.00289 | -0.01535 | -0.01247 | -0.0015 | -0.01396 |
| | z | -0.07111 | -2.10E-05 | -0.07113 | -0.07111 | 0.000647 | -0.07046 |
| P4-M1 contact (rt) | x | -0.13157 | -0.00179 | -0.13336 | -0.13157 | -0.00425 | -0.13581 |
| | y | -0.03766 | 0.001589 | -0.03607 | -0.03766 | 0.002248 | -0.03541 |
| | z | -0.07299 | 0.001539 | -0.07145 | -0.07299 | 0.001625 | -0.07136 |
| M1-M2 contact (rt) | x | -0.11948 | -0.00563 | -0.12511 | -0.11948 | -0.0076 | -0.12708 |
| | y | -0.06223 | 0.004905 | -0.05733 | -0.06223 | 0.005876 | -0.05635 |
| | z | -0.06944 | 0.001006 | -0.06843 | -0.06944 | 0.00029 | -0.06915 |
| M2-M3 contact (rt) | x | -0.10495 | -0.00602 | -0.11097 | -0.10495 | -0.00904 | -0.11399 |
| | y | -0.08953 | 0.007447 | -0.08209 | -0.08953 | 0.00818 | -0.08135 |
| | z | -0.06372 | -0.00321 | -0.06694 | -0.06372 | -0.00507 | -0.06879 |

**Table 11** Continued

| **Landmark** | | MH1 | Male Slope | *P. troglodytes* male adult | MH1 | Female Slope | *P. troglodytes* female adult |
|---|---|---|---|---|---|---|---|
| I1-I2 contact (lft) | x | -0.14612 | -0.01173 | -0.15785 | -0.14612 | -0.00855 | -0.15466 |
| | y | 0.042056 | -0.00528 | 0.036772 | 0.042056 | -0.0009 | 0.041157 |
| | z | 0.014822 | -0.00437 | 0.010454 | 0.014822 | -0.00436 | 0.010462 |
| I2-Canine contact (lft) | x | -0.14053 | -0.0058 | -0.14633 | -0.14053 | -0.0034 | -0.14393 |
| | y | 0.037814 | -0.00047 | 0.037343 | 0.037814 | 0.001764 | 0.039578 |
| | z | 0.029858 | -0.00071 | 0.029151 | 0.029858 | -0.00352 | 0.026338 |
| Canine-P3 contact (lft) | x | -0.13922 | -0.00167 | -0.14089 | -0.13922 | -0.00256 | -0.14179 |
| | y | 0.02269 | -0.006 | 0.016688 | 0.02269 | -0.0032 | 0.019487 |
| | z | 0.05416 | 0.001539 | 0.055699 | 0.05416 | -0.00075 | 0.053414 |
| P3-P4 contact (lft) | x | -0.13946 | -0.00298 | -0.14245 | -0.13946 | -0.00316 | -0.14262 |
| | y | 0.003812 | -0.00488 | -0.00107 | 0.003812 | -0.00226 | 0.001552 |
| | z | 0.060171 | -0.00128 | 0.058889 | 0.060171 | -0.00186 | 0.05831 |
| P4-M1 contact (lft) | x | -0.12576 | -0.00215 | -0.12791 | -0.12576 | -0.00334 | -0.1291 |
| | y | -0.01907 | -0.00094 | -0.02002 | -0.01907 | 0.000514 | -0.01856 |
| | z | 0.066851 | -0.00334 | 0.063511 | 0.066851 | -0.00297 | 0.06388 |
| M1-M2 contact (lft) | x | -0.11662 | -0.00502 | -0.12164 | -0.11662 | -0.00566 | -0.12228 |
| | y | -0.04389 | 0.001309 | -0.04258 | -0.04389 | 0.003516 | -0.04037 |
| | z | 0.072312 | -0.00384 | 0.068468 | 0.072312 | -0.00284 | 0.069472 |
| M2-M3 contact (lft) | x | -0.10296 | -0.00552 | -0.10847 | -0.10296 | -0.00737 | -0.11033 |
| | y | -0.06832 | 0.004137 | -0.06419 | -0.06832 | 0.005813 | -0.06251 |
| | z | 0.07292 | -0.00126 | 0.071657 | 0.07292 | 0.000326 | 0.073246 |
| Incisivion | x | -0.12264 | 0.002792 | -0.11985 | -0.12264 | 0.001812 | -0.12083 |
| | y | -0.00175 | -0.00376 | -0.00551 | -0.00175 | -0.00183 | -0.00358 |
| | z | -0.00689 | 0.000169 | -0.00672 | -0.00689 | -0.00078 | -0.00767 |
| Alveolon | x | -0.07627 | 0.007172 | -0.0691 | -0.07627 | 0.005461 | -0.07081 |
| | y | -0.08576 | 0.001981 | -0.08378 | -0.08576 | -0.00148 | -0.08724 |
| | z | 0.004303 | -0.00177 | 0.002528 | 0.004303 | -0.00068 | 0.003626 |
| Jugale (lft) | x | -0.01745 | 0.004188 | -0.01326 | -0.01745 | 0.004346 | -0.0131 |

**Table 11** Continued

| **Landmark** | | MH1 | Male Slope | *P. troglodytes* male adult | MH1 | Female Slope | *P. troglodytes* female adult |
|---|---|---|---|---|---|---|---|
| | y | -0.01038 | 0.000431 | -0.00995 | -0.01038 | 0.000175 | -0.01021 |
| | z | 0.107984 | 0.006924 | 0.114907 | 0.107984 | 0.004236 | 0.112219 |
| Zygomatico-temporal suture superior | x | -0.01107 | 0.004377 | -0.00669 | -0.01107 | 0.004679 | -0.00639 |
| | y | -0.02436 | 0.006065 | -0.0183 | -0.02436 | 0.000102 | -0.02426 |
| | z | 0.116842 | 0.005648 | 0.122489 | 0.116842 | 0.004673 | 0.121515 |
| Zygomatico-temporal suture inferior | x | -0.01112 | 0.001631 | -0.00949 | -0.01112 | 0.00674 | -0.00438 |
| | y | -0.05908 | 0.011393 | -0.04769 | -0.05908 | 0.00229 | -0.05679 |
| | z | 0.130104 | 0.004492 | 0.134596 | 0.130104 | 0.003016 | 0.13312 |
| Jugale (rt) | x | -0.01781 | 0.006306 | -0.0115 | -0.01781 | 0.004694 | -0.01311 |
| | y | -0.03985 | 0.000536 | -0.03932 | -0.03985 | -0.0014 | -0.04125 |
| | z | -0.11243 | -0.00801 | -0.12044 | -0.11243 | -0.00325 | -0.11568 |
| Pterion (lft) | x | 0.065289 | 0.005861 | 0.07115 | 0.065289 | -0.00134 | 0.063949 |
| | y | -0.03453 | 0.002239 | -0.03229 | -0.03453 | -0.00049 | -0.03501 |
| | z | 0.099798 | -0.01332 | 0.086483 | 0.099798 | -0.00882 | 0.09098 |
| Pterion (rt) | x | 0.064611 | 0.004844 | 0.069454 | 0.064611 | 0.000567 | 0.065177 |
| | y | -0.0673 | 0.006317 | -0.06099 | -0.0673 | 0.00639 | -0.06091 |
| | z | -0.08781 | 0.011877 | -0.07593 | -0.08781 | 0.010269 | -0.07754 |
| Inferior-most point of glenoid process (lft) | x | 0.001882 | 0.011286 | 0.013168 | 0.001882 | 0.011542 | 0.013424 |
| | y | -0.12161 | 0.005699 | -0.11591 | -0.12161 | 0.002651 | -0.11896 |
| | z | 0.126986 | 0.001041 | 0.128027 | 0.126986 | -0.00248 | 0.124502 |
| Inferior-most point of glenoid process (rt) | x | 0.002264 | 0.012539 | 0.014803 | 0.002264 | 0.011663 | 0.013927 |
| | y | -0.15229 | 0.004624 | -0.14767 | -0.15229 | 0.001795 | -0.1505 |
| | z | -0.09175 | -0.00318 | -0.09493 | -0.09175 | 0.002487 | -0.08927 |

**Table 11** Continued

| **Landmark** | | MH1 | Male Slope | *P. troglodytes* male adult | MH1 | Female Slope | *P. troglodytes* female adult |
|---|---|---|---|---|---|---|---|
| Infra-orbital foramen (rt) | x | -0.06224 | 0.00378 | -0.05846 | -0.06224 | 0.003503 | -0.05873 |
| | y | -8.87E-04 | 0.000691 | -0.0002 | -8.87E-04 | -0.00402 | -0.00491 |
| | z | -0.06367 | 2.65E-05 | -0.06364 | -0.06367 | -0.00308 | -0.06675 |
| Infra-orbital foramen (lft) | x | -0.06373 | 0.004052 | -0.05968 | -0.06373 | 0.003181 | -0.06055 |
| | y | 0.012899 | -0.0005 | 0.012396 | 0.012899 | -0.00342 | 0.009481 |
| | z | 0.049629 | 0.000378 | 0.050007 | 0.049629 | 0.004064 | 0.053693 |
| Alare (rt) | x | -0.07875 | -0.00218 | -0.08093 | -0.07875 | 0.001939 | -0.07681 |
| | y | 0.012917 | -0.00089 | 0.012025 | 0.012917 | -0.00241 | 0.010503 |
| | z | -0.03712 | 0.000336 | -0.03678 | -0.03712 | -0.00174 | -0.03886 |
| Alare (lft) | x | -0.07917 | -0.00283 | -0.08201 | -0.07917 | 0.002008 | -0.07716 |
| | y | 0.023512 | 0.000153 | 0.023665 | 0.023512 | -0.00208 | 0.021433 |
| | z | 0.020081 | -0.00021 | 0.019867 | 0.020081 | 0.001679 | 0.021761 |
| s1 | x | -0.04278 | -0.00022 | -0.043 | -0.04278 | -0.00126 | -0.04403 |
| | y | 0.025795 | 0.000429 | 0.026224 | 0.025795 | -0.00141 | 0.024382 |
| | z | -0.00771 | 0.000356 | -0.00736 | -0.00771 | 0.000453 | -0.00726 |
| s2 | x | -0.02305 | 0.001315 | -0.02174 | -0.02305 | 0.000116 | -0.02294 |
| | y | 0.02061 | 0.000341 | 0.020951 | 0.02061 | -0.00147 | 0.019142 |
| | z | -0.00824 | 0.000641 | -0.0076 | -0.00824 | 0.000604 | -0.00763 |
| s3 | x | -9.30E-04 | 0.003591 | 0.00266 | -9.30E-04 | 0.001524 | 0.000593 |
| | y | 0.019889 | 0.000504 | 0.020393 | 0.019889 | -1.93E-05 | 0.01987 |
| | z | -0.00789 | 0.000759 | -0.00713 | -0.00789 | 0.000325 | -0.00756 |
| s4 | x | 0.006697 | 0.004549 | 0.011246 | 0.006697 | 0.002132 | 0.008829 |
| | y | 0.033195 | 0.001408 | 0.034603 | 0.033195 | 0.00109 | 0.034286 |
| | z | -0.00707 | 0.000591 | -0.00648 | -0.00707 | 8.02E-05 | -0.00699 |
| s5 | x | 0.016078 | 0.004055 | 0.020133 | 0.016078 | 0.002111 | 0.018189 |
| | y | 0.038874 | 0.002342 | 0.041216 | 0.038874 | 0.00165 | 0.040524 |
| | z | -0.00673 | 0.000388 | -0.00634 | -0.00673 | 5.77E-06 | -0.00672 |
| s6 | x | 0.022976 | 0.002558 | 0.025535 | 0.022976 | 0.001219 | 0.024196 |
| | y | 0.044327 | 0.003221 | 0.047548 | 0.044327 | 0.002318 | 0.046645 |

**Table 11** Continued

| **Landmark** | | MH1 | Male Slope | *P. troglodytes* male adult | MH1 | Female Slope | *P. troglodytes* female adult |
|---|---|---|---|---|---|---|---|
| | z | -0.00666 | 0.0003 | -0.00636 | -0.00666 | -3.03E-05 | -0.00669 |
| s7 | x | 0.031299 | 0.001235 | 0.032534 | 0.031299 | 0.000468 | 0.031767 |
| | y | 0.047864 | 0.003473 | 0.051337 | 0.047864 | 0.001961 | 0.049824 |
| | z | -0.00672 | 0.000429 | -0.00629 | -0.00672 | 5.60E-05 | -0.00667 |
| s8 | x | 0.042526 | 0.002027 | 0.044553 | 0.042526 | 5.42E-06 | 0.042532 |
| | y | 0.048191 | 0.00347 | 0.051661 | 0.048191 | 0.000307 | 0.048498 |
| | z | -0.00663 | 0.000467 | -0.00616 | -0.00663 | 0.000122 | -0.0065 |
| s9 | x | 0.053416 | 0.003103 | 0.056519 | 0.053416 | -8.54E-07 | 0.053415 |
| | y | 0.043213 | -0.00065 | 0.042565 | 0.043213 | -4.41E-05 | 0.043169 |
| | z | -0.00594 | 0.000463 | -0.00547 | -0.00594 | -0.00031 | -0.00624 |
| s10 | x | 0.059879 | 0.002066 | 0.061946 | 0.059879 | -2.31E-05 | 0.059856 |
| | y | 0.038087 | -0.00153 | 0.036554 | 0.038087 | -0.00016 | 0.037923 |
| | z | -0.00526 | 0.000351 | -0.00491 | -0.00526 | -0.00059 | -0.00585 |
| s11 | x | 0.059879 | 0.002066 | 0.061946 | 0.059879 | -2.31E-05 | 0.059856 |
| | y | 0.038087 | -0.00153 | 0.036554 | 0.038087 | -0.00016 | 0.037923 |
| | z | -0.00526 | 0.000351 | -0.00491 | -0.00526 | -0.00059 | -0.00585 |
| s12 | x | 0.065372 | 0.000599 | 0.065972 | 0.065372 | -0.00085 | 0.064523 |
| | y | 0.033445 | -0.00192 | 0.031526 | 0.033445 | 0.000675 | 0.034121 |
| | z | -0.00471 | 0.000602 | -0.00411 | -0.00471 | -0.00076 | -0.00548 |
| s13 | x | 0.071394 | -0.0012 | 0.070197 | 0.071394 | -0.00234 | 0.06905 |
| | y | 0.029252 | -0.00298 | 0.026274 | 0.029252 | 0.000915 | 0.030167 |
| | z | -0.00425 | 0.000896 | -0.00335 | -0.00425 | -0.00085 | -0.00509 |
| s14 | x | 0.077793 | -0.00264 | 0.075156 | 0.077793 | -0.00397 | 0.073818 |
| | y | 0.025963 | -0.00438 | 0.021585 | 0.025963 | 0.000172 | 0.026134 |
| | z | -0.00393 | 0.001153 | -0.00278 | -0.00393 | -0.00081 | -0.00474 |
| s15 | x | 0.084359 | -0.00346 | 0.080899 | 0.084359 | -0.00506 | 0.079295 |
| | y | 0.023621 | -0.00503 | 0.018595 | 0.023621 | -0.0008 | 0.022818 |
| | z | -0.00378 | 0.001237 | -0.00255 | -0.00378 | -0.00075 | -0.00453 |
| s16 | x | 0.090966 | -0.00393 | 0.08704 | 0.090966 | -0.00558 | 0.08539 |

**Table 11** Continued

| **Landmark** | | MH1 | Male Slope | *P. troglodytes* male adult | MH1 | Female Slope | *P. troglodytes* female adult |
|---|---|---|---|---|---|---|---|
| | y | 0.021773 | -0.00503 | 0.016745 | 0.021773 | -0.00152 | 0.020251 |
| | z | -0.00374 | 0.001213 | -0.00253 | -0.00374 | -0.00067 | -0.00441 |
| s17 | x | 0.09745 | -0.00408 | 0.09337 | 0.09745 | -0.00549 | 0.091963 |
| | y | 0.019374 | -0.0047 | 0.014671 | 0.019374 | -0.00157 | 0.0178 |
| | z | -0.00365 | 0.00113 | -0.00252 | -0.00365 | -0.00061 | -0.00426 |
| s18 | x | 0.103896 | -0.00398 | 0.099919 | 0.103896 | -0.005 | 0.098897 |
| | y | 0.016569 | -0.00447 | 0.012101 | 0.016569 | -0.00156 | 0.015009 |
| | z | -0.00354 | 0.001009 | -0.00253 | -0.00354 | -0.00054 | -0.00408 |
| s19 | x | 0.110092 | -0.00363 | 0.106459 | 0.110092 | -0.00419 | 0.105901 |
| | y | 0.013098 | -0.00434 | 0.00876 | 0.013098 | -0.00165 | 0.011453 |
| | z | -0.00334 | 0.000858 | -0.00248 | -0.00334 | -0.00041 | -0.00375 |
| s20 | x | 0.115925 | -0.00316 | 0.112766 | 0.115925 | -0.00313 | 0.112798 |
| | y | 0.009368 | -0.0043 | 0.005069 | 0.009368 | -0.00182 | 0.007546 |
| | z | -0.00313 | 0.000691 | -0.00244 | -0.00313 | -0.00021 | -0.00334 |
| s21 | x | 0.115925 | -0.00316 | 0.112766 | 0.115925 | -0.00313 | 0.112798 |
| | y | 0.009368 | -0.0043 | 0.005069 | 0.009368 | -0.00182 | 0.007546 |
| | z | -0.00313 | 0.000691 | -0.00244 | -0.00313 | -0.00021 | -0.00334 |
| s22 | x | 0.121865 | -0.00332 | 0.118544 | 0.121865 | -0.00278 | 0.119083 |
| | y | 0.004774 | -0.00379 | 0.000985 | 0.004774 | -0.00222 | 0.002553 |
| | z | -0.00291 | 0.000421 | -0.00249 | -0.00291 | -9.09E-05 | -0.003 |
| s23 | x | 0.127559 | -0.0035 | 0.124056 | 0.127559 | -0.00263 | 0.124927 |
| | y | -2.68E-04 | -0.00336 | -0.00363 | -2.68E-04 | -0.00264 | -0.00291 |
| | z | -0.00248 | 0.000142 | -0.00234 | -0.00248 | 7.06E-05 | -0.00241 |
| s24 | x | 0.133362 | -0.00383 | 0.129536 | 0.133362 | -0.00243 | 0.130933 |
| | y | -0.00539 | -0.00312 | -0.00851 | -0.00539 | -0.00277 | -0.00817 |
| | z | -0.00192 | -0.00013 | -0.00205 | -0.00192 | 0.000147 | -0.00177 |
| s25 | x | 0.138982 | -0.00414 | 0.134845 | 0.138982 | -0.00234 | 0.136639 |
| | y | -0.01096 | -0.0029 | -0.01386 | -0.01096 | -0.00279 | -0.01375 |
| | z | -0.00114 | -0.00041 | -0.00155 | -0.00114 | 0.00021 | -0.00093 |
| s26 | x | 0.144208 | -0.00452 | 0.13969 | 0.144208 | -0.00255 | 0.141659 |
| | y | -0.01712 | -0.00275 | -0.01987 | -0.01712 | -0.00283 | -0.01995 |

**Table 11** Continued

| **Landmark** | | MH1 | Male Slope | *P. troglodytes* male adult | MH1 | Female Slope | *P. troglodytes* female adult |
|---|---|---|---|---|---|---|---|
| | z | -1.25E-04 | -0.00067 | -0.0008 | -1.25E-04 | 0.000291 | 0.000166 |
| s27 | x | 0.149371 | -0.00484 | 0.14453 | 0.149371 | -0.00284 | 0.146526 |
| | y | -0.02361 | -0.00262 | -0.02623 | -0.02361 | -0.00272 | -0.02633 |
| | z | 0.001074 | -0.00094 | 0.000137 | 0.001074 | 0.000373 | 0.001447 |
| s28 | x | 0.154314 | -0.00512 | 0.149199 | 0.154314 | -0.00318 | 0.151135 |
| | y | -0.03053 | -0.0025 | -0.03302 | -0.03053 | -0.00241 | -0.03294 |
| | z | 0.002483 | -0.0012 | 0.001281 | 0.002483 | 0.000432 | 0.002915 |
| s29 | x | 0.158956 | -0.00533 | 0.15363 | 0.158956 | -0.00329 | 0.155666 |
| | y | -0.03791 | -0.00237 | -0.04028 | -0.03791 | -0.00177 | -0.03968 |
| | z | 0.004102 | -0.00147 | 0.002635 | 0.004102 | 0.000466 | 0.004568 |
| s30 | x | 0.163511 | -0.00563 | 0.157883 | 0.163511 | -0.00338 | 0.16013 |
| | y | -0.04565 | -0.00234 | -0.04798 | -0.04565 | -0.001 | -0.04665 |
| | z | 0.005915 | -0.00176 | 0.004157 | 0.005915 | 0.000486 | 0.0064 |

**Table 12:** Data for *G. gorilla* developmental vectors and coordinates for simulated *Au. sediba* adult crania. Lower case "s" stands for semi-landmark coordinate.

| **Landmark** | | **Data for male virtual adult** | | | **Data for female virtual adult** | | |
|---|---|---|---|---|---|---|---|
| | | **MH1** | **Slope** | ***G. gorilla* male adult** | **MH1** | **Slope** | ***G. gorilla* female adult** |
| Mid-torus inferior (rt) | x | -0.03899 | -0.00146 | -0.04045 | -0.03899 | -0.00126 | -0.04026 |
| | y | 0.067924 | 0.002919 | 0.070842 | 0.067924 | 0.003239 | 0.071163 |
| | z | -0.02136 | 0.001526 | -0.01983 | -0.02136 | -0.00295 | -0.02431 |
| Mid-torus superior (rt) | x | -0.05063 | -0.00791 | -0.05853 | -0.05063 | -0.00129 | -0.05192 |
| | y | 0.070309 | 0.003002 | 0.073311 | 0.070309 | 0.003328 | 0.073636 |
| | z | -0.02193 | -0.00266 | -0.02459 | -0.02193 | -0.00636 | -0.02828 |
| Mid-torus inferior (lft) | x | -0.04133 | -0.00083 | -0.04216 | -0.04133 | -0.00088 | -0.04221 |
| | y | -0.05592 | -0.00653 | -0.06245 | -0.05592 | -0.00073 | -0.05664 |
| | z | -0.04363 | 0.000521 | -0.04311 | -0.04363 | -0.00489 | -0.04852 |

**Table 12** Continued

| **Landmark** | | MH1 | Slope | *G. gorilla* male adult | MH1 | Slope | *G. gorilla* female adult |
|---|---|---|---|---|---|---|---|
| Mid-torus superior (lft) | x | -0.05418 | -0.00815 | -0.06234 | -0.05418 | -0.00151 | -0.05569 |
| | y | -0.05567 | -0.00784 | -0.06351 | -0.05567 | -0.00131 | -0.05698 |
| | z | -0.0453 | -0.00138 | -0.04667 | -0.0453 | -0.00656 | -0.05185 |
| zygoorbitale (rt) | x | 0.03314 | -0.01258 | 0.020558 | 0.03314 | -0.00319 | 0.029952 |
| | y | 0.05997 | 0.005612 | 0.065583 | 0.05997 | -0.00262 | 0.057355 |
| | z | 0.005392 | 0.001927 | 0.00732 | 0.005392 | 0.000855 | 0.006248 |
| zygomaxillare (rt) | x | 0.067884 | -0.00965 | 0.058236 | 0.067884 | -0.00622 | 0.061668 |
| | y | 0.10115 | 0.008059 | 0.109209 | 0.10115 | 0.003444 | 0.104593 |
| | z | 0.025214 | 0.007882 | 0.033097 | 0.025214 | 0.008325 | 0.033539 |
| zygoorbitale (lft) | x | 0.033329 | -0.01406 | 0.019273 | 0.033329 | -0.00271 | 0.030621 |
| | y | -0.0471 | -0.00772 | -0.05482 | -0.0471 | -0.00525 | -0.05235 |
| | z | -0.01514 | 0.000341 | -0.0148 | -0.01514 | 0.002794 | -0.01234 |
| zygomaxillare (lft) | x | 0.059339 | -0.01019 | 0.049151 | 0.059339 | -0.0073 | 0.052043 |
| | y | -0.09391 | -0.0079 | -0.10181 | -0.09391 | -0.00722 | -0.10113 |
| | z | -0.01096 | 0.003991 | -0.00697 | -0.01096 | 0.006781 | -0.00418 |
| frontomalare orbitale (rt) | x | -0.02084 | -0.00713 | -0.02797 | -0.02084 | -0.00299 | -0.02383 |
| | y | 0.096743 | 0.003216 | 0.099959 | 0.096743 | 0.003205 | 0.099948 |
| | z | 0.011659 | -0.00165 | 0.010006 | 0.011659 | -0.0003 | 0.011362 |
| frontomalare temporale (rt) | x | -0.03941 | -0.0137 | -0.05311 | -0.03941 | -0.00526 | -0.04467 |
| | y | 0.104008 | 0.001937 | 0.105945 | 0.104008 | 0.004811 | 0.108819 |
| | z | 0.020715 | 0.00156 | 0.022275 | 0.020715 | -0.00097 | 0.019749 |
| frontomalare orbitale (lft) | x | -0.02227 | -0.00817 | -0.03044 | -0.02227 | -0.00424 | -0.02651 |
| | y | -0.08864 | -0.00226 | -0.0909 | -0.08864 | -0.00243 | -0.09107 |
| | z | -0.02424 | -0.00171 | -0.02595 | -0.02424 | -0.00281 | -0.02706 |
| frontomalare temporale (lft) | x | -0.04308 | -0.01054 | -0.05361 | -0.04308 | -0.00535 | -0.04843 |
| | y | -0.09982 | -0.00743 | -0.10725 | -0.09982 | -0.00388 | -0.1037 |

**Table 12** Continued

| **Landmark** | | MH1 | Slope | *G. gorilla* male adult | MH1 | Slope | *G. gorilla* female adult |
|---|---|---|---|---|---|---|---|
| | z | -0.01669 | -0.00068 | -0.01737 | -0.01669 | -0.00148 | -0.01817 |
| dacryon (rt | x | -0.00545 | -0.00762 | -0.01307 | -0.00545 | -0.00174 | -0.00719 |
| | y | 0.026951 | 0.00456 | 0.031511 | 0.026951 | 0.000274 | 0.027225 |
| | z | -0.01262 | 0.00359 | -0.00903 | -0.01262 | 0.000764 | -0.01186 |
| dacryon (lf) | x | -0.00484 | -0.00799 | -0.01283 | -0.00484 | -0.0032 | -0.00804 |
| | y | -0.01464 | -0.00398 | -0.01862 | -0.01464 | 0.00081 | -0.01383 |
| | z | -0.02164 | 0.001568 | -0.02007 | -0.02164 | 0.0004 | -0.02124 |
| inferolateral junction of nasal with maxilla (rt) | x | 0.04571 | -0.00672 | 0.038995 | 0.04571 | -0.00314 | 0.042568 |
| | y | 0.024806 | -0.00027 | 0.024537 | 0.024806 | -0.00089 | 0.023917 |
| | z | -0.01758 | 0.005837 | -0.01174 | -0.01758 | 0.003798 | -0.01378 |
| inferolateral junction of nasal with maxilla (lft) | x | 0.043942 | -0.00685 | 0.037093 | 0.043942 | -0.00331 | 0.040636 |
| | y | -0.00654 | 0.000434 | -0.00611 | -0.00654 | -0.00129 | -0.00783 |
| | z | -0.02254 | 0.00486 | -0.01768 | -0.02254 | 0.004898 | -0.01764 |
| anterior attachment of nasal septum | x | 0.096673 | -0.00537 | 0.0913 | 0.096673 | -0.00643 | 0.090241 |
| | y | 0.005738 | 0.001226 | 0.006964 | 0.005738 | 3.60E-05 | 0.005774 |
| | z | -0.02038 | 0.00108 | -0.0193 | -0.02038 | 0.001639 | -0.01874 |
| prosthion | x | 0.148541 | 0.000865 | 0.149406 | 0.148541 | -0.00232 | 0.146223 |
| | y | 0.00958 | 0.002176 | 0.011756 | 0.00958 | -0.00048 | 0.009104 |
| | z | -0.03778 | -0.00346 | -0.04124 | -0.03778 | 0.001408 | -0.03638 |
| I1-I2 contact (rt) | x | 0.149183 | 0.001846 | 0.151029 | 0.149183 | -0.00143 | 0.147752 |
| | y | 0.032687 | 0.000266 | 0.032954 | 0.032687 | -0.00382 | 0.028871 |
| | z | -0.03066 | -0.00707 | -0.03773 | -0.03066 | -0.00121 | -0.03187 |
| I2-canine contact (rt) | x | 0.147131 | 0.001271 | 0.148402 | 0.147131 | -0.00482 | 0.142316 |
| | y | 0.048155 | 0.003715 | 0.05187 | 0.048155 | -0.00168 | 0.046479 |
| | z | -0.02088 | -0.00852 | -0.0294 | -0.02088 | -0.00236 | -0.02324 |

**Table 12** Continued

| **Landmark** | | MH1 | Slope | *G. gorilla* male adult | MH1 | Slope | *G. gorilla* female adult |
|---|---|---|---|---|---|---|---|
| Canine-P3 contact (rt) | x | 0.145521 | 0.001316 | 0.146837 | 0.145521 | -0.00261 | 0.142911 |
| | y | 0.063516 | 0.005143 | 0.068659 | 0.063516 | 0.005354 | 0.06887 |
| | z | 0.002305 | -0.00099 | 0.00131 | 0.002305 | -0.00294 | -0.00063 |
| P3-P4 contact (rt) | x | 0.142729 | 0.003909 | 0.146638 | 0.142729 | -0.00018 | 0.142552 |
| | y | 0.067432 | 0.003454 | 0.070885 | 0.067432 | 0.006401 | 0.073833 |
| | z | 0.017488 | -0.00268 | 0.014804 | 0.017488 | -0.0046 | 0.012885 |
| P4-M1 contact (rt) | x | 0.132786 | 0.007887 | 0.140673 | 0.132786 | 0.004489 | 0.137275 |
| | y | 0.068814 | 0.001733 | 0.070547 | 0.068814 | 0.006016 | 0.07483 |
| | z | 0.044144 | -0.00542 | 0.038728 | 0.044144 | -0.00527 | 0.038874 |
| M1-M2 contact (rt) | x | 0.119852 | 0.011402 | 0.131254 | 0.119852 | 0.007867 | 0.127718 |
| | y | 0.065487 | 0.002475 | 0.067962 | 0.065487 | 0.007968 | 0.073455 |
| | z | 0.067662 | -0.00614 | 0.061521 | 0.067662 | -0.00576 | 0.061899 |
| M2-M3 contact (rt) | x | 0.104488 | 0.017157 | 0.121645 | 0.104488 | 0.011828 | 0.116316 |
| | y | 0.060009 | 0.006376 | 0.066385 | 0.060009 | 0.010565 | 0.070574 |
| | z | 0.093481 | -0.00771 | 0.08577 | 0.093481 | -0.00693 | 0.086551 |
| I1-I2 contact (lft) | x | 0.147491 | 0.001191 | 0.148681 | 0.147491 | -0.00214 | 0.145352 |
| | y | -0.0152 | 0.005788 | -0.00941 | -0.0152 | 0.004592 | -0.01061 |
| | z | -0.03963 | -0.00631 | -0.04594 | -0.03963 | 0.000685 | -0.03894 |
| I2-Canine contact (lft) | x | 0.140476 | -0.00062 | 0.139857 | 0.140476 | -0.00444 | 0.136041 |
| | y | -0.0303 | 0.003996 | -0.02631 | -0.0303 | 0.003891 | -0.02641 |
| | z | -0.03645 | -0.00938 | -0.04583 | -0.03645 | -0.00175 | -0.0382 |
| Canine-P3 contact (lft) | x | 0.139508 | -0.00041 | 0.139101 | 0.139508 | -0.00151 | 0.138002 |
| | y | -0.05734 | 0.000655 | -0.05669 | -0.05734 | -0.00125 | -0.05859 |
| | z | -0.01938 | -0.0037 | -0.02308 | -0.01938 | -0.00259 | -0.02196 |
| P3-P4 contact (lft) | x | 0.136477 | 0.001823 | 0.138301 | 0.136477 | 0.001445 | 0.137923 |
| | y | -0.06474 | -0.00025 | -0.06499 | -0.06474 | -0.00234 | -0.06708 |
| | z | -0.00448 | -0.00239 | -0.00687 | -0.00448 | -0.00286 | -0.00735 |

**Table 12** Continued

| **Landmark** | | MH1 | Slope | *G. gorilla* male adult | MH1 | Slope | *G. gorilla* female adult |
|---|---|---|---|---|---|---|---|
| P4-M1 contact (lft) | x | 0.124337 | 0.006095 | 0.130432 | 0.124337 | 0.004555 | 0.128892 |
| | y | -0.07107 | 0.00109 | -0.06998 | -0.07107 | -0.003 | -0.07407 |
| | z | 0.014788 | -0.00379 | 0.011 | 0.014788 | -0.00401 | 0.01078 |
| M1-M2 contact (lft) | x | 0.114291 | 0.010843 | 0.125134 | 0.114291 | 0.005787 | 0.120078 |
| | y | -0.07707 | 0.001389 | -0.07568 | -0.07707 | -0.00371 | -0.08078 |
| | z | 0.043096 | -0.00595 | 0.037146 | 0.043096 | -0.00429 | 0.038806 |
| M2-M3 contact (lft) | x | 0.100858 | 0.014601 | 0.115459 | 0.100858 | 0.010776 | 0.111634 |
| | y | -0.07846 | -0.00124 | -0.0797 | -0.07846 | -0.00372 | -0.08218 |
| | z | 0.065913 | -0.00766 | 0.058256 | 0.065913 | -0.00704 | 0.058872 |
| Incisivion | x | 0.123476 | -0.00335 | 0.120122 | 0.123476 | -0.00693 | 0.116545 |
| | y | 0.005258 | 0.00187 | 0.007128 | 0.005258 | -0.00144 | 0.003816 |
| | z | 0.003859 | -0.00063 | 0.003226 | 0.003859 | 0.002968 | 0.006826 |
| Alveolon | x | 0.076876 | -0.00619 | 0.070689 | 0.076876 | -0.0079 | 0.068978 |
| | y | -0.00971 | -0.00053 | -0.01024 | -0.00971 | 0.001668 | -0.00804 |
| | z | 0.086509 | 0.00856 | 0.095069 | 0.086509 | 0.003869 | 0.090378 |
| Jugale (lft) | x | 0.014561 | -0.01253 | 0.002031 | 0.014561 | -0.00726 | 0.007298 |
| | y | -0.10816 | -0.01184 | -0.12 | -0.10816 | -0.00595 | -0.11411 |
| | z | 0.006112 | -0.00163 | 0.004484 | 0.006112 | -0.00146 | 0.004653 |
| Zygomatico-temporal suture superior | x | 0.008303 | -0.01418 | -0.00587 | 0.008303 | -0.00573 | 0.002577 |
| | y | -0.11873 | -0.01175 | -0.13049 | -0.11873 | -0.00572 | -0.12445 |
| | z | 0.019612 | 0.002983 | 0.022595 | 0.019612 | 0.000185 | 0.019797 |
| Zygomatico-temporal suture inferior | x | 0.007632 | -0.01423 | -0.0066 | 0.007632 | -0.00618 | 0.001453 |
| | y | -0.13209 | -0.01242 | -0.14451 | -0.13209 | -0.00971 | -0.14179 |
| | z | 0.055516 | 0.006672 | 0.062187 | 0.055516 | 0.005628 | 0.061144 |
| Jugale (rt) | x | 0.018071 | -0.01022 | 0.007848 | 0.018071 | -0.00684 | 0.011228 |
| | y | 0.109888 | 0.011466 | 0.121354 | 0.109888 | 0.007136 | 0.117025 |
| | z | 0.046299 | 0.007552 | 0.053851 | 0.046299 | 0.003194 | 0.049493 |
| Pterion (lft) | x | -0.06608 | -0.00946 | -0.07554 | -0.06608 | -0.00021 | -0.06629 |

**Table 12** Continued

| **Landmark** | | MH1 | Slope | *G. gorilla* male adult | MH1 | Slope | *G. gorilla* female adult |
|---|---|---|---|---|---|---|---|
| | y | -0.09877 | 0.012625 | -0.08615 | -0.09877 | 0.007759 | -0.09101 |
| | z | 0.026975 | 0.00972 | 0.036695 | 0.026975 | -0.00337 | 0.02361 |
| Pterion (rt) | x | -0.06326 | -0.00895 | -0.07221 | -0.06326 | 0.005387 | -0.05787 |
| | y | 0.085819 | -0.01669 | 0.069125 | 0.085819 | -0.0069 | 0.07892 |
| | z | 0.070419 | 0.004091 | 0.07451 | 0.070419 | -0.00332 | 0.067096 |
| Inferior-most point of glenoid process (lft) | x | -0.00843 | -0.01906 | -0.02749 | -0.00843 | -0.00651 | -0.01495 |
| | y | -0.13342 | -0.0034 | -0.13682 | -0.13342 | -0.00626 | -0.13969 |
| | z | 0.114629 | 0.009096 | 0.123725 | 0.114629 | 0.002313 | 0.116943 |
| Inferior-most point of glenoid process (rt) | x | -0.00484 | -0.01971 | -0.02455 | -0.00484 | -0.00793 | -0.01277 |
| | y | 0.08525 | -0.00272 | 0.082531 | 0.08525 | 3.64E-05 | 0.085286 |
| | z | 0.156999 | 0.010247 | 0.167246 | 0.156999 | 0.005045 | 0.162044 |
| Infra-orbital foramen (rt) | x | 0.063594 | -0.00805 | 0.055543 | 0.063594 | -0.00524 | 0.058353 |
| | y | 0.062607 | 0.004346 | 0.066953 | 0.062607 | -0.00024 | 0.062368 |
| | z | 0.005151 | 0.006403 | 0.011554 | 0.005151 | 0.006644 | 0.011794 |
| Infra-orbital foramen (lft) | x | 0.063596 | -0.00858 | 0.055014 | 0.063596 | -0.00636 | 0.057234 |
| | y | -0.05035 | -0.00378 | -0.05413 | -0.05035 | 0.000102 | -0.05025 |
| | z | -0.01354 | 0.004572 | -0.00896 | -0.01354 | 0.004778 | -0.00876 |
| Alare (rt) | x | 0.083556 | 0.001636 | 0.085193 | 0.083556 | -0.00235 | 0.081205 |
| | y | 0.036352 | 0.003596 | 0.039948 | 0.036352 | 0.000188 | 0.03654 |
| | z | -0.01001 | 0.000738 | -0.00927 | -0.01001 | 0.002331 | -0.00767 |
| Alare (lft) | x | 0.083548 | 0.002098 | 0.085646 | 0.083548 | -0.00224 | 0.081312 |
| | y | -0.01959 | -7.77E-05 | -0.01967 | -0.01959 | -0.00079 | -0.02038 |
| | z | -0.02263 | -0.00031 | -0.02294 | -0.02263 | 0.003325 | -0.01931 |
| s1 | x | 0.04383 | -0.00765 | 0.036181 | 0.04383 | -0.00435 | 0.039484 |
| | y | 0.009164 | -0.0004 | 0.008767 | 0.009164 | -0.0003 | 0.008862 |
| | z | -0.02471 | 0.006483 | -0.01823 | -0.02471 | 0.005479 | -0.01923 |
| s2 | x | 0.025326 | -0.00477 | 0.020555 | 0.025326 | -0.00159 | 0.023737 |

**Table 12** Continued

| **Landmark** | | MH1 | Slope | *G. gorilla* male adult | MH1 | Slope | *G. gorilla* female adult |
|---|---|---|---|---|---|---|---|
| | y | 0.009289 | -0.00085 | 0.008437 | 0.009289 | -0.00025 | 0.009042 |
| | z | -0.02006 | 0.006282 | -0.01377 | -0.02006 | 0.003425 | -0.01663 |
| s3 | x | 0.006136 | -0.00435 | 0.001791 | 0.006136 | 0.000542 | 0.006678 |
| | y | 0.008766 | -0.0008 | 0.007961 | 0.008766 | -0.00021 | 0.008552 |
| | z | -0.01983 | 0.006033 | -0.0138 | -0.01983 | 0.002732 | -0.0171 |
| s4 | x | -0.00343 | -0.00294 | -0.00637 | -0.00343 | 0.002268 | -0.00116 |
| | y | 0.008602 | -0.00059 | 0.008016 | 0.008602 | -0.00023 | 0.008376 |
| | z | -0.03125 | 0.004795 | -0.02645 | -0.03125 | 0.002088 | -0.02916 |
| s5 | x | -0.01322 | -0.00046 | -0.01367 | -0.01322 | 0.003381 | -0.00983 |
| | y | 0.008581 | -0.00064 | 0.007943 | 0.008581 | -0.00027 | 0.008311 |
| | z | -0.03744 | 0.00347 | -0.03397 | -0.03744 | 0.001693 | -0.03575 |
| s6 | x | -0.02088 | 0.002177 | -0.0187 | -0.02088 | 0.00455 | -0.01633 |
| | y | 0.008994 | -0.00087 | 0.008124 | 0.008994 | -0.0003 | 0.008698 |
| | z | -0.04416 | 0.00246 | -0.0417 | -0.04416 | 0.001056 | -0.0431 |
| s7 | x | -0.03018 | 0.004975 | -0.02521 | -0.03018 | 0.006497 | -0.02369 |
| | y | 0.009472 | -0.0011 | 0.008368 | 0.009472 | -0.00015 | 0.00932 |
| | z | -0.04854 | 0.00033 | -0.04821 | -0.04854 | -0.00103 | -0.04957 |
| s8 | x | -0.04204 | 0.00474 | -0.0373 | -0.04204 | 0.004741 | -0.03729 |
| | y | 0.009511 | -0.00075 | 0.008758 | 0.009511 | 0.001016 | 0.010527 |
| | z | -0.04908 | -0.00473 | -0.05381 | -0.04908 | -0.00725 | -0.05633 |
| s9 | x | -0.05323 | -0.00292 | -0.05615 | -0.05323 | 0.002186 | -0.05104 |
| | y | 0.00841 | 0.000134 | 0.008544 | 0.00841 | 0.000682 | 0.009092 |
| | z | -0.04403 | -0.0039 | -0.04793 | -0.04403 | -0.0007 | -0.04473 |
| s10 | x | -0.06029 | -0.00218 | -0.06248 | -0.06029 | 0.003146 | -0.05715 |
| | y | 0.007192 | 0.000678 | 0.00787 | 0.007192 | 0.001396 | 0.008588 |
| | z | -0.03866 | -0.00511 | -0.04377 | -0.03866 | -0.00142 | -0.04008 |
| s11 | x | -0.06029 | -0.00218 | -0.06248 | -0.06029 | 0.003146 | -0.05715 |
| | y | 0.007192 | 0.000678 | 0.00787 | 0.007192 | 0.001396 | 0.008588 |
| | z | -0.03866 | -0.00511 | -0.04377 | -0.03866 | -0.00142 | -0.04008 |
| s12 | x | -0.06567 | -0.00065 | -0.06633 | -0.06567 | 0.004455 | -0.06122 |
| | y | 0.006831 | 0.000657 | 0.007488 | 0.006831 | 0.001258 | 0.008088 |
| | z | -0.03432 | -0.00454 | -0.03886 | -0.03432 | -0.00124 | -0.03556 |
| s13 | x | -0.0717 | 0.002704 | -0.069 | -0.0717 | 0.00602 | -0.06568 |

**Table 12** Continued

| **Landmark** | | MH1 | Slope | *G. gorilla* male adult | MH1 | Slope | *G. gorilla* female adult |
|---|---|---|---|---|---|---|---|
| | y | 0.00657 | 0.000477 | 0.007046 | 0.00657 | 0.001027 | 0.007596 |
| | z | -0.03041 | -0.00379 | -0.0342 | -0.03041 | -0.00058 | -0.03098 |
| s14 | x | -0.07819 | 0.006771 | -0.07142 | -0.07819 | 0.007621 | -0.07057 |
| | y | 0.006473 | 0.000105 | 0.006578 | 0.006473 | 0.000694 | 0.007167 |
| | z | -0.0274 | -0.00156 | -0.02896 | -0.0274 | 0.000728 | -0.02667 |
| s15 | x | -0.08489 | 0.0101 | -0.07479 | -0.08489 | 0.008334 | -0.07656 |
| | y | 0.006512 | -0.00027 | 0.006241 | 0.006512 | 0.000395 | 0.006907 |
| | z | -0.02529 | 0.001161 | -0.02413 | -0.02529 | 0.001595 | -0.02369 |
| s16 | x | -0.09168 | 0.012531 | -0.07915 | -0.09168 | 0.008367 | -0.08331 |
| | y | 0.006565 | -0.00062 | 0.005941 | 0.006565 | 0.000189 | 0.006754 |
| | z | -0.02347 | 0.003562 | -0.0199 | -0.02347 | 0.001867 | -0.0216 |
| s17 | x | -0.09845 | 0.014369 | -0.08408 | -0.09845 | 0.007707 | -0.09075 |
| | y | 0.00647 | -0.00088 | 0.005587 | 0.00647 | 0.00015 | 0.00662 |
| | z | -0.02101 | 0.005243 | -0.01577 | -0.02101 | 0.001372 | -0.01964 |
| s18 | x | -0.10527 | 0.015656 | -0.08961 | -0.10527 | 0.006428 | -0.09884 |
| | y | 0.00625 | -0.00104 | 0.005213 | 0.00625 | 0.000209 | 0.00646 |
| | z | -0.01801 | 0.00608 | -0.01193 | -0.01801 | 0.000591 | -0.01742 |
| s19 | x | -0.11196 | 0.016391 | -0.09556 | -0.11196 | 0.004871 | -0.10709 |
| | y | 0.005876 | -0.00107 | 0.004805 | 0.005876 | 0.000254 | 0.006129 |
| | z | -0.01434 | 0.006138 | -0.0082 | -0.01434 | 0.000291 | -0.01405 |
| s20 | x | -0.11833 | 0.016445 | -0.10189 | -0.11833 | 0.003144 | -0.11519 |
| | y | 0.005384 | -0.001 | 0.004381 | 0.005384 | 0.00022 | 0.005604 |
| | z | -0.01027 | 0.005705 | -0.00457 | -0.01027 | 0.000434 | -0.00984 |
| s21 | x | -0.11833 | 0.016445 | -0.10189 | -0.11833 | 0.003144 | -0.11519 |
| | y | 0.005384 | -0.001 | 0.004381 | 0.005384 | 0.00022 | 0.005604 |
| | z | -0.01027 | 0.005705 | -0.00457 | -0.01027 | 0.000434 | -0.00984 |
| s22 | x | -0.12344 | 0.017182 | -0.10626 | -0.12344 | 0.003436 | -0.12 |
| | y | 0.005111 | -0.0005 | 0.004608 | 0.005111 | 0.000107 | 0.005218 |
| | z | -0.00639 | 0.004249 | -0.00215 | -0.00639 | -0.00023 | -0.00663 |
| s23 | x | -0.12853 | 0.017085 | -0.11145 | -0.12853 | 0.003403 | -0.12513 |
| | y | 0.004617 | 6.33E-05 | 0.00468 | 0.004617 | 1.74E-05 | 0.004634 |
| | z | -0.00203 | 0.002594 | 0.00056 | -0.00203 | -0.00079 | -0.00283 |
| s24 | x | -0.13394 | 0.016516 | -0.11743 | -0.13394 | 0.003232 | -0.13071 |

**Table 12** Continued

| **Landmark** | | MH1 | Slope | *G. gorilla* male adult | MH1 | Slope | *G. gorilla* female adult |
|---|---|---|---|---|---|---|---|
| | y | 0.003994 | 0.000538 | 0.004532 | 0.003994 | -0.00011 | 0.003884 |
| | z | 0.002487 | 0.000596 | 0.003083 | 0.002487 | -0.00101 | 0.001481 |
| s25 | x | -0.13937 | 0.01541 | -0.12396 | -0.13937 | 0.002764 | -0.1366 |
| | y | 0.003146 | 0.000944 | 0.004091 | 0.003146 | -0.00026 | 0.002886 |
| | z | 0.007555 | -0.00158 | 0.005973 | 0.007555 | -0.00106 | 0.006494 |
| s26 | x | -0.14459 | 0.013756 | -0.13083 | -0.14459 | 0.002114 | -0.14248 |
| | y | 0.002025 | 0.001242 | 0.003267 | 0.002025 | -0.00046 | 0.001566 |
| | z | 0.013343 | -0.00349 | 0.009853 | 0.013343 | -0.0008 | 0.012545 |
| s27 | x | -0.14996 | 0.010702 | -0.13925 | -0.14996 | 0.001219 | -0.14874 |
| | y | 7.05E-04 | 0.001858 | 0.002563 | 7.05E-04 | -0.00069 | 1.72E-05 |
| | z | 0.019564 | -0.00663 | 0.012932 | 0.019564 | -0.00024 | 0.019325 |
| s28 | x | -0.1552 | 0.006481 | -0.14872 | -0.1552 | 0.000435 | -0.15477 |
| | y | -8.67E-04 | 0.002906 | 0.002039 | -8.67E-04 | -0.00103 | -0.0019 |
| | z | 0.026409 | -0.01107 | 0.015338 | 0.026409 | 0.00095 | 0.027358 |
| s29 | x | -0.16027 | 0.001758 | -0.15852 | -0.16027 | -0.00065 | -0.16092 |
| | y | -0.00269 | 0.003773 | 0.001088 | -0.00269 | -0.00137 | -0.00406 |
| | z | 0.03388 | -0.01453 | 0.01935 | 0.03388 | 0.002339 | 0.036219 |
| s30 | x | -0.16523 | -0.00358 | -0.16881 | -0.16523 | -0.00157 | -0.1668 |
| | y | -0.00473 | 0.00386 | -0.00087 | -0.00473 | -0.00182 | -0.00655 |
| | z | 0.041896 | -0.01832 | 0.023577 | 0.041896 | 0.004136 | 0.046032 |
| | | | | | | | |

**Table 13:** Data for *H. sapiens* developmental vectors and coordinates for simulated *Au. sediba* adult crania. Lower case "s" stands for semi-landmark coordinate.

| **Landmark** | | **Data for male virtual adult** | | | **Data for female virtual adult** | | |
|---|---|---|---|---|---|---|---|
| | | **MH1** | **Slope** | ***H. sapiens* male adult** | **MH1** | **Slope** | ***H. sapiens* female adult** |
| Mid-torus inferior (rt) | x | 0.042758 | -0.00074 | 0.042014 | 0.042758 | -0.00204 | 0.040718 |
| | y | 0.020977 | 0.000751 | 0.021728 | 0.020977 | 0.000932 | 0.021909 |
| | z | -0.0681 | -0.0019 | -0.07001 | -0.0681 | -0.00034 | -0.06844 |

**Table 13** Continued

| **Landmark** | | MH1 | Slope | *H. sapiens* male adult | MH1 | Slope | *H. sapiens* female adult |
|---|---|---|---|---|---|---|---|
| Mid-torus superior (rt) | x | 0.057704 | -0.00067 | 0.057036 | 0.057704 | -0.00329 | 0.054413 |
| | y | 0.019493 | -0.00068 | 0.018809 | 0.019493 | 3.43E-05 | 0.019527 |
| | z | -0.06913 | -0.00245 | -0.07158 | -0.06913 | -0.00029 | -0.06942 |
| Mid-torus inferior (lft) | x | 0.041598 | -0.00143 | 0.040172 | 0.041598 | -0.00257 | 0.039032 |
| | y | 0.041225 | 0.001425 | 0.042649 | 0.041225 | 0.001477 | 0.042702 |
| | z | 0.062807 | 0.001285 | 0.064091 | 0.062807 | -0.00011 | 0.062695 |
| Mid-torus superior (lft) | x | 0.05467 | -0.0015 | 0.053175 | 0.05467 | -0.00377 | 0.0509 |
| | y | 0.039524 | 0.0003 | 0.039823 | 0.039524 | 0.000513 | 0.040036 |
| | z | 0.065085 | 0.001784 | 0.066869 | 0.065085 | -0.00013 | 0.064952 |
| zygoorbitale (rt) | x | -0.03044 | 0.004587 | -0.02585 | -0.03044 | 0.003042 | -0.0274 |
| | y | -0.00267 | -0.00172 | -0.00439 | -0.00267 | 0.000979 | -0.00169 |
| | z | -0.06163 | 0.001768 | -0.05986 | -0.06163 | 0.002534 | -0.0591 |
| zygomaxillare (rt) | x | -0.06658 | 0.000801 | -0.06578 | -0.06658 | -0.00054 | -0.06712 |
| | y | -0.01937 | 0.001264 | -0.01811 | -0.01937 | 0.001093 | -0.01828 |
| | z | -0.10445 | -0.00254 | -0.10699 | -0.10445 | -0.00156 | -0.10601 |
| zygoorbitale (lft) | x | -0.03393 | 0.002725 | -0.03121 | -0.03393 | 0.002125 | -0.03181 |
| | y | 0.013799 | -0.0007 | 0.013098 | 0.013799 | -0.00012 | 0.013682 |
| | z | 0.047007 | -1.31E-05 | 0.046994 | 0.047007 | -0.00138 | 0.045626 |
| zygomaxillare (lft) | x | -0.06493 | 0.000827 | -0.0641 | -0.06493 | -0.00062 | -0.06555 |
| | y | 0.007863 | 0.000501 | 0.008365 | 0.007863 | 0.000924 | 0.008787 |
| | z | 0.091221 | 0.002155 | 0.093376 | 0.091221 | 0.001379 | 0.092599 |
| frontomalare orbitale (rt) | x | 0.023476 | -0.00015 | 0.023324 | 0.023476 | 0.000164 | 0.02364 |
| | y | -0.00989 | -0.00055 | -0.01044 | -0.00989 | 0.000902 | -0.00899 |
| | z | -0.09833 | -0.00117 | -0.0995 | -0.09833 | -0.00077 | -0.0991 |
| frontomalare temporale (rt) | x | 0.042156 | 0.002278 | 0.044435 | 0.042156 | 0.002225 | 0.044381 |
| | y | -0.01928 | 0.002257 | -0.01702 | -0.01928 | 0.001547 | -0.01773 |
| | z | -0.10492 | -0.00063 | -0.10555 | -0.10492 | -0.00059 | -0.10551 |
| frontomalare orbitale (lft) | x | 0.020928 | 5.44E-05 | 0.020983 | 0.020928 | 0.000155 | 0.021084 |

**Table 13** Continued

| **Landmark** | | MH1 | Slope | *H. sapiens* male adult | MH1 | Slope | *H. sapiens* female adult |
|---|---|---|---|---|---|---|---|
| | y | 0.019401 | 0.000159 | 0.01956 | 0.019401 | 0.002189 | 0.02159 |
| | z | 0.092559 | 0.001597 | 0.094156 | 0.092559 | 0.000633 | 0.093192 |
| frontomalare temporale (lft) | x | 0.041037 | 0.001893 | 0.042929 | 0.041037 | 0.001262 | 0.042299 |
| | y | 0.009544 | 0.001499 | 0.011043 | 0.009544 | 0.002632 | 0.012176 |
| | z | 0.103454 | 0.000509 | 0.103963 | 0.103454 | 0.000399 | 0.103853 |
| dacryon (rt) | x | 0.006902 | 0.001028 | 0.00793 | 0.006902 | -0.00075 | 0.006153 |
| | y | 0.013019 | 0.002386 | 0.015405 | 0.013019 | 0.001023 | 0.014042 |
| | z | -0.02643 | -0.00171 | -0.02814 | -0.02643 | -0.0016 | -0.02804 |
| dacryon (lft) | x | 0.004218 | 0.000763 | 0.004982 | 0.004218 | -0.00107 | 0.003146 |
| | y | 0.019345 | 0.000807 | 0.020152 | 0.019345 | 0.001611 | 0.020956 |
| | z | 0.016279 | 0.002084 | 0.018363 | 0.016279 | 0.001628 | 0.017907 |
| inferolateral junction of nasal with maxilla (rt) | x | -0.04426 | -0.00434 | -0.04861 | -0.04426 | -0.00185 | -0.04611 |
| | y | 0.019984 | -0.00167 | 0.018319 | 0.019984 | -0.00011 | 0.01987 |
| | z | -0.02695 | -0.0032 | -0.03015 | -0.02695 | -0.00163 | -0.02859 |
| inferolateral junction of nasal with maxilla (lft) | x | -0.04259 | -0.00437 | -0.04696 | -0.04259 | -0.00151 | -0.0441 |
| | y | 0.024142 | 0.000817 | 0.02496 | 0.024142 | 0.000282 | 0.024424 |
| | z | 0.006232 | 0.002195 | 0.008427 | 0.006232 | 0.002372 | 0.008603 |
| anterior attachment of nasal septum | x | -0.09577 | -0.00149 | -0.09726 | -0.09577 | -0.0019 | -0.09767 |
| | y | 0.022975 | 0.001332 | 0.024307 | 0.022975 | -0.00195 | 0.021027 |
| | z | -0.00901 | 0.000296 | -0.00871 | -0.00901 | 0.000703 | -0.00831 |
| | x | -0.14762 | -0.00514 | -0.15277 | -0.14762 | -0.00447 | -0.15209 |
| prosthion | y | 0.042609 | -0.00184 | 0.04077 | 0.042609 | -0.00225 | 0.040358 |
| | z | -0.01227 | -5.42E-05 | -0.01232 | -0.01227 | 0.000327 | -0.01194 |
| I1-I2 contact (rt) | x | -0.1454 | -0.00479 | -0.15019 | -0.1454 | -0.00408 | -0.14948 |
| | y | 0.036068 | -0.00255 | 0.033519 | 0.036068 | -0.00301 | 0.03306 |
| | z | -0.03648 | 0.001101 | -0.03538 | -0.03648 | 0.001378 | -0.0351 |
| I2-canine contact (rt) | x | -0.14544 | -0.00411 | -0.14956 | -0.14544 | -0.00488 | -0.15033 |

**Table 13** Continued

| **Landmark** | | MH1 | Slope | *H. sapiens* male adult | MH1 | Slope | *H. sapiens* female adult |
|---|---|---|---|---|---|---|---|
| | y | 0.02619 | -0.00171 | 0.024484 | 0.02619 | -0.00257 | 0.023624 |
| | z | -0.05308 | 0.000938 | -0.05214 | -0.05308 | 0.001605 | -0.05148 |
| Canine-P3 contact (rt) | x | -0.14424 | -0.00372 | -0.14796 | -0.14424 | -0.00438 | -0.14861 |
| | y | 0.005277 | -0.00171 | 0.003568 | 0.005277 | -0.001 | 0.004277 |
| | z | -0.06781 | 0.001084 | -0.06672 | -0.06781 | 0.002304 | -0.0655 |
| P3-P4 contact (rt) | x | -0.14088 | -0.00368 | -0.14456 | -0.14088 | -0.00419 | -0.14507 |
| | y | -0.01164 | -0.00069 | -0.01233 | -0.01164 | -0.00056 | -0.0122 |
| | z | -0.07347 | 0.002067 | -0.0714 | -0.07347 | 0.003131 | -0.07034 |
| P4-M1 contact (rt) | x | -0.1323 | -0.00288 | -0.13518 | -0.1323 | -0.00367 | -0.13597 |
| | y | -0.03559 | 0.000864 | -0.03473 | -0.03559 | 0.001108 | -0.03448 |
| | z | -0.07601 | 0.001771 | -0.07424 | -0.07601 | 0.001914 | -0.0741 |
| M1-M2 contact (rt) | x | -0.11877 | -0.00415 | -0.12292 | -0.11877 | -0.00434 | -0.12311 |
| | y | -0.06079 | 0.000832 | -0.05996 | -0.06079 | 0.001421 | -0.05937 |
| | z | -0.07398 | 0.00179 | -0.07219 | -0.07398 | 0.00207 | -0.07191 |
| M2-M3 contact (rt) | x | -0.10461 | -0.0072 | -0.11181 | -0.10461 | -0.00724 | -0.11185 |
| | y | -0.0907 | 0.003042 | -0.08766 | -0.0907 | 0.003767 | -0.08694 |
| | z | -0.06666 | -0.00115 | -0.06781 | -0.06666 | -0.00056 | -0.06722 |
| I1-I2 contact (lft) | x | -0.14658 | -0.00489 | -0.15148 | -0.14658 | -0.00391 | -0.15049 |
| | y | 0.043328 | -0.00241 | 0.040913 | 0.043328 | -0.00323 | 0.040093 |
| | z | 0.012711 | -0.00078 | 0.011929 | 0.012711 | -0.00127 | 0.01144 |
| I2-Canine contact (lft) | x | -0.13971 | -0.00372 | -0.14343 | -0.13971 | -0.00393 | -0.14363 |
| | y | 0.039172 | -0.00213 | 0.03704 | 0.039172 | -0.00368 | 0.035491 |
| | z | 0.028591 | -0.00106 | 0.027535 | 0.028591 | -0.00045 | 0.028136 |
| Canine-P3 contact (lft) | x | -0.14073 | -0.00362 | -0.14435 | -0.14073 | -0.00253 | -0.14326 |
| | y | 0.021628 | -0.00114 | 0.020484 | 0.021628 | -0.00184 | 0.019784 |
| | z | 0.053923 | -0.00151 | 0.052408 | 0.053923 | -0.00206 | 0.051867 |
| P3-P4 contact (lft) | x | -0.13903 | -0.00407 | -0.14311 | -0.13903 | -0.0032 | -0.14223 |
| | y | 0.00594 | -0.00147 | 0.004474 | 0.00594 | -0.00159 | 0.004348 |
| | z | 0.061104 | -0.00279 | 0.05831 | 0.061104 | -0.00301 | 0.058091 |

**Table 13** Continued

| **Landmark** | | MH1 | Slope | *H. sapiens* male adult | MH1 | Slope | *H. sapiens* female adult |
|---|---|---|---|---|---|---|---|
| P4-M1 contact (lft) | x | -0.12798 | -0.00453 | -0.13251 | -0.12798 | -0.00374 | -0.13172 |
| | y | -0.01335 | -0.00013 | -0.01348 | -0.01335 | -0.00086 | -0.01422 |
| | z | 0.067239 | -0.00267 | 0.064572 | 0.067239 | -0.00226 | 0.064979 |
| M1-M2 contact (lft) | x | -0.11953 | -0.00514 | -0.12467 | -0.11953 | -0.00479 | -0.12431 |
| | y | -0.03863 | 0.000911 | -0.03771 | -0.03863 | 0.001083 | -0.03754 |
| | z | 0.072149 | -0.00299 | 0.069159 | 0.072149 | -0.00343 | 0.068719 |
| M2-M3 contact (lft) | x | -0.10548 | -0.0062 | -0.11168 | -0.10548 | -0.00583 | -0.11132 |
| | y | -0.06469 | 0.000346 | -0.06434 | -0.06469 | 0.000722 | -0.06396 |
| | z | 0.074291 | -0.00162 | 0.072666 | 0.074291 | -0.0031 | 0.071189 |
| Incisivion | x | -0.12328 | 0.000431 | -0.12285 | -0.12328 | 0.001133 | -0.12215 |
| | y | 1.09E-04 | -0.00042 | -0.00031 | 1.09E-04 | 0.000109 | 0.000218 |
| | z | -0.00704 | 2.02E-05 | -0.00702 | -0.00704 | -0.00018 | -0.00722 |
| Alveolon | x | -0.08237 | 0.004968 | -0.0774 | -0.08237 | 0.004745 | -0.07762 |
| | y | -0.08492 | -0.00588 | -0.0908 | -0.08492 | -0.00077 | -0.08569 |
| | z | 0.002517 | 0.00072 | 0.003238 | 0.002517 | 9.99E-05 | 0.002617 |
| Jugale (lft) | x | -0.01762 | 0.002978 | -0.01465 | -0.01762 | 0.001389 | -0.01623 |
| | y | -0.01014 | -0.00087 | -0.011 | -0.01014 | 0.001918 | -0.00822 |
| | z | 0.109048 | 0.004794 | 0.113842 | 0.109048 | 0.002403 | 0.111451 |
| Zygomatico-temporal suture superior | x | -0.01282 | 0.004297 | -0.00852 | -0.01282 | 0.001543 | -0.01128 |
| | y | -0.02442 | 0.001171 | -0.02325 | -0.02442 | 0.003037 | -0.02138 |
| | z | 0.118758 | 0.003846 | 0.122604 | 0.118758 | 0.001045 | 0.119803 |
| Zygomatico-temporal suture inferior | x | -0.01268 | 0.004406 | -0.00828 | -0.01268 | 0.004195 | -0.00849 |
| | y | -0.059 | -0.0009 | -0.0599 | -0.059 | 0.000547 | -0.05845 |
| | z | 0.133136 | 0.006307 | 0.139443 | 0.133136 | 0.002313 | 0.135449 |
| Jugale (rt) | x | -0.01525 | 0.004266 | -0.01099 | -0.01525 | 0.002347 | -0.01291 |
| | y | -0.04229 | -0.0026 | -0.04489 | -0.04229 | -0.00016 | -0.04244 |
| | z | -0.11389 | -0.00416 | -0.11805 | -0.11389 | -0.00306 | -0.11695 |
| Pterion (lft) | x | 0.063117 | -0.00501 | 0.05811 | 0.063117 | -0.00207 | 0.061042 |
| | y | -0.03719 | -0.00137 | -0.03857 | -0.03719 | -0.0009 | -0.0381 |
| | z | 0.103582 | -0.00493 | 0.098657 | 0.103582 | -0.00358 | 0.1 |
| Pterion (rt) | x | 0.0658 | -0.0009 | 0.064897 | 0.0658 | 0.001685 | 0.067485 |
| | y | -0.06948 | -0.00099 | -0.07047 | -0.06948 | 0.000586 | -0.06889 |

**Table 13** Continued

| **Landmark** | | MH1 | Slope | *H. sapiens* male adult | MH1 | Slope | *H. sapiens* female adult |
|---|---|---|---|---|---|---|---|
| | z | -0.08854 | 0.005734 | -0.08281 | -0.08854 | 0.005566 | -0.08298 |
| Inferior-most point of glenoid process (lft) | x | -0.00128 | 0.005068 | 0.003783 | -0.00128 | 0.008596 | 0.007311 |
| | y | -0.12391 | -0.00198 | -0.12588 | -0.12391 | 0.000598 | -0.12331 |
| | z | 0.129139 | -0.00142 | 0.127715 | 0.129139 | -0.00423 | 0.124912 |
| Inferior-most point of glenoid process (rt) | x | 0.002736 | 0.006216 | 0.008952 | 0.002736 | 0.009958 | 0.012694 |
| | y | -0.15602 | 0.000123 | -0.1559 | -0.15602 | 0.00249 | -0.15353 |
| | z | -0.093 | -5.69E-05 | -0.09306 | -0.093 | 0.00167 | -0.09133 |
| Infra-orbital foramen (rt) | x | -0.06134 | 0.002334 | -0.05901 | -0.06134 | 0.001474 | -0.05987 |
| | y | -0.00154 | -0.00207 | -0.00361 | -0.00154 | -0.00346 | -0.005 |
| | z | -0.06626 | -0.00258 | -0.06884 | -0.06626 | -0.00395 | -0.07021 |
| Infra-orbital foramen (lft) | x | -0.06427 | 0.002946 | -0.06133 | -0.06427 | 0.002155 | -0.06212 |
| | y | 0.013364 | -0.00132 | 0.012041 | 0.013364 | -0.00231 | 0.011059 |
| | z | 0.049847 | 0.001446 | 0.051293 | 0.049847 | 0.004015 | 0.053862 |
| Alare (rt) | x | -0.0797 | 0.002739 | -0.07696 | -0.0797 | 0.004467 | -0.07524 |
| | y | 0.014334 | -0.00081 | 0.013523 | 0.014334 | -0.00043 | 0.013904 |
| | z | -0.03958 | -0.00093 | -0.04051 | -0.03958 | -0.00139 | -0.04097 |
| Alare (lft) | x | -0.0811 | 0.003227 | -0.07787 | -0.0811 | 0.004536 | -0.07656 |
| | y | 0.023599 | -0.00062 | 0.022978 | 0.023599 | -0.00069 | 0.022912 |
| | z | 0.018603 | 0.001338 | 0.019941 | 0.018603 | 0.001899 | 0.020502 |
| s1 | x | -0.04217 | 0.003618 | -0.03855 | -0.04217 | -8.76E-05 | -0.04226 |
| | y | 0.026888 | 0.002785 | 0.029674 | 0.026888 | 0.001223 | 0.028111 |
| | z | -0.00961 | 0.00043 | -0.00918 | -0.00961 | 0.000531 | -0.00908 |
| s2 | x | -0.02229 | 0.003855 | -0.01843 | -0.02229 | 0.000169 | -0.02212 |
| | y | 0.021347 | 0.001479 | 0.022826 | 0.021347 | 0.001228 | 0.022575 |
| | z | -0.00916 | 0.000349 | -0.00881 | -0.00916 | 0.000273 | -0.00889 |
| s3 | x | -0.00425 | 0.00479 | 0.000535 | -0.00425 | 0.0002 | -0.00406 |
| | y | 0.020829 | 0.00143 | 0.022259 | 0.020829 | 0.001356 | 0.022186 |
| | z | -0.0078 | 0.000125 | -0.00767 | -0.0078 | -0.00011 | -0.0079 |
| s4 | x | 0.003654 | 0.005162 | 0.008816 | 0.003654 | 6.59E-05 | 0.00372 |
| | y | 0.030006 | 0.001806 | 0.031812 | 0.030006 | 0.001812 | 0.031818 |

**Table 13** Continued

| **Landmark** | | MH1 | Slope | *H. sapiens* male adult | MH1 | Slope | *H. sapiens* female adult |
|---|---|---|---|---|---|---|---|
| | z | -0.0066 | -9.30E-05 | -0.00669 | -0.0066 | -0.00039 | -0.007 |
| s5 | x | 0.012125 | 0.004998 | 0.017122 | 0.012125 | 0.000153 | 0.012277 |
| | y | 0.035885 | 0.002302 | 0.038186 | 0.035885 | 0.001616 | 0.037501 |
| | z | -0.00601 | -0.00024 | -0.00624 | -0.00601 | -0.00044 | -0.00645 |
| s6 | x | 0.020393 | 0.00426 | 0.024653 | 0.020393 | 0.000187 | 0.02058 |
| | y | 0.04091 | 0.00363 | 0.04454 | 0.04091 | 0.002072 | 0.042982 |
| | z | -0.00582 | -0.00045 | -0.00627 | -0.00582 | -0.00048 | -0.0063 |
| s7 | x | 0.028625 | 0.00393 | 0.032555 | 0.028625 | 0.000269 | 0.028894 |
| | y | 0.046568 | 0.004243 | 0.050811 | 0.046568 | 0.00211 | 0.048678 |
| | z | -0.00609 | -0.00047 | -0.00656 | -0.00609 | -0.00037 | -0.00646 |
| s8 | x | 0.039809 | 0.004311 | 0.044119 | 0.039809 | 0.000547 | 0.040355 |
| | y | 0.048748 | 0.004223 | 0.052971 | 0.048748 | 0.002149 | 0.050896 |
| | z | -0.00613 | -0.00058 | -0.00671 | -0.00613 | -0.00043 | -0.00656 |
| s9 | x | 0.050839 | 0.005116 | 0.055956 | 0.050839 | 0.000892 | 0.051731 |
| | y | 0.045838 | 0.003632 | 0.04947 | 0.045838 | 0.002202 | 0.04804 |
| | z | -0.00552 | -0.00072 | -0.00624 | -0.00552 | -0.00061 | -0.00613 |
| s10 | x | 0.057708 | 0.005317 | 0.063025 | 0.057708 | 0.001132 | 0.05884 |
| | y | 0.041733 | 0.002775 | 0.044509 | 0.041733 | 0.001907 | 0.04364 |
| | z | -0.00493 | -0.0008 | -0.00573 | -0.00493 | -0.00066 | -0.00559 |
| s11 | x | 0.057708 | 0.005317 | 0.063025 | 0.057708 | 0.001132 | 0.05884 |
| | y | 0.041733 | 0.002775 | 0.044509 | 0.041733 | 0.001907 | 0.04364 |
| | z | -0.00493 | -0.0008 | -0.00573 | -0.00493 | -0.00066 | -0.00559 |
| s12 | x | 0.062464 | 0.005385 | 0.067849 | 0.062464 | 0.003944 | 0.066408 |
| | y | 0.037821 | 0.001306 | 0.039127 | 0.037821 | 0.001233 | 0.039054 |
| | z | -0.00458 | -0.00045 | -0.00504 | -0.00458 | -0.00029 | -0.00488 |
| s13 | x | 0.067621 | 0.005414 | 0.073035 | 0.067621 | 0.006127 | 0.073748 |
| | y | 0.033738 | 0.000262 | 0.034 | 0.033738 | 0.000545 | 0.034283 |
| | z | -0.00422 | -0.00017 | -0.00439 | -0.00422 | 4.35E-05 | -0.00417 |
| s14 | x | 0.073369 | 0.005318 | 0.078687 | 0.073369 | 0.007718 | 0.081087 |
| | y | 0.029889 | -0.001 | 0.028893 | 0.029889 | -0.00015 | 0.029739 |
| | z | -0.00389 | 0.000108 | -0.00378 | -0.00389 | 0.000327 | -0.00356 |
| s15 | x | 0.079801 | 0.004959 | 0.08476 | 0.079801 | 0.008582 | 0.088383 |
| | y | 0.026565 | -0.0026 | 0.023961 | 0.026565 | -0.00152 | 0.025047 |
| | z | -0.00365 | 0.000402 | -0.00325 | -0.00365 | 0.00064 | -0.00301 |
| s16 | x | 0.086962 | 0.00421 | 0.091171 | 0.086962 | 0.008667 | 0.095629 |
| | y | 0.023897 | -0.00329 | 0.020612 | 0.023897 | -0.00282 | 0.021074 |
| | z | -0.00352 | 0.000523 | -0.003 | -0.00352 | 0.000914 | -0.00261 |
| s17 | x | 0.094826 | 0.0031 | 0.097926 | 0.094826 | 0.007849 | 0.102675 |

**Table 13** Continued

| **Landmark** | | MH1 | Slope | *H. sapiens* male adult | MH1 | Slope | *H. sapiens* female adult |
|---|---|---|---|---|---|---|---|
| | y | 0.021643 | -0.00435 | 0.017294 | 0.021643 | -0.00471 | 0.016934 |
| | z | -0.00348 | 0.000647 | -0.00283 | -0.00348 | 0.001209 | -0.00227 |
| s18 | x | 0.102882 | 0.001848 | 0.104729 | 0.102882 | 0.006428 | 0.10931 |
| | y | 0.018474 | -0.00483 | 0.013639 | 0.018474 | -0.00597 | 0.012505 |
| | z | -0.00329 | 0.000664 | -0.00262 | -0.00329 | 0.001347 | -0.00194 |
| s19 | x | 0.11102 | 0.000618 | 0.111639 | 0.11102 | 0.004739 | 0.11576 |
| | y | 0.014425 | -0.00466 | 0.009765 | 0.014425 | -0.00638 | 0.008045 |
| | z | -0.00295 | 0.000588 | -0.00236 | -0.00295 | 0.001327 | -0.00162 |
| s20 | x | 0.118956 | -0.00066 | 0.118297 | 0.118956 | 0.00297 | 0.121926 |
| | y | 0.009518 | -0.00412 | 0.005395 | 0.009518 | -0.00618 | 0.003342 |
| | z | -0.00247 | 0.000435 | -0.00204 | -0.00247 | 0.001207 | -0.00127 |
| s21 | x | 0.118956 | -0.00066 | 0.118297 | 0.118956 | 0.00297 | 0.121926 |
| | y | 0.009518 | -0.00412 | 0.005395 | 0.009518 | -0.00618 | 0.003342 |
| | z | -0.00247 | 0.000435 | -0.00204 | -0.00247 | 0.001207 | -0.00127 |
| s22 | x | 0.125923 | -0.00219 | 0.123735 | 0.125923 | 0.001016 | 0.12694 |
| | y | 0.004199 | -0.00303 | 0.001166 | 0.004199 | -0.00532 | -0.00112 |
| | z | -0.00182 | 0.000221 | -0.00159 | -0.00182 | 0.000784 | -0.00103 |
| s23 | x | 0.132418 | -0.0035 | 0.12892 | 0.132418 | -0.00072 | 0.1317 |
| | y | -0.0016 | -0.00187 | -0.00347 | -0.0016 | -0.0042 | -0.00579 |
| | z | -9.87E-04 | 8.03E-06 | -0.00098 | -9.87E-04 | 0.000381 | -0.00061 |
| s24 | x | 0.138814 | -0.00454 | 0.134273 | 0.138814 | -0.00218 | 0.136632 |
| | y | -0.00744 | -0.00061 | -0.00804 | -0.00744 | -0.00278 | -0.01022 |
| | z | -5.99E-05 | -0.00021 | -0.00027 | -5.99E-05 | -9.92E-07 | -6.1E-05 |
| s25 | x | 0.144847 | -0.00538 | 0.139471 | 0.144847 | -0.00324 | 0.14161 |
| | y | -0.01365 | 0.000679 | -0.01297 | -0.01365 | -0.00102 | -0.01468 |
| | z | 0.001021 | -0.0004 | 0.000623 | 0.001021 | -0.00037 | 0.000648 |
| s26 | x | 0.150327 | -0.00605 | 0.144277 | 0.150327 | -0.00415 | 0.146178 |
| | y | -0.02038 | 0.00194 | -0.01844 | -0.02038 | 0.000835 | -0.01955 |
| | z | 0.002276 | -0.00056 | 0.001719 | 0.002276 | -0.00071 | 0.001569 |
| s27 | x | 0.155534 | -0.00662 | 0.148912 | 0.155534 | -0.00512 | 0.150414 |
| | y | -0.02736 | 0.003142 | -0.02422 | -0.02736 | 0.002671 | -0.02469 |
| | z | 0.003665 | -0.00068 | 0.002988 | 0.003665 | -0.00098 | 0.002688 |
| s28 | x | 0.160435 | -0.00726 | 0.153179 | 0.160435 | -0.00616 | 0.154273 |
| | y | -0.03465 | 0.004242 | -0.03041 | -0.03465 | 0.004552 | -0.0301 |
| | z | 0.005196 | -0.00074 | 0.004458 | 0.005196 | -0.00117 | 0.004022 |
| s29 | x | 0.164985 | -0.00759 | 0.157399 | 0.164985 | -0.00693 | 0.158052 |
| | y | -0.04227 | 0.005418 | -0.03686 | -0.04227 | 0.006688 | -0.03559 |

**Table 13** Continued

| **Landmark** | | MH1 | Slope | *H. sapiens* male adult | MH1 | Slope | *H. sapiens* female adult |
|---|---|---|---|---|---|---|---|
| | z | 0.006873 | -0.00081 | 0.006063 | 0.006873 | -0.00135 | 0.005521 |
| s30 | x | 0.169162 | -0.00748 | 0.161685 | 0.169162 | -0.00719 | 0.161971 |
| | y | -0.05023 | 0.006552 | -0.04368 | -0.05023 | 0.00909 | -0.04114 |
| | z | 0.008694 | -0.00106 | 0.007634 | 0.008694 | -0.0016 | 0.007098 |